CHAPTER-V

Section A

An efficient and green protocol for the synthesis of 1-hydroxy-2-arylimidazole-3-oxide derivatives under solvent free condition using inexpensive Copper borate (CuB_4O_7) catalyst.

5.A.1 Background of the present investigation:

During the past, drugs containing heterocyclic scaffold has occupied a unique position because of their high therapeutic values. A lot of drug motif heterocyclic core are in clinical use to treat many infectious diseases[1]. Among a large and diverse variety of heterocyclic compounds, imidazole, five membered nitrogen containing heterocyclic compound has gained a lot of interest in the field of drug discovery and has occupied a special position in the field of heterocyclic chemistry[2]. A unique feature of the imidazole scaffold is its polar nature and this property could be largely exploited to improve the pharmacokinetic property of drug molecule containing imidazole core as this moiety could help in improving the aqueous solubility of many drugs which are poorly soluble in water[3]. A large variety of compounds containing imidazole scaffold shows a lot of promising therapeutic activities such as antiviral[2], antitumor[4], antiinflamatory[5], antidiabetic[6], anticonvulsant[7], antiasthamatic[8] and antiamoebic[19] etc. A large variety of drugs containing imidazole scaffold such as Etonitazene (analgesics)[10] (104), Enviroxime (antiviral)[11] (105), pantoprazole (antiulcer)[10](106), Metronidazole (antibacterial)[3] (107) and Carbimazole (antithyroid)[7] (108) etc. are commercially available in the market (Fig. 5A.1). Among the various types of heterocyclic compounds consisting of imidazole core, 1-hydroxy-imidazole-3-oxide is regarded as a versatile heterocyclic compound as these compounds are mostly involved in the synthesis of room temperature ionic liquids[11]. Particularly, the incorporation of N-O moiety into the imidazolium based ionic liquid may give rise to greener solvent which is degradable by design and may fulfill the primary aspect of green chemistry principles[12]. Moreover, the imidazolium salt namely 1-alkoxy-3-alkyl-imidazolium salt were found to be liquid at room temperature and the synthesis of such room temperature ILs requires a two-step alkylation of the precursor 1-hydroxyimidazole[13].

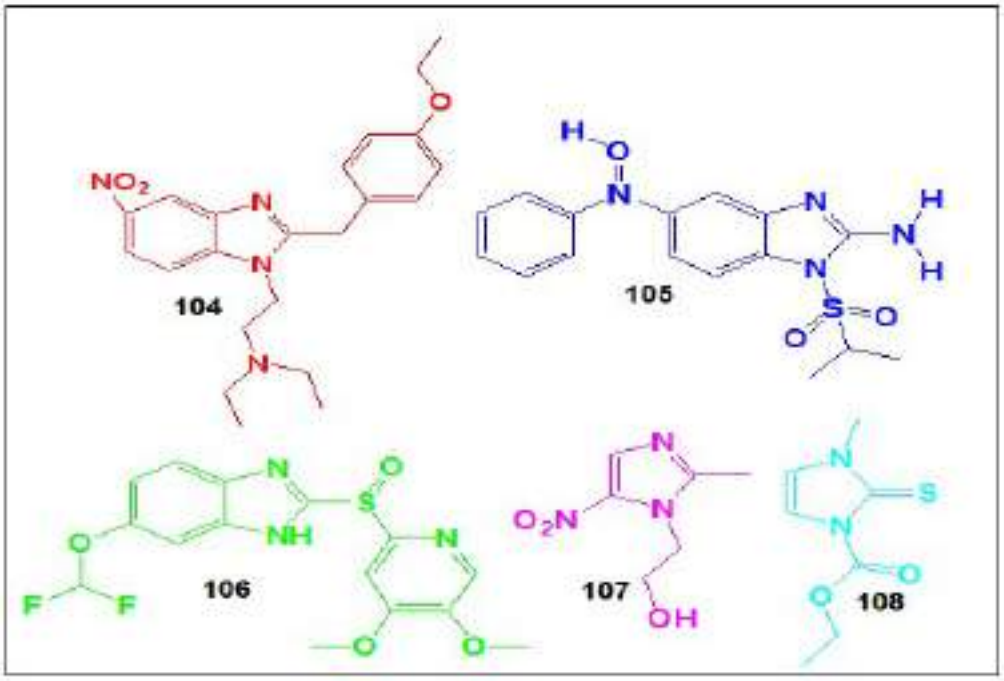

Fig. 5.A.1. Examples of drugs containing imidazole scaffold

The precursor 1-hydroxy-imidazole3-oxide could readily be obtained by cyclization of glyoxime and formaldehyde[14]. The employment of alkyl or aryl aldehydes in the synthesis of 1-hydroxyimidazole results in the formation of corresponding 1-hydroxy-2-alkylimidazole3-oxide and 1-hydroxy-2-arylimidazole-3-oxide derivatives respectively. In general, Heterocyclic compounds commonly containing a dipolar R_3-N-O linkage in which the nitrogen either sp3 or sp2 hybridized are known as Heterocyclic-N-oxides[15-16]. Interestingly, the incorporation of a negative charge on oxygen changes most of the physical properties including the reactivity of the heterocyclic compounds and the most common Heterocyclic-N-Oxide is Pyridine-N-oxide which has excellent donor properties as compared to normal pyridine[17-18]. Imidazole –N-oxides are the compounds which have N-O group attached to the imidazole ring. Imidazole-N-oxides fall under the category of N-substituted imidazole which have a wide variety of applications. These compounds have gained popularity due to their anti-protozoal[19], fungicidal, herbicidal, pesticidal[20], hypotensive properties[21], anti-tumor[22] and anti-viral[23] properties (Fig.5.A.2). Apart from its pharmaceutical applications, imidazole-N-oxides are also used for the generation of N-containing heterocyclic carbenes (NHCs) which acts as intermediates in various organic reactions[24].

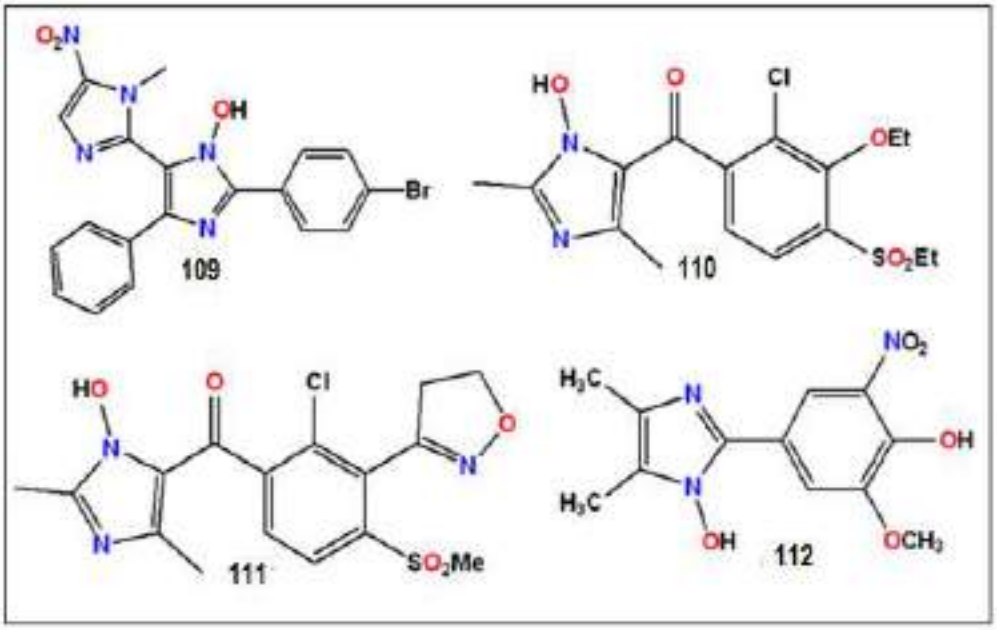

Fig. 5.A.2. Examples of 1-hydroxyimidazole compounds having biological activities.

The current literature survey revealed that only few works on the synthesis of 1-hydroxy-2-arylimidazole3-oxide has been documented in the literature[25]. Thus, it was thought worthwhile to undertake the research work in the synthesis of 1-hydroxy-2-arylimidazole-3-oxide derivatives under green chemical condition by employing inexpensive and unconventional copper borate as a catalyst.

5.A.2 Result and Discussions

By looking at the diverse applications of Imidazole-3-oxides and 1-hydroxyimidazole3-oxide, various methodologies have been developed in the past for the synthesis of these compounds. The most common and the conventional method for the synthesis of imidazole-3-oxides (4) is from mono-oximes(α-hydroxyiminoketones) (1) and aldehydes (2) in the presence of amines (3)[20,26] (Scheme 5.A.1)

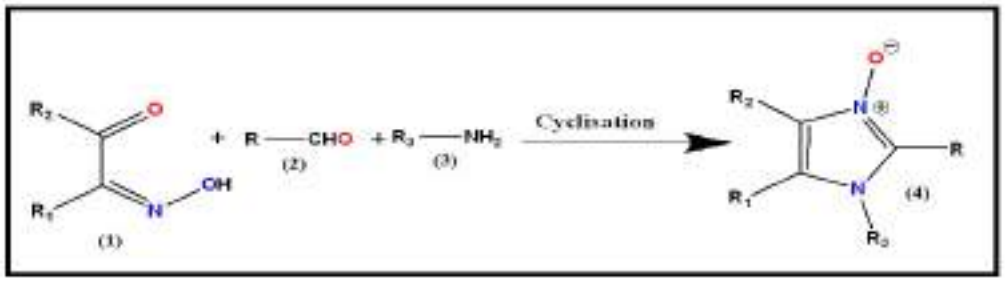

Scheme. 5.A.1. Method of synthesis of N-alkylimidazole3-oxide (4)

Substitution of the amine precursor with NH_4OAc for the above reaction results in the formation of the 1-hydroxyimidazole derivatives (4)[27-28] (Scheme 5.A.2).

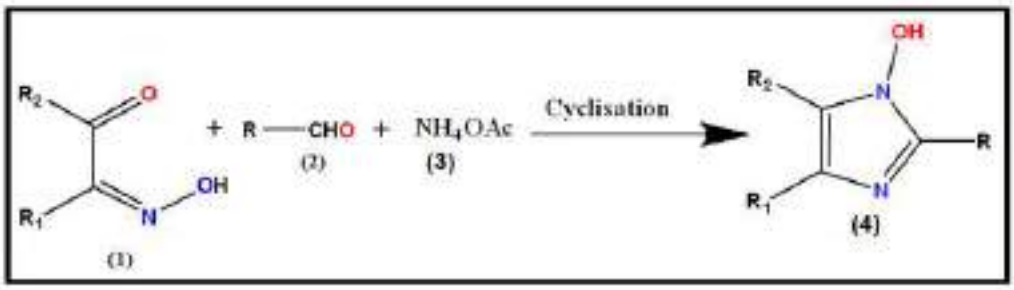

Scheme. 5.A.2. Synthesis of 1-hydroxyimidazole derivatives (4)

However, when hydroxylamine hydrochloride ($NH_2OH.HCl$) is used instead of amine and NH_4OAc, the corresponding 1-hydroxy-2-alkylimidazole 3-oxide (4) or 1-hydroxy-2-arylimidazole-3-oxide (4) is formed respectively depending upon the aldehyde precursor used[29-30] (Scheme 5.A.3).

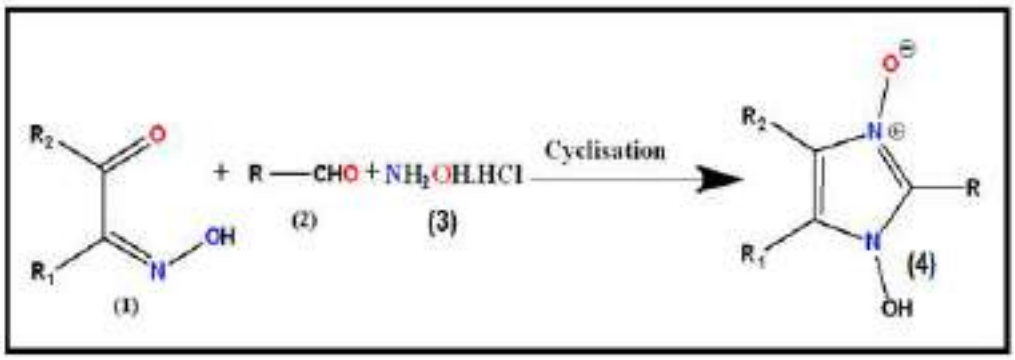

Scheme. 5.A.3. Synthesis of 1-hydroxy-2-(aryl)-4,5-dimethylimidazole-3-oxide (4).

Although the above-mentioned procedures are widely used for the synthesis of imidazole-N-oxides and 1 hydroxy imidazole-3-oxides, yet there are a very few reports for the solvent free and green procedures for the synthesis of the above said compounds[35]. These factors prompted us to devise a synthetic method for the synthesis of 1-hydroxy-2-arylimidazole-3-oxide derivatives under solvent free conditions using copper borate as a catalyst. Thus, in this chapter we are representing the catalytic efficacy of the inexpensive copper borate (CuB_4O_7) as a catalyst for the solvent free synthesis of 1-hydroxy-2-(aryl)-4,5-dimethylimidazole-3-oxide derivatives.

Initially, for the synthesis of 1-hydroxy-2-(aryl)-4,5-dimethylimidazole-3-oxide (4), we selected diacetylmonoxime (1), benzaldehyde (2) and hydroxylamine hydrochloride ($NH_2OH.HCl$)(3) as a model compounds under different reaction conditions at 100 ºC for 2 hours using varied amount of catalyst (0.5 to 3.5 mol %) (Scheme5.A.4).

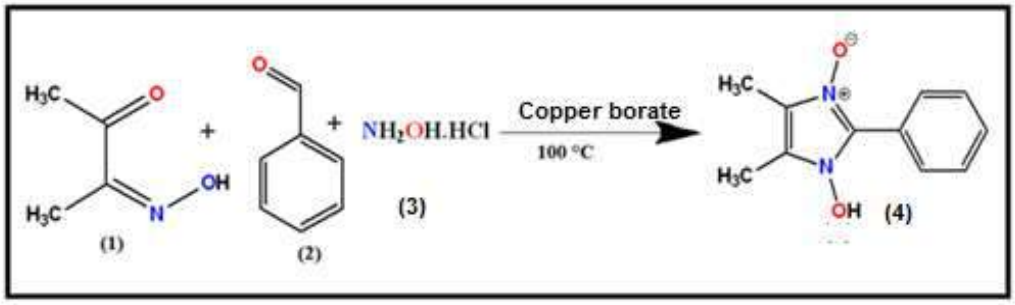

Scheme. 5.A.4. Model reaction for the synthesis of 1-hydroxy-2-(aryl)-4,5-dimethylimidazole-3-oxide using diacetyl monoxime(1) 1mmol, benzaldehyde (2) 1mmol, hydroxylamine hydrochloride (3) 2.5 mmol under different mole % of catalyst.

Again, for the optimization of the reaction condition, we choose different solvent systems for the above reaction. At least we choose 5 polar protic and polar aprotic solvents to screen the efficacy of the employed catalyst for the desired reaction (Table 5.A.1). Interestingly we observed that the above reaction proceeds well in more polar protic and aprotic solvents like alcohol and DMF, DMSO respectively (Table 5.A.1. entry 1, 2, 3 and 4) but we encountered that under this reaction condition, the reaction needs more time for the completion. Therefore, we focused our study towards the green protocol by utilizing solvent free condition for the synthesis of the 1-hydroxy-2-arylimidazole3-oxide. Moreover, we observed that under solvent free condition, the reaction proceeds well and requires less time for completion without forming the by-product and therefore making the work-up procedure more facile and efficient (Table 5.A.1, entry 6).

Table. 5.A.1. Screening of the reaction condition (solvent) for model reaction

Entry	Solvent[a]	Yield[b]
1	Ethanol	90
2	Methanol	86
3	DMF	88
4	DMSO	79
5	Water	55
6	**Neat**	**98**

[a]The reaction was carried out with diacetyl monoxime (1) (1 mmol), benzaldehyde (2) (1 mmol) and hydroxylamine hydrochloride (2.5 mmol) with the catalyst using different solvents at 100°C.After having recognized the optimum reaction conditions, we carried forward this protocol to other aromatic aldehydes to synthesize 1-hydroxy-2-(aryl)-4,5-dimethylimidazole-3-oxide derivatives (4) and in almost all the cases, the reaction proceeded in a short time with excellent yield of the products (90-98 %) and [b]isolated yields

We carried out the above reaction with model components using different mol % of the catalyst to optimize the catalyst loading for the desired product and we observed that the reaction proceeds well when the amount of catalyst loading is 2.5 mol % at the optimized reaction temperature of 100 ºC (Table5.A.2). Then we optimized the reaction time for the modelled reaction and we found that the reaction completes within 10 minutes under solvent free condition (Scheme.5.A.5). Therefore, we concluded that the model reaction goes for completion when the amount of catalyst loading is 2.5 mole % at 100 ºC and 10 minutes of reaction time (Table 5.A.2, entry5). It was also observed that only a negligible amount of product was formed without catalyst (Table 5.A.2, entry1).

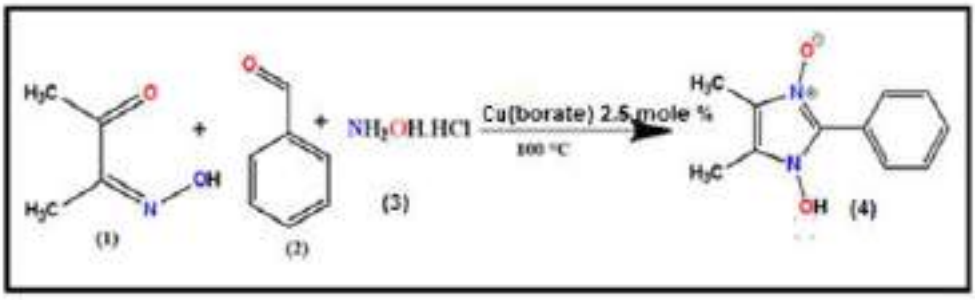

Scheme. 5.A.5. Optimized reaction condition for the synthesis of 1-hydroxy-2-(aryl)-4,5-dimethylimidazole-3-oxide

Table. 5.A.2. Screening of the amount of catalyst loading for the model reaction

Entry	Catalyst mol %[a]	Temperature (°C)	Time (Minutes)	Yield[b] (%)
1	0	100	10	12
2	0.5	100	10	59
3	1.0	100	10	62
4	2.0	100	10	85
5	**2.5**	**100**	**10**	**97**
6	3.0	100	10	95
7	3.5	100	10	94

[a]The reaction was carried out with diacetyl monoxime (1) (1 mmol), benzaldehyde (2) (1 mmol) and hydroxylamine hydrochloride (2.5 mmol) with the catalyst using different solvents at 100°C. After having recognized the optimum reaction conditions, we carried forward this protocol to other aromatic aldehydes to synthesize 1-hydroxy-2-(aryl)-4,5-dimethylimidazole-3-oxide derivatives (4) and in almost all the cases, the reaction proceeded in a short time with excellent yield of the products (90-98 %), [b]isolated yield

It was observed that when the amount of catalyst loading is more than or less than 2.5 mole %, the isolated yield of the product found to be decreased. Having recognized the optimized reaction condition, we therefore extended this reaction protocol for a number of aromatic aldehydes having electron withdrawing and electron releasing groups and we found that this catalytic protocol works well with both type of aldehyde precursors. However, it reflects from this study that aldehydes having electron withdrawing group successfully afforded the desired product more efficiently in excellent yield than the aldehydes having the electron releasing group (Table 5.A.3, Fig. 5.A.3).

Table. 5.A.3. CuB_4O_7 catalyzed solvent free synthesis of 1-hydroxy-2-(aryl)-4,5-dimethylimidazole-3-oxide (4a-4m)

Entry	α-hydroxyiminoketone	Aldehyde	Product	Yield[b] (%)
1	Diacetyl monoxime	Benzaldehyde	4a	97
2	Diacetyl monoxime	3-nitro-benzaldehyde	4b	98
3	Diacetyl monoxime	4-fluoro-benzaldehyde	4c	98
4	Diacetyl monoxime	3-hydroxy-benzaldehyde	4d	95
5	Diacetyl monoxime	2,4-dihydroxy-benzaldehyde	4e	93
6	Diacetyl monoxime	2-hydroxy-benzaldehyde	4f	94
7	Diacetyl monoxime	4-hydroxybenzaldehyde	4g	94
8	Diacetyl monoxime	2-hydroxy-5-chloro-benzaldehyde	4h	96
9	Diacetyl monoxime	2-hydroxy-5-bromo-benzaldehyde	4i	95
10	Diacetyl monoxime	2-hydroxy-3-methoxy-benzaldehyde	4j	95
11	Diacetyl monoxime	4-hydroxy-3-methoxy-benzaldehyde	4k	94
12	Diacetyl monoxime	3,4,5-trimethoxy-benzaldehyde	4l	94
13	Diacetyl monoxime	4-methoxy-benzaldehyde	4m	93

[b]isolated yield

After recognizing the catalytic efficacy of the copper borate catalyst, we were interested to study the recyclability of the catalyst for the given reaction protocol and we observed that the catalyst is easily recoverable with simple filtration from the reaction mixture. Thus, we recovered the catalyst after the first run of the reaction and purified the catalyst by simply washing with methanol and dried at 100 ºC in an oven. The recovered catalyst again used for further reaction and interestingly we observed that catalyst did not lose its efficiency up to 5th run of the reaction (Table 5.A.4). However, after the 5th run, we observed that the product yield changed little and from this we can infer that the catalyst could be used up to 5th run for the studied reaction protocol. The bar diagram for the catalytic recyclability of the studied catalyst is given in Fig. 5.A.4.

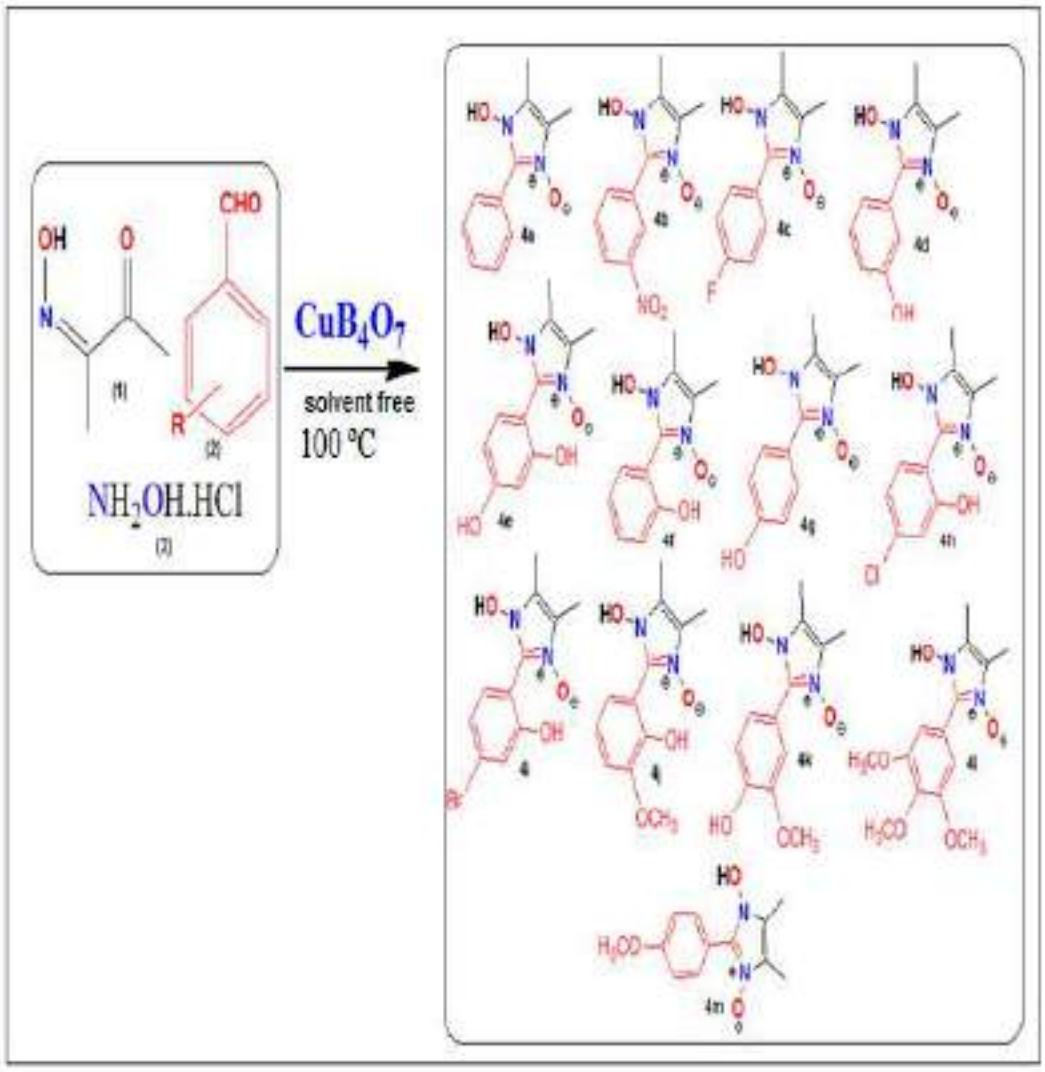

Fig. 5.A.3. Schematic representation of product formed under the stated reaction condition

Table. 5.A.4. Recyclability of copper borate in model reaction

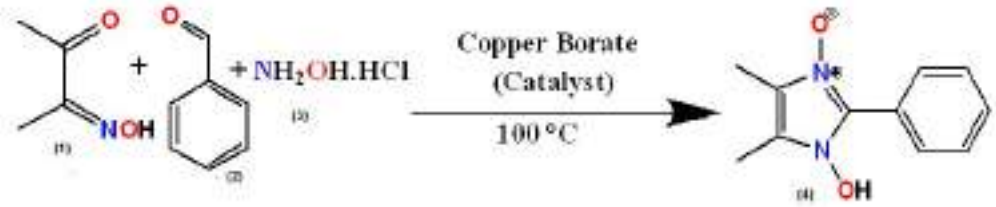

Entry	No. of runs	Isolated yields (%)
1	1	97
2	2	96
3	3	95
4	4	95
5	5	94
6	6	84

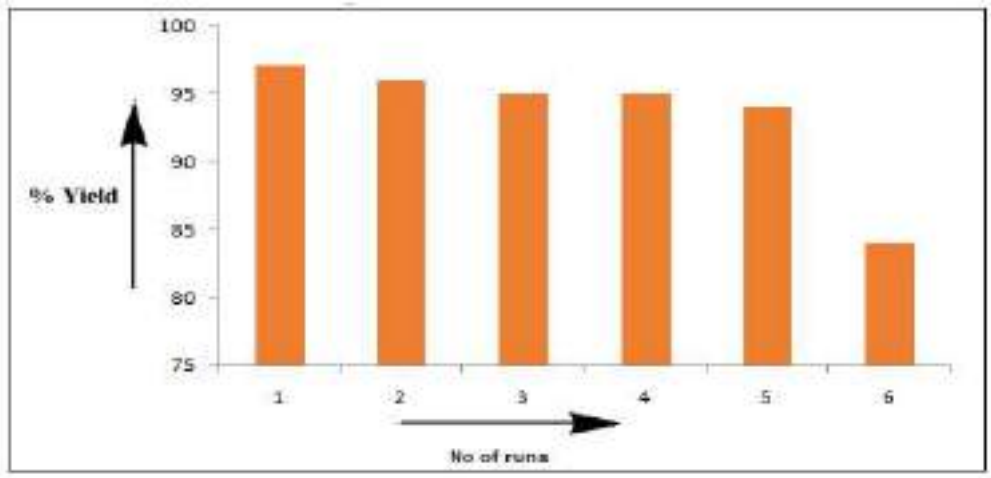

Fig. 5.A.4. Recyclability of the catalyst

Interestingly, it has been observed that the 1-hydroxyimidazole derivatives and N-hydroxybenzimidazole derivatives know to show prototropic tautomerism and this type of tautomerism plays an important role in drug discovery. Therefore, due to prototropic tautomerism, either N-hydroxy (a/a$^{/}$) or N-oxide (b/b$^{/}$) tautomeric form exist for these type of molecules[31-33] (Fig.5A.5).

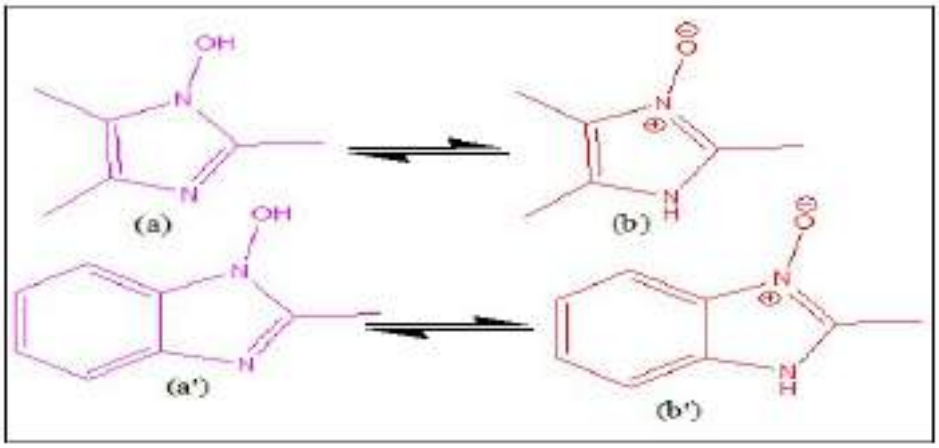

Fig. 5.A.5. Prototropic tautomeric equilibrium of 1-hydroxyimidazole and N-hydroxybenzimidazole, a/a/) N-hydroxy form and b/b/) N-oxide form.

While recrystallizing the synthesized 1-hydroxy-2-arylimidazole3-oxide derivatives using aqueous ethanol (20:80), we observed that the compound 4m crystallized in a needle shaped crystal and therefore, we carried out the X-ray single crystal diffraction study of 4m. From the single crystal diffraction study, it was revealed that the compound 4m exist as a 1, 3-dihydroxy form instead of 1-hydroxy 3-oxide form as shown in Fig 5.A.6.

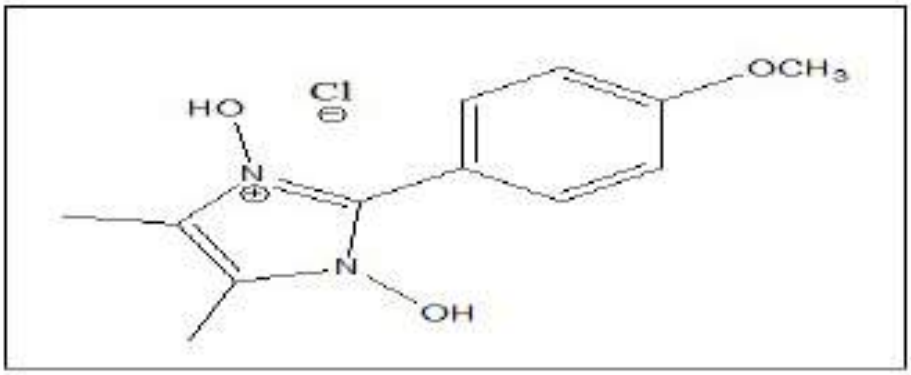

Fig. 5.A.6. Structure of 1,3-dihydroxy-2-(4-methoxyphenyl)-4,5-dimethyl-1*H*-imidazol-3-ium chloride (4m).

5.A.2.1 Description of crystal structure of (4m)

The compound, 1,3-dihydroxy-2-(4-methoxyphenyl)-4,5-dimethyl-1*H*-imidazol-3-ium chloride, **4m**, crystallizes in the monoclinic P 21/n space group. Crystal data and experimental details for **4m** are listed in Table 5.A.5. Selected bond lengths and torsion angles are presented in Table 5.A.6. The asymmetric unit has been shown in Fig. 5.A.7. The three-dimensional packing arrangement of **4m** has been shown in Fig. 5.A.8. The molecule is not a planner molecule as is evident from the torsion angles around C1–C8 bond. There is puckering in the C1–C8 bond. The puckering is envisioned by the dihedral angle between the planes containing the phenyl and imidazole moiety which is *ca*. 44.62 (0.05). There are two intermolecular O–H···Cl interactions (Table 5.A.7, Fig. 5.A.9) which stabilizes the crystal packing and is further stabilized by an intermolecular C–H···*Cg* interaction (Table 5.A.8, Fig. 5.A.10) between C12–H12B and *Cg*2 (centroid of C1 – C6 ring).

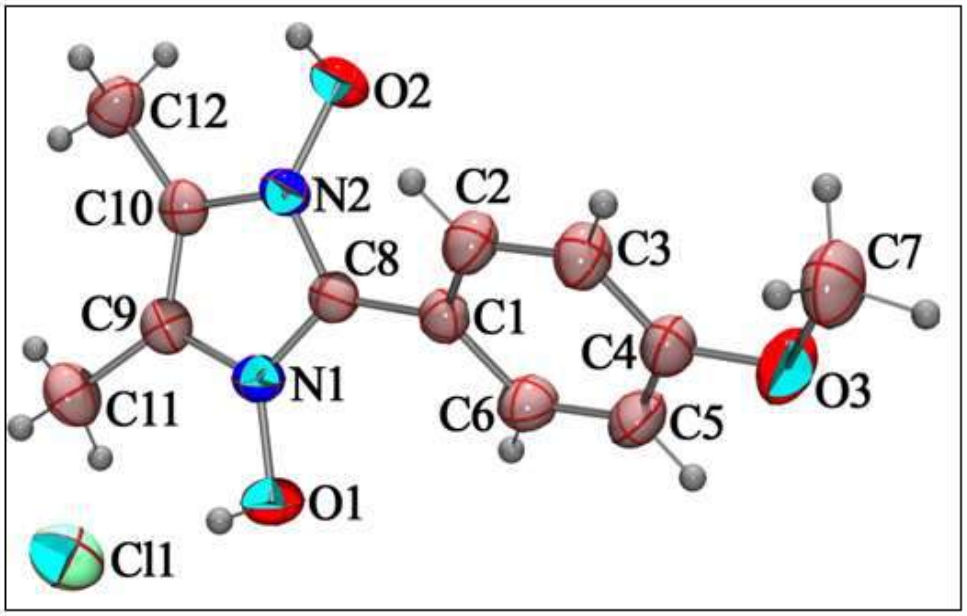

Fig. 5.A.7. Asymmetric unit of **4m** with displacement ellipsoids drawn at 50% probability level.

Table. 5.A.5 Crystal data collection and structure refinement for (**4m**)

Crystal data	
CCDC reference number	2183509
Empirical formula	$C_{12}H_{15}N_2O_3Cl$
Moiety formula	$C_{12}H_{15}N_2O_3$, Cl
Formula weight	270.71
Crystal system	Monoclinic
Space group	P 21/n
Color, habit	Pale white, rod
Size, mm	0.28 × 0.26 × 0.25
Unit cell dimensions	
a = 8.5143(4)Å	α = 90°
b = 7.6289(4)Å	β = 94.228(4)°
c = 20.1962(9)Å	γ = 90°
Volume Å^3	1308.27(11)
Z	4
Density (calculated), Mg/m^3	1.374
Absorption coefficient, mm^{-1}	0.294
F(000)	568
Data collection	
Temperature, K	293(2)
Theta range for data collection	3.35° to 25.00°
Index ranges	$-10 \le h \le 9$ $-7 \le k \le 9$ $-24 \le l \le 23$
Reflections collected	5168
Unique reflections	2299
Observed reflections (>2σ(I))	1890
R_{int}	0.0169
Completeness to θ, %	25.00°, 99.8
Absorption correction	Multi-scan (SADABS; Bruker, 2000) T_{min} = 0.922, T_{max} = 0.923
Refinement	
Refinement method	Full-matrix least-squares on F^2
Data / restraints / parameters	2299 / 0 / 223
Calculated weights, *w*	$1/[\sigma^2(F_o^2) + (0.0378P)^2 + 0.3138P]$ where $P = (F_o^2 + 2F_c^2)/3$
Goodness-of-fit on F^2	1.051
Final R indices [I > 2σ(I)]	R_1 = 0.0356, wR_2 = 0.0843
R indices (all data)	R_1 = 0.0456, wR_2 = 0.0909
Largest diff. peak and hole	0.169 and -0.199 e.Å^{-3}

Table. 5.A.6. Selected bond lengths (Å), bond angles (°) and torsion angles (°) for (**4m**)

Bond lengths (Å)			
O(1)–N(1)	1.3798(18)	O(2)–N(2)	1.3716(18)
C(1)–C(8)	1.460(2)	C(9)–C(10)	1.356(2)
Torsion angles (°)			
N(1)–C(8)–C(1)–C(6)	46.1(3)	N(2)–C(8)–C(1)–C(2)	42.9(3)

Table 5.A.7. Hydrogen bonded geometries in (**4m**)

Bond	D - H	H···A	D···A	D - H···A
O(1)–H(1)···Cl(1)^{i}	0.88(3)	2.10(3)	2.9732(16)	172(2)
O(2)–H(2A)···Cl(1)^{ii}	1.00(3)	1.95(3)	2.9393(14)	170(2)

Symmetry codes: (i) -1+x, y, z; (iii) 3/2-x, 1/2+y, 1/2-z

Table 5.A.8 X–H···*Cg* interactions in (**4m**)

X–H···*Cg*	H···*Cg*	H_{perp}	γ	X–H···*Cg*	X···*Cg*
C(12)–H(12B)···*Cg*(2)^{iii}	2.93(2)	2.92	4.19	133.2(18)	3.669(2)

Symmetry codes: (iii) 1/2-x, -1/2+y, 1/2-z
Note: *Cg*2 is the centroid of the C1–C6 ring.

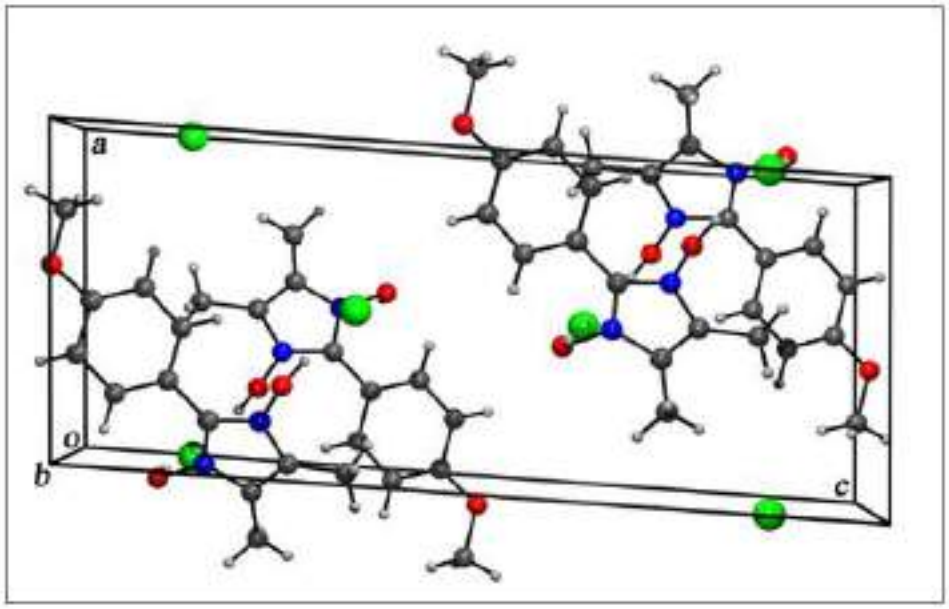

Fig. 5.A.8. The molecular arrangement of **4m** in the *ac* plane

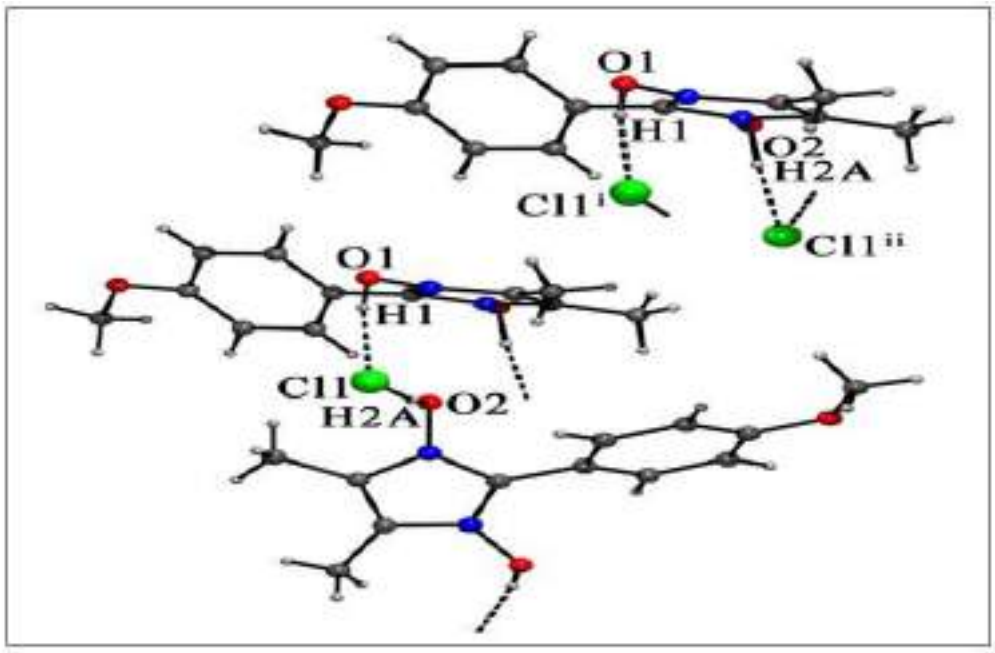

Fig. 5.A.9. Hydrogen bonding interaction in 4m, (dotted lines indicate the interionic C–H···Cl interactions in **4m).**

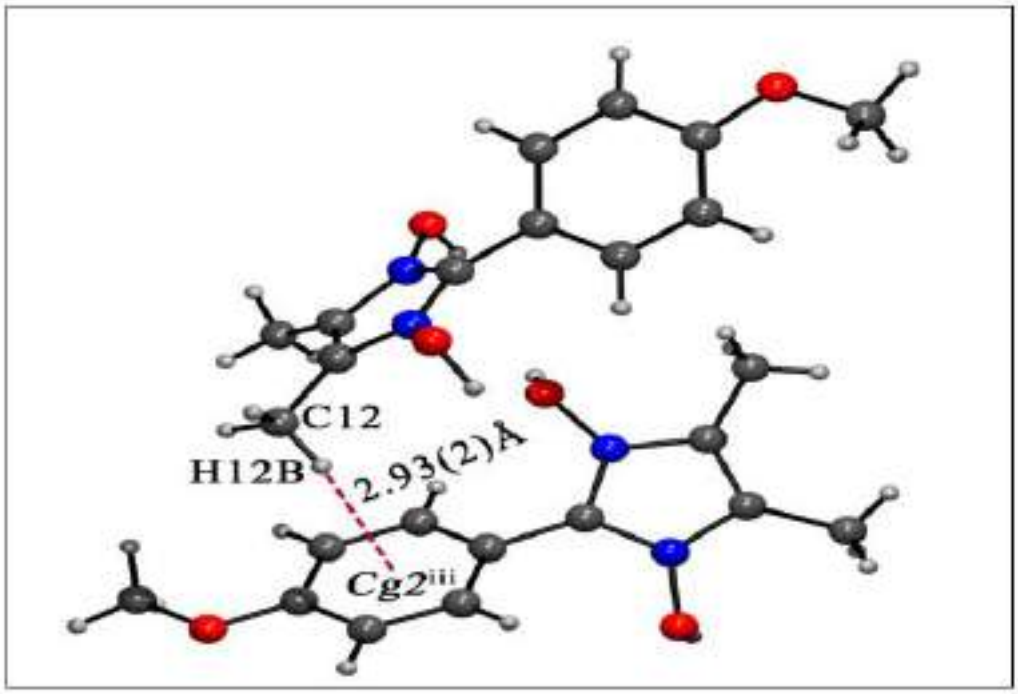

Fig. 5.A.10. C–H···Cg interaction in the cationic unit of **4m (**Dotted line indicates the C–H···Cg interaction)

Thus, it is evident from the crystallography study that the title compound 4m exist as a 1,3-dihydroxy form in the solid state and more work towards the understanding of the tautomeric form of 1-hydroxy-2-arylimidazole3-oxide is under progress in our laboratory.

5.A.3 Experimental section

5.A.3.1 Materials and methods:

All starting materials of high purity for the desired synthesis were purchased commercially and used as received. The FT-IR spectra of the prepared compounds were recorded in Bruker Alpha III spectrophotometer operating in the wave number region 4000 to 400 cm^{-1} in dry KBr. The melting points of the synthesized compounds were determined by open capillary method. ^{1}HNMR of the synthesized 1-hydroxy-2arylimidazole-3-oxide derivatives were recorded at room temperature on a FT-IR (Bruker Advance-II 400 MHz) spectrometer by using DMSO-d_6 as solvents and chemical shifts are quoted in ppm downfield of internal standard tetramethyl silane (TMS).X-ray single crystal study of 1,3-dihydroxy-2-(4-methoxyphenyl)-4,5-dimethyl-1*H*-imidazol-3-ium chloride (4m), was recorded on a Bruker SMART-APEX CCD diffractometer and the Diffraction data was collected using monochromatic Mo Kα radiation (λ = 0.71073 Å) with the ω and φ scan technique. The unit cell was determined using Bruker SMART, the diffraction data were integrated with Bruker SAINT system and the data were corrected for absorption using SADABS[34]. The structure was solved by direct method and was refined by full matrix least squares based on F^2 using SHELXL 97[35]. All the H atoms were localized from the difference electron-density map and refined isotropically. ORTEP-plot and packing diagram were generated with ORTEP-3 for Windows[36] and PLATON[37]. WinGX[38-39] was used to prepare the material for publication.

5.A.3.2 General procedure for the synthesis of 1-hydroxy-imidazole-3-oxide derivatives (4a-4m):

In a typical green procedure, a mixture of diacetyl monoxime (1 mmol), substituted benzaldehyde (1 mmol), hydroxylamine hydrochloride (2.5 mmol) and copper borate (2.5 mmol) were thoroughly ground and mixed in a mortar and pestle to make a homogeneous mixture. The mixture was then transferred to a test tube. The reaction was heated at 100°C for 10 minutes. The progress of the reaction was monitored by TLC using hexane/ethyl acetate (80:20) solvent. After completion of the reaction, the reaction mixture was dissolved in methanol and filtered. The filtrate was evaporated under vacuum and subsequently dried to afford the desired product. All the synthesized products (4a-4m) were recrystallized from ethanol and have been characterized by their analytical (yield and melting point) and spectroscopic data (FT-IR and ^{1}HNMR) and compared with the literature value.

5.A.3.2 Crystallization procedure for compound 4m

The compound 4m after recrystallized from ethanol were further dissolved in aqueous ethanol solution (20:80) and the solution was left for evaporation at room temperature. After 5 days a pale white needle shaped crystals were start appearing in the solution. After seven days, we obtained the crystals of compound 4m suitable for single crystal x-ray diffraction study.

5.A.4 Analytical and Spectroscopic data

5.A.4.1 1-hydroxy-2-phenyl-4,5-dimethylimidazole-3-oxide (4a): white solid, yield= 97 %, melting point found (^{0}C) = 155-157, IR (KBr, cm^{-1}) υ_{max}:3441 (br, OH), 3054, 3039 (C-H, Aromatic), 2969, 2927 (C-H, Aliphatic), 2231, 1713, 1639, 1545 (C=C), 1602, 1582 (C=N), 1347, 1253, 815, ^{1}HNMR (400 MHz, DMSO d_6): δppm = 12.68 (S, 1H, OH), 6.81-7.69 3.15 (S, 3H, CH_3), 2.31 (s, 3H, CH_3).

5.A.4.2 1-hydroxy-2-(3-nitrophenyl)-4,5-dimethylimidazole-3-oxide (4b): Pale yellow solid, yield= 98 %, melting point found (^{0}C) = 208-211, IR (KBr, cm^{-1}) υ_{max}:3442 (br, OH), 3060 (C-H, Aromatic), 2974, 2926 (C-H, Aliphatic), 1657 (C=C), 1625, 1610 (C=N), 1394, 1267, 833, ^{1}HNMR (400 MHz, DMSO d_6): δppm = 11.65 (S, 1H, OH), 7.66-8.40 (m, 4H, Ar-H), 3.36 (S, 3H, CH_3), 1.96 (s, 3H, CH_3).

5.A.4.3 1-hydroxy-2-(4-fluorophenyl)-4,5-dimethylimidazole-3-oxide (4c): Pale white solid, yield= 98 %, , IR (KBr, cm^{-1}) υ_{max}:3424 (br, OH), 3062 (C-H, Aromatic), 2984, 2926 (C-H, Aliphatic), 1632 (C=C), 1550, 1487 (C=N), 1391, 1257, 839, ^{1}HNMR (400 MHz, DMSO d_6): δppm = 11.00 (S, 1H, OH), 7.07-7.80 (m, 4H, Ar-H), 3.34 (S, 3H, CH_3), 2.24 (s, 3H, CH_3).

5.A.4.4 1-hydroxy-2-(3-hydroxyphenyl)-4,5-dimethylimidazole-3-oxide (4d): Pale white solid, yield= 95 %, IR (KBr, cm^{-1}) υ_{max}:3430 (br, OH), 3298, 3051 (C-H, Aromatic), 2995, 2962 (C-H, Aliphatic), 1627 (C=C), 1602, 1545 (C=N), 1334, 1243, 854, ^{1}HNMR (400 MHz, DMSO d_6): δppm = 11.37 (s, 1H, OH), 9.99 (s, 1H, OH), 7.40-7.46 (m, 4H, Ar-H), 3.35 (s, 3H, CH_3), 1.96 (s, 3H, CH_3).

5.A.4.5 1-hydroxy-2-(2,4-dihydroxyphenyl)-4,5-dimethylimidazole-3-oxide (4e): Pale brown, yield= 93 %, IR (KBr, cm^{-1}) υ_{max}:3549, 3452 (br, OH), 3288, 3112 (C-H, Aromatic), 2972, 2930 (C-H, Aliphatic), 1718, 1677 (C=C), 1618

(C=N), 1364, 1257, 810, ^{1}HNMR (400 MHz, DMSO d_6): δppm = 13.57 (s, 1H, OH), 11.48 (s, 1H, OH), 11.37 (s, 1H, OH), 6.79-7.70 (m, 3H, Ar-H), 3.34 (S, 3H, CH_3), 2.21 (s, 3H, CH_3).

5.A.4.6 1-hydroxy-2-(2-hydroxyphenyl)-4,5-dimethylimidazole-3-oxide (4f): Dirty white, yield= 94 %, IR (KBr, cm^{-1}) υ_{max}: 3430 (br, OH), 3098, 3064 (C-H, Aromatic), 2958, 2927 (C-H, Aliphatic), 1658, 1640 (C=C), 1615, 1542 (C=N), 1343, 1260, 832, ^{1}HNMR (400 MHz, DMSO d_6): δppm = 12.16 (s, 1H, OH), 9.87 (s, 1H, OH), 6.87-7.67 (m, 4H, Ar-H), 3.26 (s, 3H, CH_3), 2.42 (s, 3H, CH_3).

5.A.4.7 1-hydroxy-2-(4-hydroxyphenyl)-4,5-dimethylimidazole-3-oxide (4g): white flakes yield= 94 %, melting point found (^{0}C) = 165-168, IR (KBr, cm^{-1}) υ_{max}: 3400 (br, OH), 3000 (C-H, Aromatic), 2671 (C-H, Aliphatic), 1611 (C=C), 1560 (C=N), 1382, 1252, 837, ^{1}HNMR (400 MHz, DMSO d_6): δppm = 11.32 (s, 1H, OH), 9.88 (s, 1H, OH), 7.04-7.86 (m, 4H, Ar-H), 2.27 (s, 3H, CH_3), 2.19 (s, 3H, CH_3).

5.A.4.8 1-hydroxy-2-(5-chloro-2-hydroxyphenyl)-4,5-dimethylimidazole-3-oxide (4h): Pale yellow solid yield= 96%, IR (KBr, cm^{-1}) υ_{max}: 3416 (br, OH), 3212, 3136, 3053 (C-H, Aromatic), 2929, 2855 (C-H, Aliphatic), 1691, 1630 (C=C), 1572 (C=N), 1381, 1261, 815, ^{1}HNMR (400 MHz, DMSO d_6): δppm = 13.49 (s, 1H, OH), 10.29 (s, 1H, OH), 7.03-7.70 (m, 3H, Ar-H), 3.34 (s, 3H, CH_3), 2.50 (s, 3H, CH_3).

5.A.4.9 1-hydroxy-2-(5-bromo-2-hydroxyphenyl)-4,5-dimethylimidazole-3-oxide (4i): Pale yellow solid yield= 95%, IR (KBr, cm^{-1}) υ_{max}: 3417 (br, OH), 3059, 3027 (C-H, Aromatic), 2924, 2853 (C-H, Aliphatic), 1658 (C=C), 1602, 1580 (C=N), 1384, 1252, 828, ^{1}HNMR (400 MHz, DMSO d_6): δppm = 11.48 (s, 1H, OH), 10.31 (s, 1H, OH), 6.83-7.63 (m, 3H, Ar-H), 3.32 (s, 3H, CH_3), 1.91 (s, 3H, CH_3).

5.A.4.10 1-hydroxy-2-(2-hydroxy-3-methoxyphenyl)-4,5-dimethylimidazole-3-oxide (4j): white solid, yield= 95%, IR (KBr, cm^{-1}) υ_{max}: 3335 (br, OH), 3097, 3065 (C-H, Aromatic), 2929, 2837 (C-H, Aliphatic), 1625 (C=C), 1578 (C=N), 1366, 1246, 839, ^{1}HNMR (400 MHz, DMSO d_6): δppm = 12.87 (s, 1H, OH), 11.38 (s, 1H, OH), 6.87-7.17 (m, 3H, Ar-H), 3.81 (s, 3H, OCH_3), 2.43 (s, 3H, CH_3), 2.18 (s, 3H, CH_3).

5.A.4.11 1-hydroxy-2-(4-hydroxy-3-methoxyphenyl)-4,5-dimethylimidazole-3-oxide (4k): white solid, yield= 94%, melting point found (^{0}C) = 200-202, IR (KBr,

cm^{-1}) υ_{max}: 3389 (br, OH), 3076 (C-H, Aromatic), 2928 (C-H, Aliphatic), 1636 (C=C), 1596 (C=N), 1388, 1279, 856, ^{1}HNMR (400 MHz, DMSO d_6): δppm = 12.65 (s, 1H, OH), 10.35 (s, 1H, OH), 6.64-8.52 (m, 3H, Ar-H), 3.76 (s, 3H, OCH_3), 2.35 (s, 3H, CH_3), 2.10 (s, 3H, CH_3).

5.A.4.12 1-hydroxy-2-(3,4,5-methoxyphenyl)-4,5-dimethylimidazole-3-oxide (4l): white solid, yield= 94%, IR (KBr, cm^{-1}) υ_{max}: 3424 (br, OH), 3001 (C-H, Aromatic), 2930, 2836 (C-H, Aliphatic), 1732, 1632 (C=C), 1586, 1534 (C=N), 1364, 1246, ^{1}HNMR (400 MHz, DMSO d_6): δppm = 11.37 (s, 1H, OH), 7.33 (s, 2H, Ar-H), 3.78 (s, 6H, OCH_3), 3.33 (s, 3H, OCH_3), 2.49 (s, 3H, CH_3), 1.37 (s, 3H, CH_3).

5.A.4.13 1-hydroxy-2-(4-methoxyphenyl)-4,5-dimethylimidazole-3-oxide (4m): white solid, yield= 93%, melting point found (^{0}C) = 196-198, IR (KBr, cm^{-1}) υ_{max}: 3418 (br, OH), 3003 (C-H, Aromatic), 2929 (C-H, Aliphatic), 1610, 1541 (C=N), 1380, 1256, 837 ^{1}HNMR (400 MHz, DMSO d_6): δppm = 10.95 (s, 1H, OH), 8.12 (d, 2H, Ar-H), 3.78 (s, 3H, OCH_3), 1.83 (s, 6H, CH_3).

5.A.5 Supporting spectra

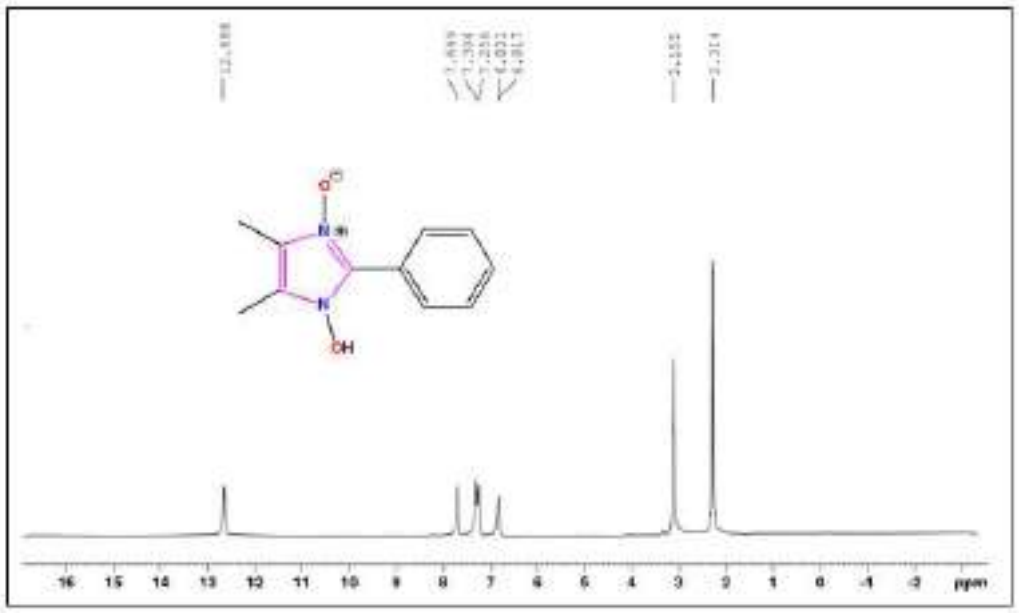

Fig. 5.A.5.1. ^{1}H NMR spectra of 1-hydroxy-2-phenyl-4,5-dimethylimidazole-3-oxide (4a)

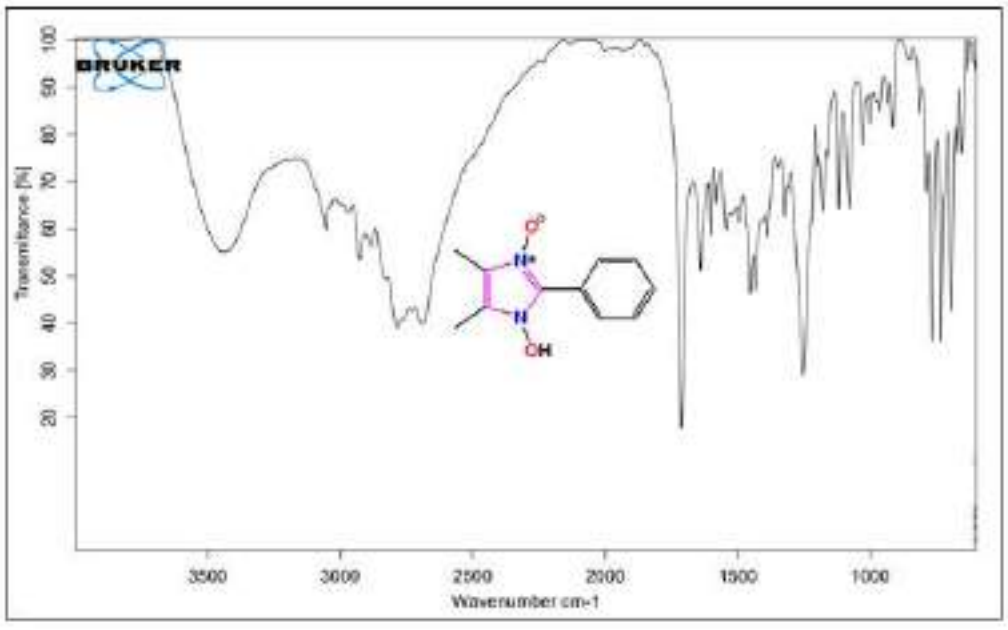

Fig. 5.A.5.2. FT-IR spectra of 1-hydroxy-2-phenyl-4,5-dimethylimidazole-3-oxide (4a)

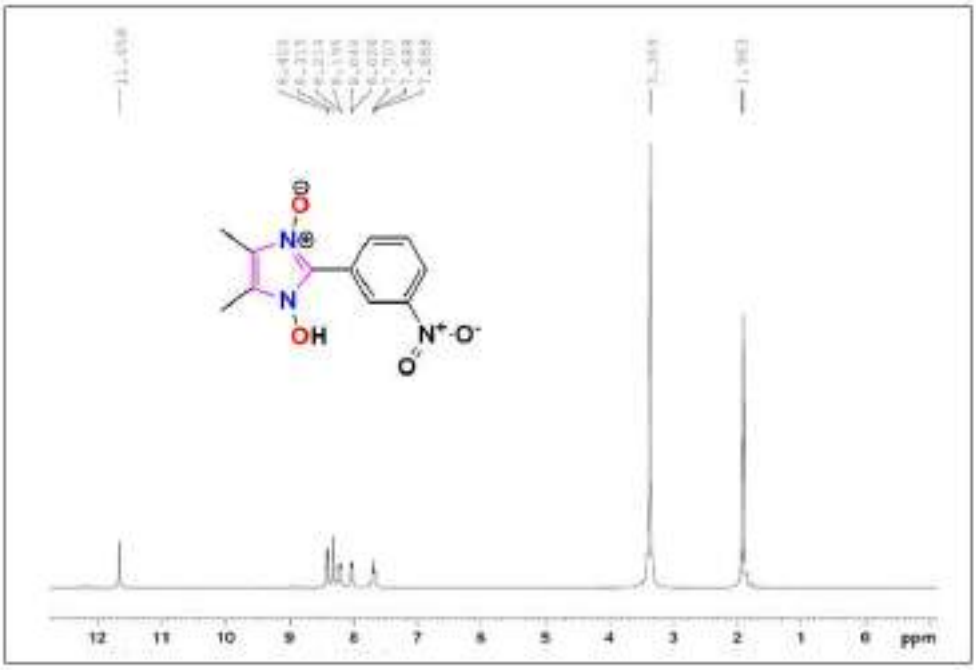

Fig. 5.A.5.3. ^{1}H NMR spectra of 1-hydroxy-2(3-nitrophenyl)-4,5-dimethylimidazole-3-oxide (4b)

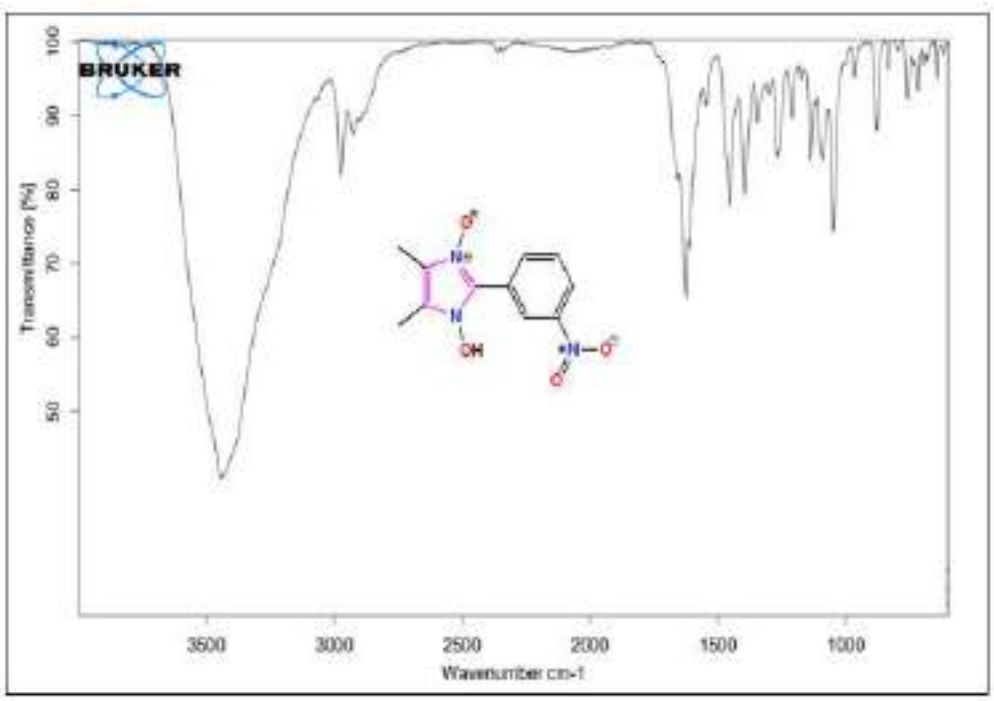

Fig. 5.A.5.4. FT-IR spectra of -hydroxy-2(3-nitrophenyl)-4,5-dimethylimidazole-3-oxide (4b)

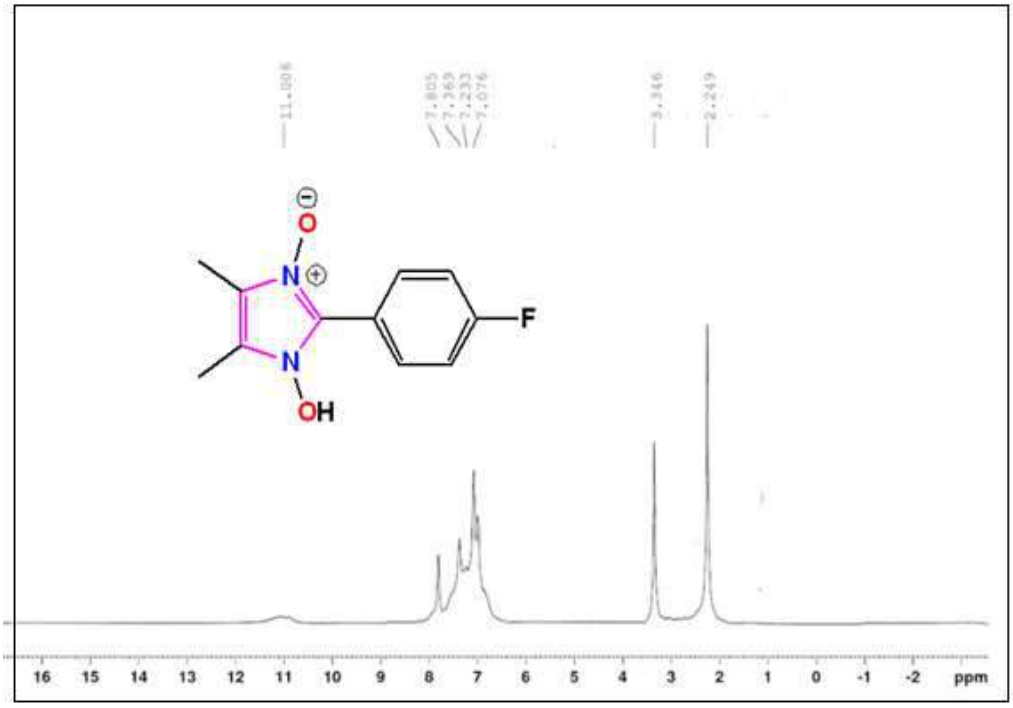

Fig. 5.A.5.5. [1]HNMR spectra of 1-hydroxy-2(4-fluorophenyl)-4, 5-dimethylimidazole-3-oxide (4c)

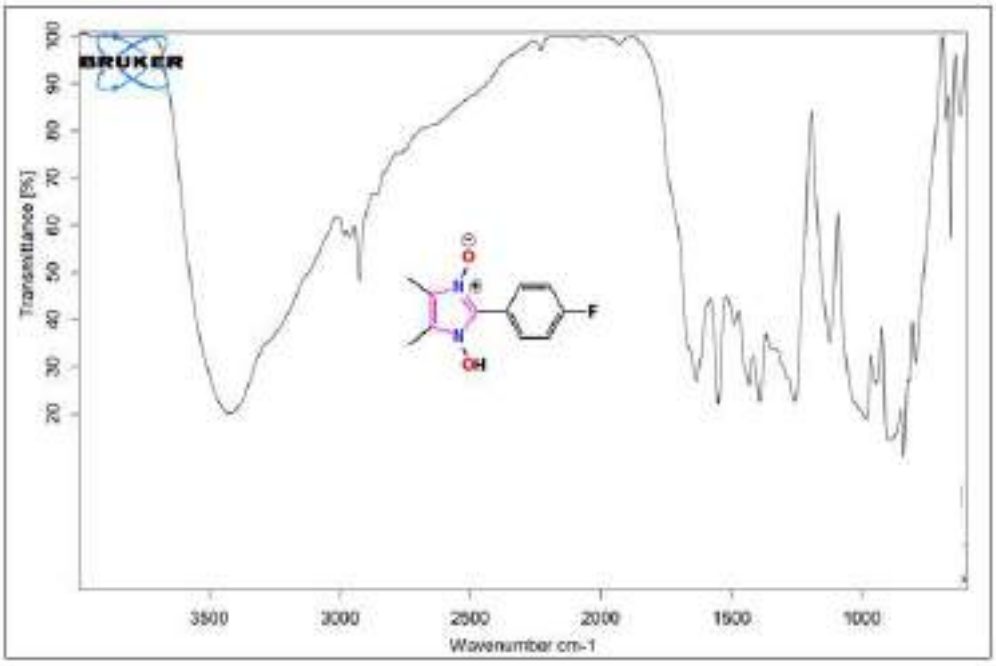

Fig. 5.A.5.6. FT-IR spectra of -hydroxy-2(4-fluorophenyl)-4,5-dimethylimidazole-3-oxide (4c)

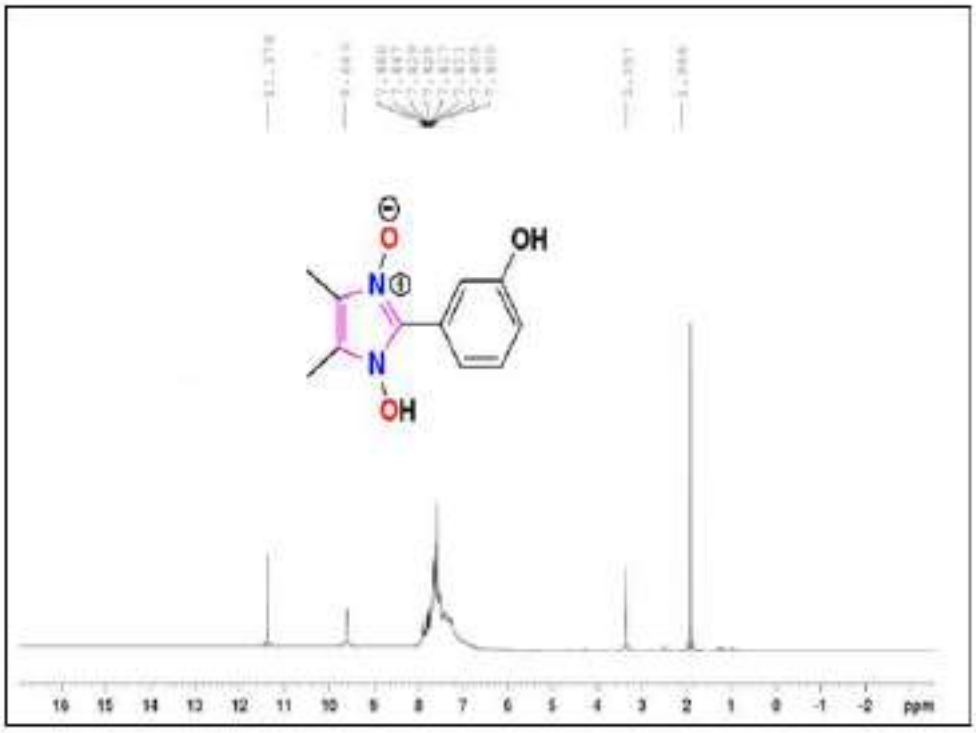

Fig. 5.A.5.7.[1]HNMR spectra of 1-hydroxy-2(3-hydroxyphenyl)-4, 5-dimethylimidazole-3- oxide (4d).

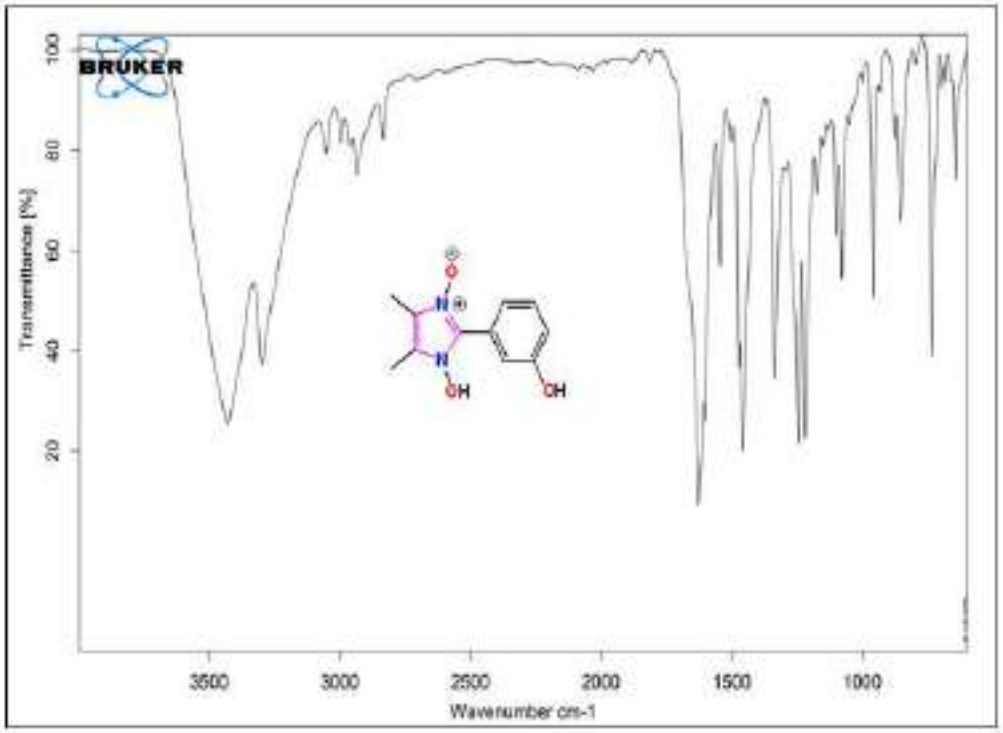

Fig. 5.A.5.8. FT-IR spectra of -hydroxy-2(3-hydroxyphenyl)-4,5-dimethylimidazole-3-oxide (4d)

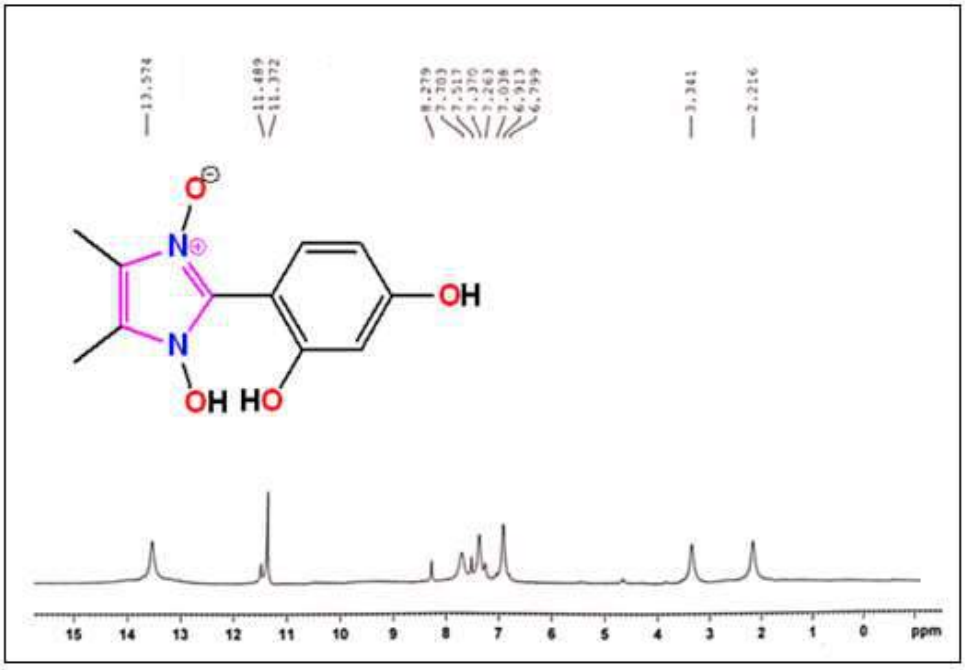

Fig. 5.A.9.[1]HNMR spectra of 1-hydroxy-2(2, 4-dihydroxyphenyl)-4, 5-dimethylimidazole-3- oxide (4e).

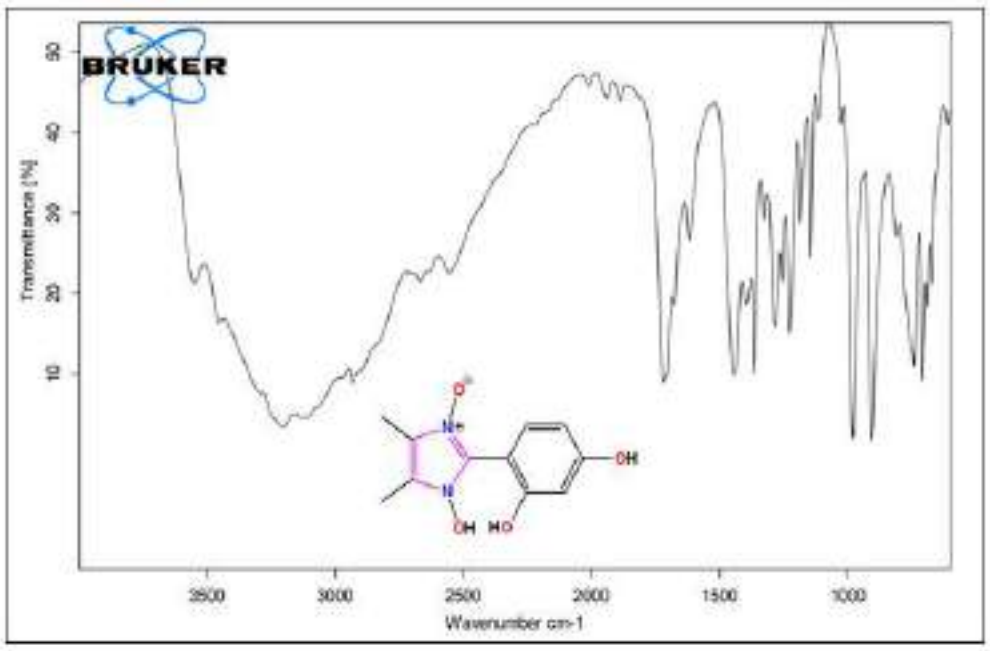

Fig. 5.A.5.10. FT-IR spectra of 1-hydroxy-2(2, 4-dihydroxyphenyl)-4, 5-dimethylimidazole-3- oxide (4e).

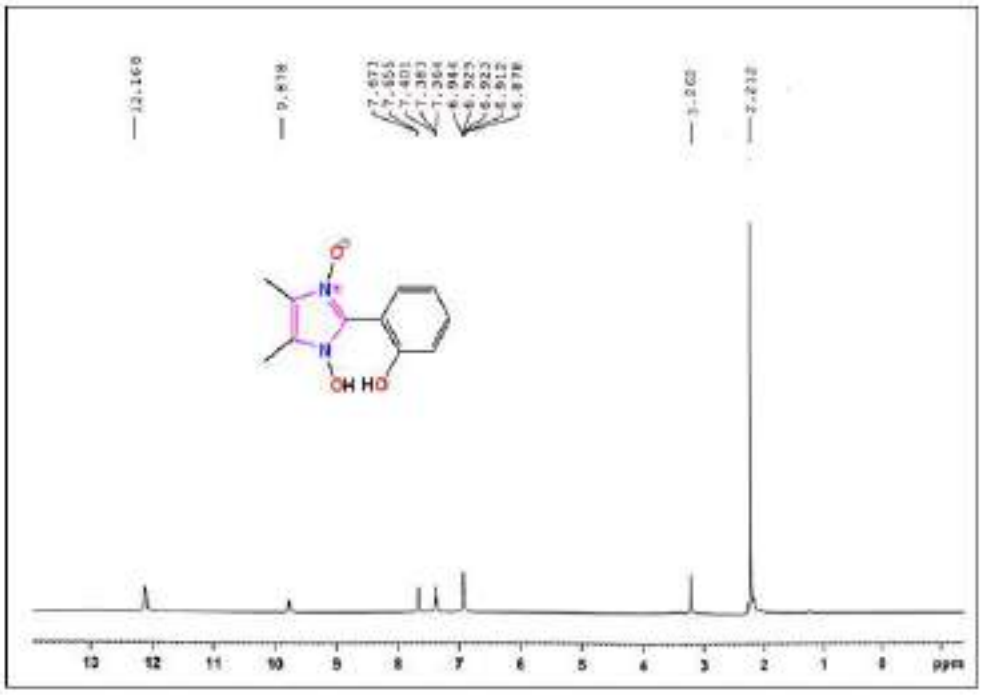

Fig. 5.A.11.[1]HNMR spectra of 1-hydroxy-2(2-hydroxyphenyl)-4, 5-dimethylimidazole-3- oxide (4f).

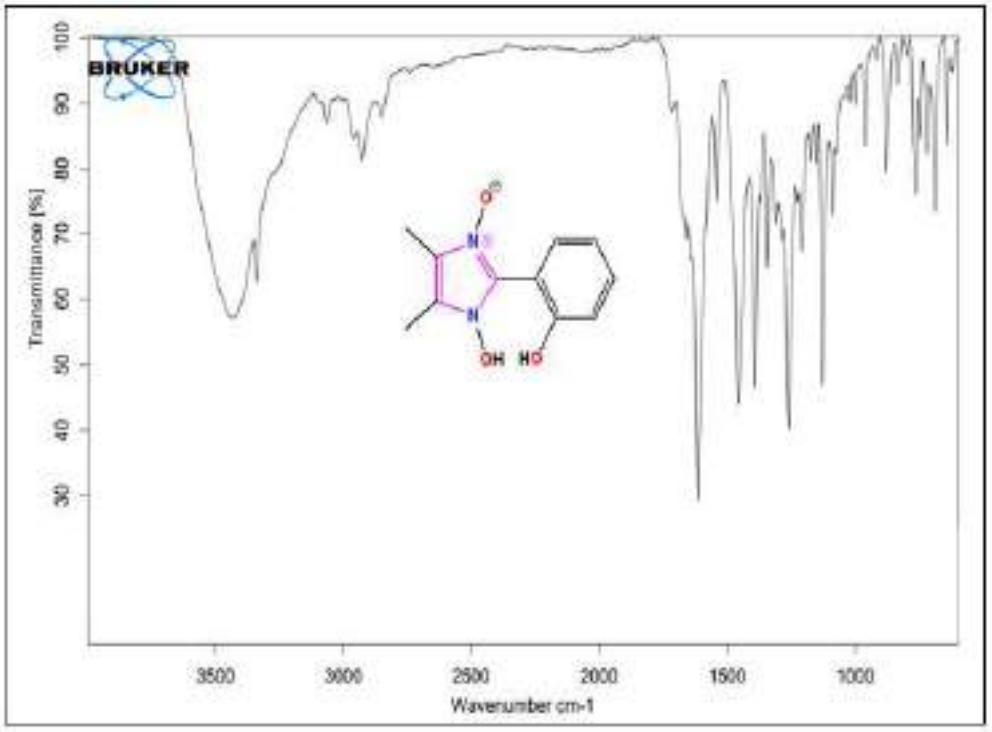

Fig. 5.A.5.12. FT-IR spectra of 1-hydroxy-2(2-hydroxyphenyl)-4, 5-dimethylimidazole-3- oxide (4f).

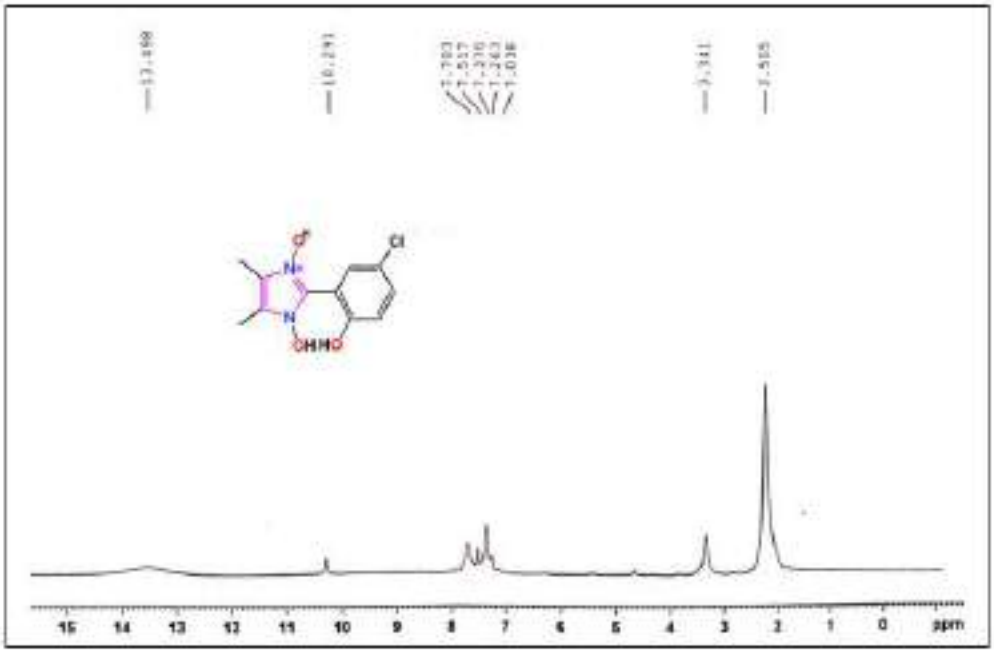

Fig. 5.A.5.13.[1]HNMR spectra of 1-hydroxy-2(5-chloro-2-hydroxyphenyl)-4, 5-dimethylimidazole-3- oxide (4h).

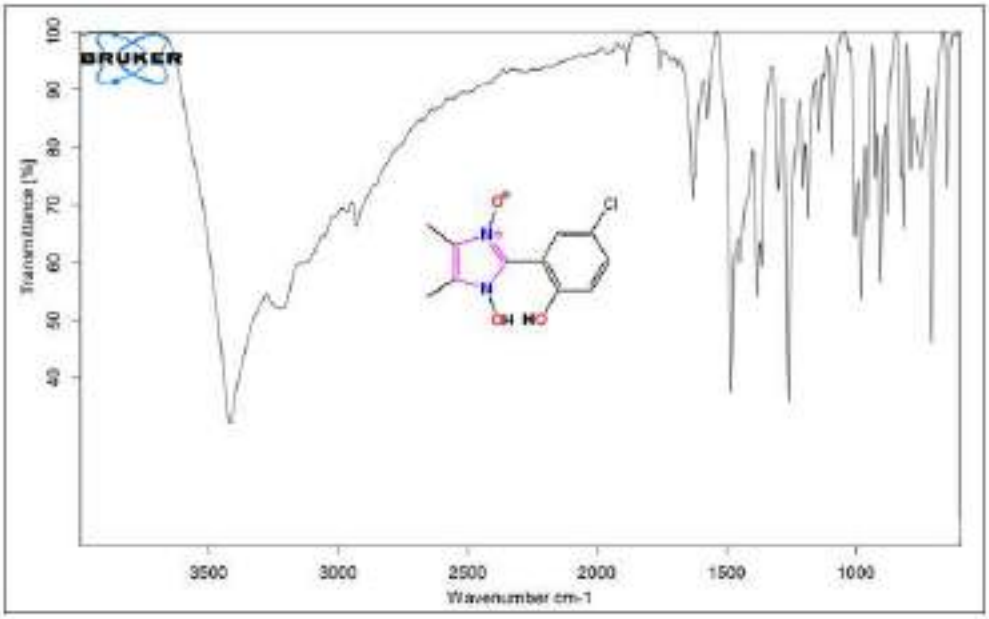

Fig. 5.A.5.14. FT-IR spectra of 1-hydroxy-2(5-chloro-2-hydroxyphenyl)-4, 5-dimethylimidazole-3- oxide (4h).

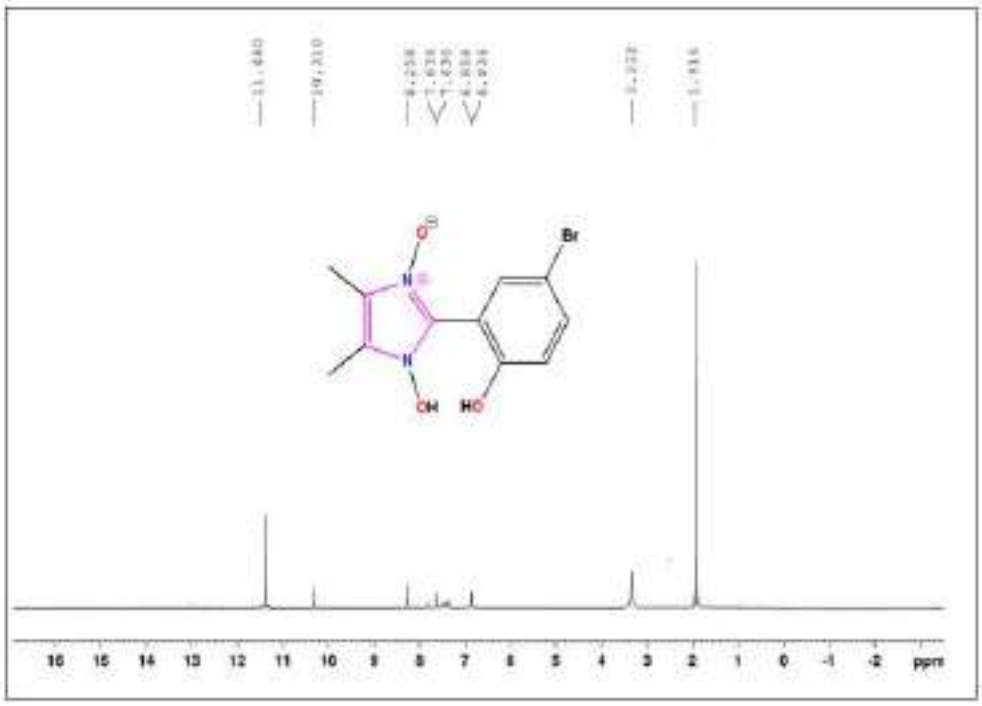

Fig. 5.A.5.15.[1]HNMR spectra of 1-hydroxy-2(5-bromo-2-hydroxyphenyl)-4, 5-dimethylimidazole-3- oxide (4i).

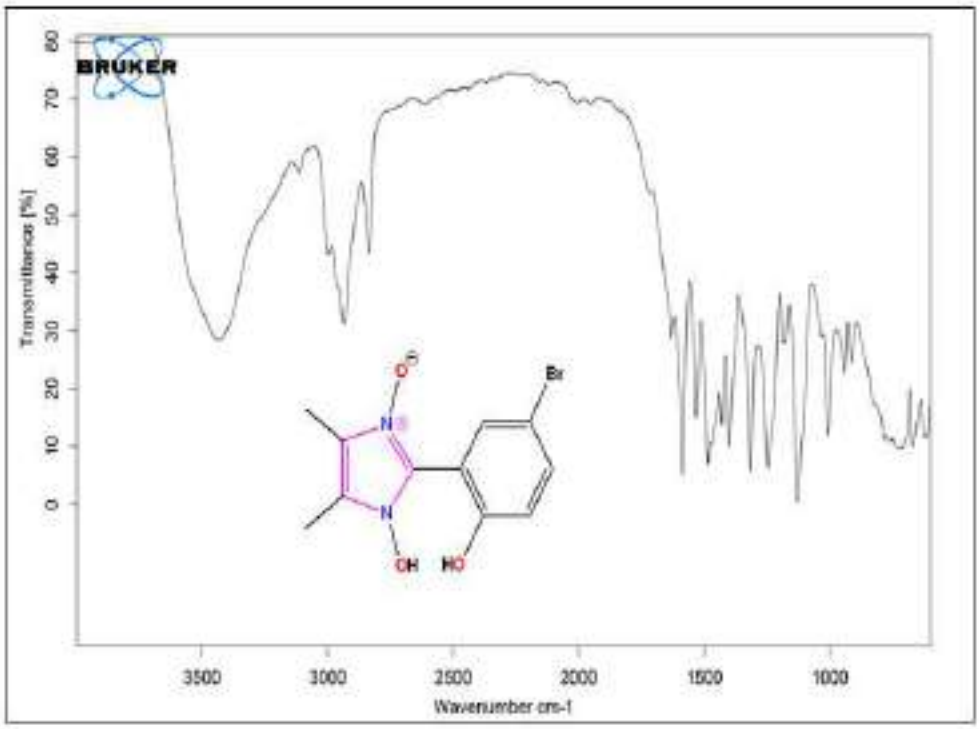

Fig. 5.A.5.16. FT-IR spectra of 1-hydroxy-2(5-bromo-2-hydroxyphenyl)-4, 5-dimethylimidazole-3- oxide (4i).

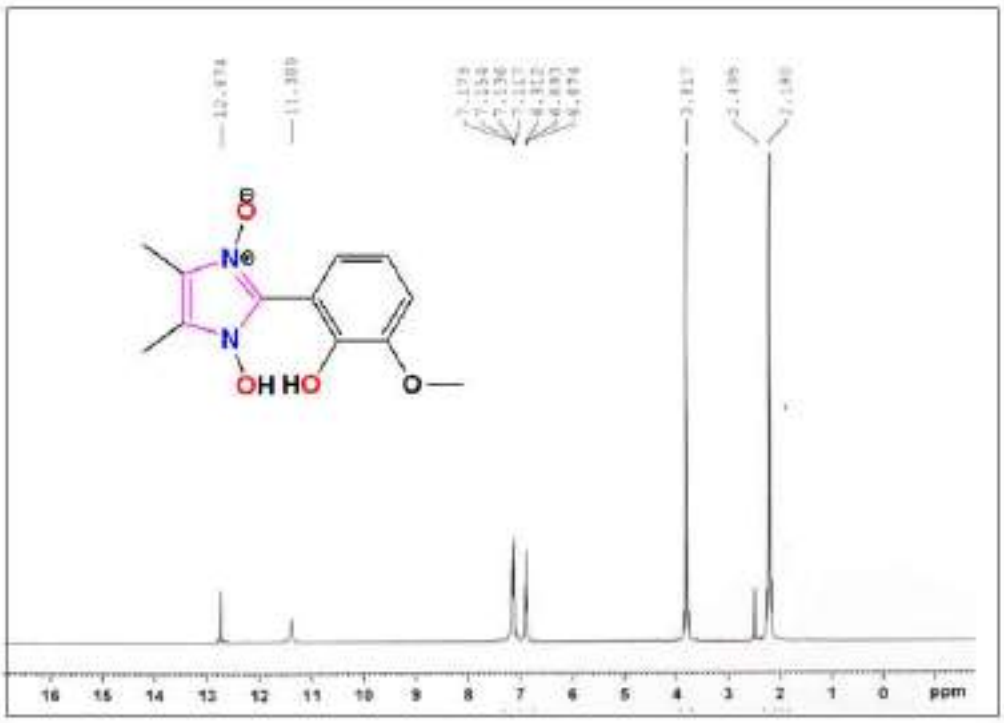

Fig. 5.A.5.17.[1]HNMR spectra of 1-hydroxy-2(2-hydroxy-3-methoxyphenyl)-4, 5-dimethylimidazole-3- oxide (4j).

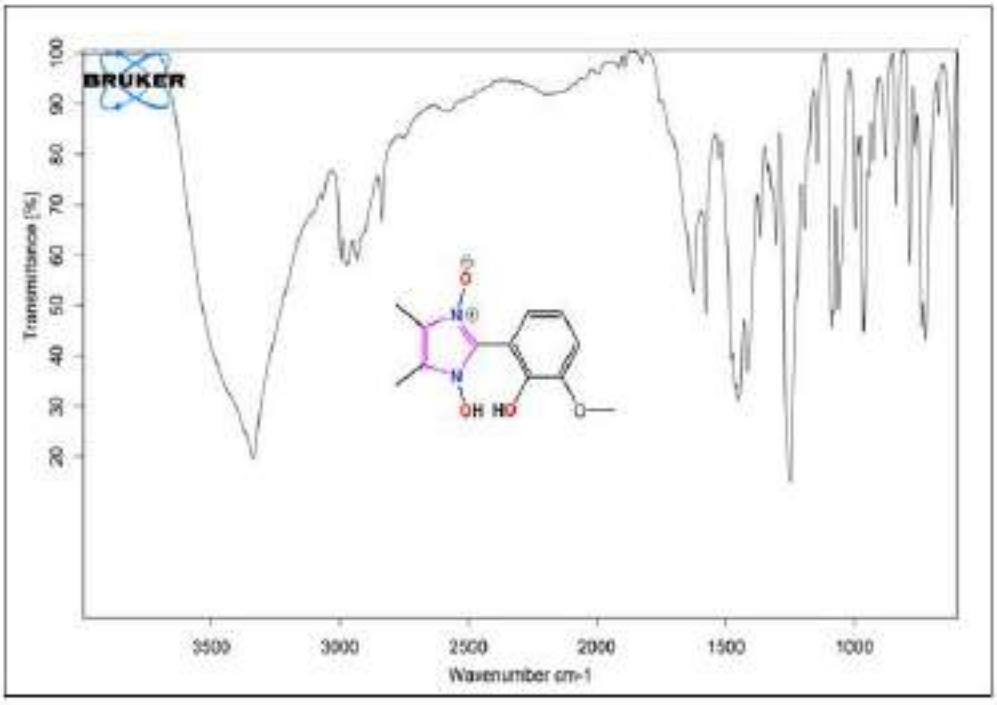

Fig. 5.A.5.18. FT-IR spectra of 1-hydroxy-2(2-hydrox-3-methoxyyphenyl)-4, 5-dimethylimidazole-3- oxide (4j).

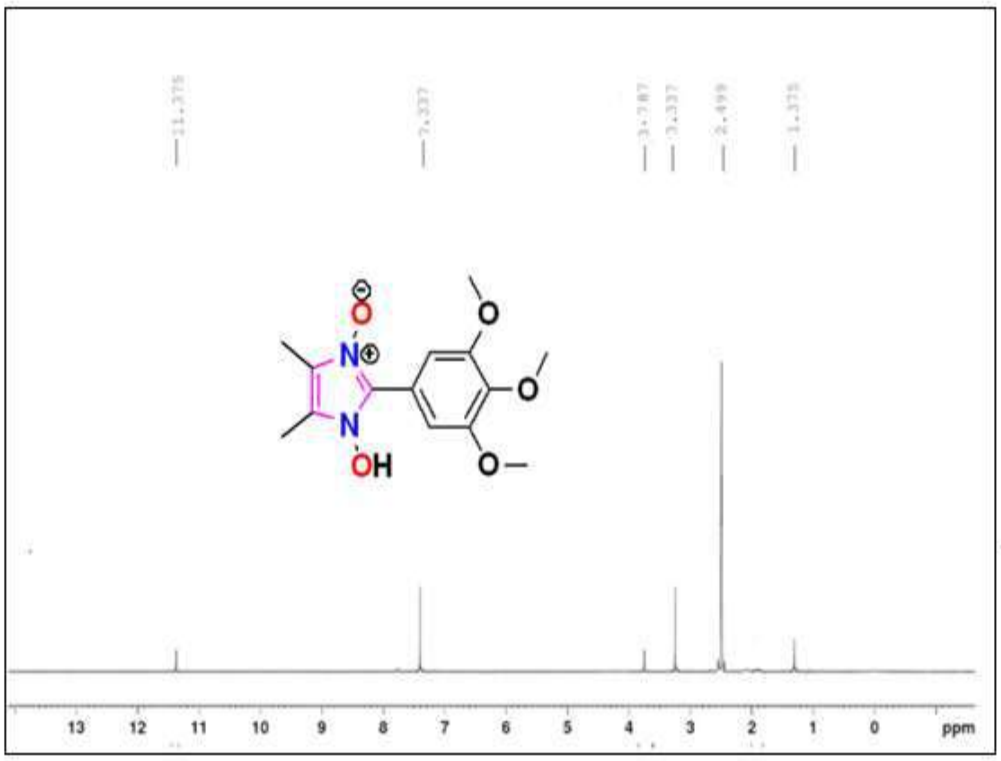

Fig. 5.A.5.19. [1]HNMR spectra of 1-hydroxy-2(3, 4, 5-tri-methoxyphenyl)-4, 5-dimethylimidazole-3- oxide (4l).

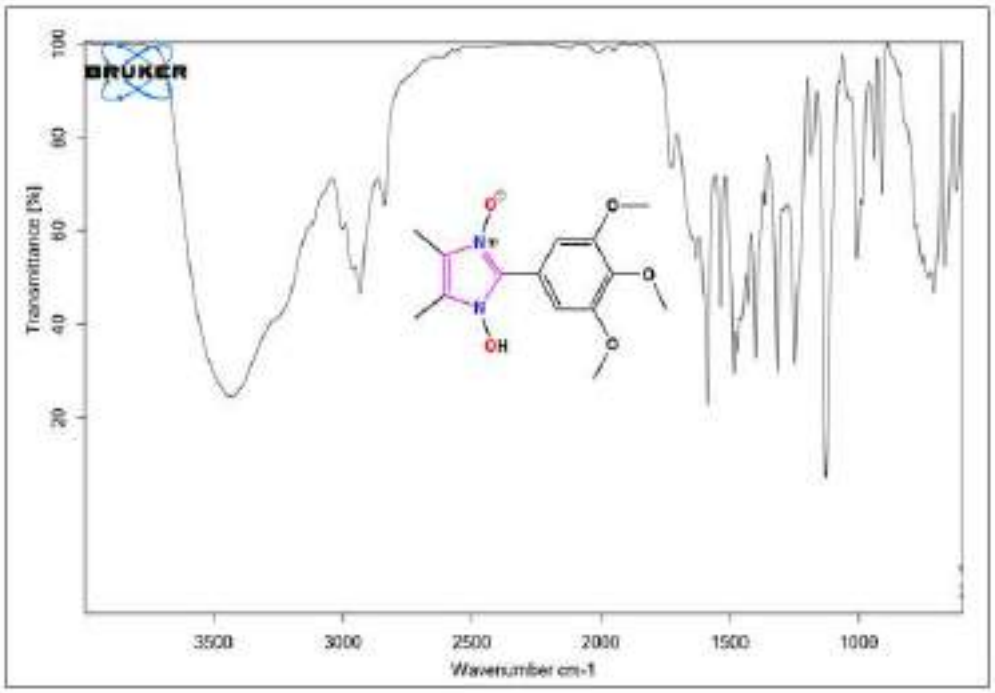

Fig. 5.A.5.20. FT-IR spectra of 1-hydroxy-2(3, 4, 5-tri-methoxyyphenyl)-4, 5-dimethylimidazole-3- oxide (4l).

5.A.6 References

(1) H. Brahmbhatt, M. Molnar, V. Pavić., *Karbala International Journal of Modern Science*, **2018**, *4* (2), 200–206.

(2) A. Verma, S. Joshi, D. Singh., *Journal of Chemistry*, **2013**, *2013* (Article ID 392412).

(3) P. Manocha, S. R. Wakode, A. Kaur, H. Kumar., *International Journal of Pharmaceutical Science and Research*, **2016**, *1* (7), 12–16.

(4) A. Reyes-Arellano, O. Gómez-García, J. Torres-Jaramillo., *Medicinal Chemistry*, **2016**, *6* (9), 561–566.

(5) D. H. Romero, V. E. T. Heredia, O. García-Barradas, Ma. E. M. López, E. S. Pavón., *Journal of Chemistry and Biochemistry*, **2014**, *2* (2), 45–83.

(6) K. Anand, S. Wakode., *International Journal of Chemical Studies*, **2017**, *5* (2), 350–362.

(7) B. K. Verma, S. Kapoor, U. Kumar, S. Pandey, P. Arya., *Indian Journal of Pharmaceutical and Biological Research*, **2017**, *5* (01), 1–9.

(8) M. W. Bhade, P. R. Rajput., *International Journal of Applied and Pure Science and Agriculture*, **2016**, *2* (11), 80–84.

(9) R. Katikireddy, R. Kakkerla, M. P. S. M. Krishna, G. Durgaiah, Y. N. Reddy, M. Satyanarayana., *Heterocyclic Communications*, **2019**, *25* (1), 27–38.

(10) A. Goyal, J. Singh, D. P. Pathak., *Journal of Pharmaceutical Technology, Research and Management*, **2013**, *1* (1), 69–79.

(11) D. R. MacFarlane, K. R. Seddon., *Australian Journal of Chemistry*, **2007**, *60* (1), 3–5.

(12) R. Rogers, G. Garau., *Materials world*, **2007**, *15* (12), 25–27.

(13) G. Laus, J. Sladlwieser, W. Klötzer., *Synthesis (Stuttg)*, **1989**, *1989* (10), 773–775.

(14) K. Hayes., *Journal of Heterocyclic Chemistry*, **1974**, *11* (4), 615–618.

(15) A. Albini, S. Pietra., *Heterocyclic N-Oxides*; CRC Press: Boca Raton, Ann Arbor, Boston USA, **1991**.

(16) A. Albini., *Synthesis (Stuttg)*, **1993**, *1993* (3), 263–277.

(17) Y. Wang, L. Zhang., *Synthesis (Stuttg)*, **2015**, *47* (03), 289–305.

(18) J. V. Quagliano, J. Fujita, G. Franz, D. J. Phillips, J. A. Walmsley, S. Y. Tyree., *J Am Chem Soc*, **1961**, *83* (18), 3770–3773.

(19) R. B. da Silva, V. B. Loback, K. Salomão, S. L. de Castro, J. L. Wardell, S. M. S. V. Wardell, T. E. M. M. Costa, C. Penido, M. D. G. M. de Oliveira Henriques, S. A. Carvalho, E. F. da Silva, C. A. M. Fraga., *Molecules*, **2013**, *18* (3), 3445–3457.

(20) M. Witschel., *Bioorganic & Medicinal Chemistry*, **2009**, *17* (12), 4221–4229.

(21) T. B. Stensbøl, P. Uhlmann, S. Morel, B. L. Eriksen, J. Felding, H. Kromann, M. B. Hermit, J. R. Greenwood, H. Braüner-Osborne, U. Madsen, F. Junager, P. Krogsgaard-Larsen, M. Begtrup, P. Vedsø., *Journal of Medicinal Chemistry*, **2002**, *45* (1), 19–31.

(22) M. L. Richardson, K. A. Croughton, C. S. Matthews, M. F. G. Stevens., *Journal of Medicinal Chemistry*, **2004**, *47* (16), 4105–4108.

(23) O. K. Kim, L. K. Garrity-Ryan, V. J. Bartlett, M. C. Grier, A. K. Verma, G. Medjanis, J. E. Donatelli, A. B. Macone, S. K. Tanaka, S. B. Levy, M. N. Alekshun., *Journal of Medicinal Chemistry*, **2009**, *52* (18), 5626–5634.

(24) G. Mloston, M. Celeda, M. Jasinski, K. Urbaniak, P. J. Boratynski, P. R. Schreiner, H. Heimgartner., *Molecules*, **2019**, *24* (23), 4398.

(25) S. A. Amitina, A. Y. Tikhonov, I. A. Grigor'Ev, Y. V. Gatilov, B. A. Selivanov., *Chemistry of Heterocyclic Compounds*, **2009**, *45* (6), 691–697.

(26) F. J. Allan, G. G. Allan., *Chemistry & Industry*, **1964**, *44*, 1837–1837.

(27) P. A. Nikitina, L. G. Kuz'Mina, V. P. Perevalov, I. I. Tkach., *Tetrahedron*, **2013**, *69* (15), 3249–3256.

(28) P. A. Nikitina, A. S. Peregudov, T. Y. Koldaeva, L. G. Kuz'Mina, E. I. Adiulin, I. I. Tkach, V. P. Perevalov., *Tetrahedron*, **2015**, *71* (33), 5217–5228.

(29) K. Pradhan, B. K. Tiwary, M. Hossain, R. Chakraborty, A. K. Nanda., *RSC Advances*, **2016**, *6* (13), 10743–10749.

(30) S. Bartz, B. Blumenröder, A. Kern, J. Fleckenstein, S. Frohnapfel, J. Schatz, A. Wagner., *Zeitschrift fur Naturforschung*, **2009**, *64b* (6), 629–638.

(31) S. O. Chua, M. J. Cook, A. R. Katritzky., *Journal of the Chemical Society B: Physical Organic*, **1971**, 2350–2355.

(32) W. Schilf, L. Stefaniak, M. Witanowski, G. A. Webb., *Journal of Molecular Structure*, **1986**, *140* (3–4), 311–315.

(33) M. Boiani, H. Cerecetto, M. Gonzalez, O. E. Piro, E. E. Castellano., *Journal of Physical Chemistry A*, **2004**, *108* (51), 11241–11248.

(34) *SADABS, SMART and SAINT*; Bruker AXS Inc., Madison, Wisconsin, USA, **2000**.

(35) G. M. Sheldrick., *SHELXS-97 and SHELXL-97, Program for Crystal Structure Solution and Refinement*; University of Gottingen, Gottingen: Germany, **1997**.

(36) L. J. Farrugia., *Journal of Applied Crystallography*, **1997**, *30* (5), 565–565.

(37) A. L. Spek., *Acta Crystallographica*, **2009**, *D65* (2), 148–155.

(38) L. J. Farrugia., *Journal of Applied Crystallography*, **1999**, *32* (4), 837–838.

(39) L. J. Farrugia., *Journal of Applied Crystallography*, **2012**, *45* (4), 849–854.

CHAPTER-V

Section B

DFT, Molecular Docking and Pharmacokinetic study of some selected 1-hydroxy-2-arylimidazole-3-oxide derivatives

5.B.1 Background of the present investigation

The imidazole scaffold is an important moiety present in natural products and biologically active compounds[1-2]. Imidazole derivatives are present in various classes of anti-cancer, anti-diabetic, anti-viral and anti-diabetic drugs[3-4]. Apart from biological applications, imidazole derivatives also various other important properties like electroluminescence and hence can also be used in diodes[5]. Imidazole-3-oxide derivatives are important derivatives of imidazole compounds. These compounds have gained immense popularity due to their anti-protozoal[6], fungicidal, herbicidal, pesticidal[7], hypotensive properties[8], anti-tumor[9] and anti-viral[10] properties. Furthermore, these compounds are also used as intermediates in some organic reactions[11].

Theoretical studies based on quantum mechanics using computational methods is an emerging field of research for understanding mechanism, geometry and reaction pathways of organic molecules[12-13]. With the introduction of Computer Aided Drug Design (CADD), the process of drug designing taken a new dimension as this method reduces the time and is cost effective for drug design[14]. In order to understand the Thermodynamic properties and other important parameters like dipole moments, optical properties, vibration frequencies theoretically, DFT or Density Functional Theory is widely used[15-17] and the results obtained from DFT can be used for comparing with the experimental results.

5.B.2 Results and Discussion

5.B.2.1 Computational Study

The molecular geometry, molecular orbital (HOMO,LUMO), Non-linear Optical property (NLO), Global chemical descriptors and Molecular Electrostatic Potential (MEP) of the selected 1-hydroxy-2-arylimidazole-3-oxide derivatives namely, 1-hydroxy-2-(2-hydroxyphenyl)-4,5-dimethylimidazole-3-oxide(IMO-1), 1-hydroxy-2-(5-nitro-2-hydroxyphenyl)-4,5-dimethylimidazole-3-oxide(IMO-2), 1-hydroxy-2-(5-chloro-2-hydroxyphenyl)-4,5-dimethylimidazole-3-oxide(IMO-3), 1-hydroxy-2-(5-bromo-2-hydroxyphenyl)-4,5-dimethylimidazole-3-oxide(IMO-4), 1-hydroxy-2-(2,4-dihydroxyphenyl)-4,5-dimethylimidazole-3-oxide(NO-5) and 1-hydroxy-2-(2-hydroxy-3-methoxyphenyl)-4,5-dimethylimidazole-3-oxide(IMO-6) have been optimized by Density Functional Theory (DFT) using Becke's three-parameter hybrid method (B3) with Lee, Yang and Parr correlation functional methods (LYP) with B3LYP/631G+(d,2p) level of basis set[18-19]. All the

computational calculations were calculated by Gaussian 16, Revision A.03 programme package[20]and the results were visualized using GAUSSVIEW 6.0 software[21] on a hp-Z640 desktop P.C. with an Intel Xeon processor (Specifications: E5-2630 V4 @ 220GHz).

5.B.2.1.1 Optimization of Molecular Geometry

To the best of our knowledge, the X-Ray single crystal structure of only a few 1-hydroxy-2-arylimidazole-3-oxide derivatives have been reported so far, therefore, structure optimization using DFT method serves as a good alternative to ascertain the different geometrical parameters of the selected compounds under study. The geometrical parameters of the studied compounds (IMO-1 to IMO-6) were calculated by DFT assay using B3LYP/631G+(d,2p) level of basis set. The optimized gas phase molecular geometry of the compounds (IMO-1 to IMO-6) with atom labelling scheme is shown in Fig. 5.B.1 and Fig 5.B.2 and the structural parameters like bond lengths, bond angles and dihedral angles are listed in Table 5.B.1.

Form the Table 5.B.1, the dihedral angles C6-C5-C7-N9 and C6-C5-C7-N12 in IMO-1 are 34.178˚ and -143.86˚ respectively. In IMO-2, the dihedral angles, C6-C5-C7-N9 and C6-C5-C7-N12 are -32.60˚ and 149.34˚ respectively. In IMO-3, the dihedral angles, C7-C6-C8-N13 and C7-C6-C8-N10 are -144.14˚ and 33.96˚ respectively. In IMO-4, the dihedral angles, C7-C6-C8-N13 and C7-C6-C8-N10 are -144.099˚ and 33.98˚ respectively. In IMO-5, the dihedral angles, C9-C8-C5-N4 and C9-C8-C5-N1 are -33.67˚ and 148.31˚ respectively. Finally for IMO-6, dihedral angles, C6-C5-C7-N9 and C6-C5-C7-N12 are -145.62˚ and 36.132˚ respectively. Therefore, from the analysis of the dihedral angles it is evident that the phenyl ring 2 is not planar with the imidazole ring 1. From the Table 5.B.1, it is seen that the C-N bond lengths of imidazole ring in all the studied compoundsIMO-1, IMO-3 and IMO-4 namely C8-N10, C8-N13, C11-N10 and C11-N13 are 1.351 Å, 1.374 Å, 1.391 Å and 1.380 Å respectively. For the compounds IMO-2 and IMO-6, the C-N bond lengths, namely C7-N9, C7-N12, C10-N9 and C10-N12 are in the range 1.350 Å, 1.374 Å, 1.389-1.391 Å and 1.380-1.381 Å respectively. For the compound IMO-5, the C-N bond lengths namely, C5-N1, C5-N4, C2-N1 and C3-N4 are 1.350 Å, 1.374 Å, 1.391 Å and 1.382 Å respectively. The shortening of the C-N bond lengths reveals the effect of resonance in this part of the molecule and this can be attributed to the difference in hybridization state of different carbon atoms in the imidazole ring[22].

Table. 5.B.1. Structural parameters (bond lengths, bond angle and dihedral angle) of the studied compounds (IMO-1 to IMO-6)

C-C bond length (Å)					
IMO-1		**IMO-2**		**IMO-3**	
C1-C2	1.403	C1-C2	1.402	C2-C3	1.400
C2-C3	1.389	C2-C3	1.382	C3-C4	1.388
C3-C4	1.408	C3-C4	1.413	C4-C5	1.408
C4-C5	1.425	C4-C5	1.433	C5-C6	1.424
C5-C6	1.414	C5-C6	1.404	C6-C7	1.413
C6-C1	1.389	C6-C1	1.390	C7-C2	1.386
C5-C7	1.458	C5-C7	1.460	C6-C8	1.458
C10-C11	1.376	C10-C11	1.376	C11-C12	1.376
C10-C14	1.488	C10-C14	1.488	C11-C15	1.488
C11-C13	1.491	C11-C13	1.491	C12-C14	1.491
IMO-4		**IMO-5**		**IMO-6**	
C2-C3	1.399	C10-C11	1.404	C1-C2	1.401
C3-C4	1.387	C11-C12	1.391	C2-C3	1.391
C4-C5	1.407	C12-C13	1.405	C3-C4	1.419
C5-C6	1.424	C13-C8	1.426	C4-C5	1.423
C6-C7	1.413	C8-C9	1.414	C5-C6	1.414
C7-C2	1.385	C9-C10	1.385	C6-C1	1.387
C6-C8	1.457	C8-C5	1.455	C5-C7	1.459
C11-C12	1.376	C2-C3	1.375	C10-C11	1.375
C11-C15	1.488	C2-C6	1.488	C10-C14	1.488
C12-C14	1.491	C3-C7	1.491	C11-C13	1.491
C-H, C-O, N-O, C-Cl, C-Br and O-H bond distances (Å)					
IMO-1(Å)		**IMO-2(Å)**		**IMO-3(Å)**	
C1-H26	1.084	C2-H29	1.082	C3-H28	1.084
C2-H27	1.085	C3-H28	1.083	C4-H27	1.084
C3-H28	1.084	C6-H30	1.081	C7-H26	1.082
C6-H25	1.083	C13-H25	1.094	C14-H18	1.090
C13-H19	1.090	C13-H26	1.090	C14-H19	1.094
C13-H20	1.094	C13-H27	1.095	C14-H20	1.095
C13-H21	1.095	C14-H22	1.091	C15-H21	1.091

C14-H22	1.094	C14-H23	1.094	C15-H22	1.094
C14-H23	1.091	C14-H24	1.094	C15-H23	1.094
C14-H24	1.094	C4-O8	1.325	C5-O9	1.339
C4-O8	1.341	N17-O18	1.236	N10-O16	1.324
N9-O15	1.325	N17-O19	1.235	N13-O17	1.379
N12-O16	1.380	O8-H20	1.047	O17-H24	0.973
O16-H18	0.973	O16-H21	0.973	O9-H25	1.028
O8-H17	1.023			C2-Cl1	1.762
IMO-4		**IMO-5**		**IMO-6**	
C3-H19	1.084	C9-H24	1.083	C1-H27	1.084
C4-H29	1.084	C10-H25	1.083	C2-H28	1.085
C7-H18	1.082	C12-H26	1.086	C6-H26	1.083
C14-H25	1.090	C6-H18	1.091	C14-H22	1.094
C14-H26	1.094	C6-H19	1.094	C14-H23	1.091
				C14-H24	1.094
C14-H27	1.095	C6-H20	1.094	C13-H19	1.090
C15-H22	1.091	C7-H21	1.096	C13-H20	1.094
C15-H23	1.094	C7-H23	1.094	C13-H21	1.095
C15-H24	1.094	C7-H22	1.091	C18-H31	1.341
C5-O9	1.338	C13-O17	1.338	C18-H32	1.372
N10-O16	1.324	C11-O14	1.368	C18-H30	1.379
N13-O21	1.379	O17-H29	1.033	C4-O8	1.341
O9-H28	1.029	O14-H27	0.966	C3-O17	1.372
O17-H21	0.973	O16-H28	0.973	N12-O16	1.379
C2-Br1	1.909	N1-O15	1.327	N9-O15	1.326
		N4-O16	1.380	O16-H25	0.973
				O8-H29	1.034
Bond Angle (°)					
IMO-1		**IMO-2**		**IMO-3**	
C3-C2-C1	120.394	C3-C2-C1	118.925	C3-C2-Cl1	119.664
C4-C3-C2	121.156	C4-C3-C2	121.577	C4-C3-C2	119.340
C5-C4-C3	118.729	C5-C4-C3	118.765	C5-C4-C3	121.625
C6-C1-C2	119.394	C6-C1-C2	121.419	C6-C5-C4	118.525
C7-C5-C4	120.945	C7-C5-C4	121.125	C7-C2-Cl1	119.548
O8-C4-C3	118.214	O8-C4-C3	118.125	C8-C6-C5	121.008
N9-C7-C5	128.145	N9-C7-C5	127.966	O9-C5-C4	118.267

C10-N9-C7	111.037	C10-N9-C7	111.178	N10-C8-C6	127.940
C11-C10-N9	107.214	C11-C10-N9	107.080	C11-N10-C8	111.014
N12-C7-C5	127.429	N12-C7-C5	127.630	C12-C11-N10	107.199
C13-C11-C10	132.159	C13-C11-C10	132.156	N13-C8-C6	127.588
C14-C10-N9	120.287	C14-C10-N9	120.424	C14-C12-C11	132.145
O15-N9-C7	125.466	O15-N9-C7	125.461	C15-C11-C10	120.306
O16-N12-C7	125.099	O16-N12-C7	125.020	O16-N10-C8	125.492
H17-O8-C4	109.111	N17-C1-C6	118.967	O17-N13-C8	125.072
H19-C13-C11	109.651	O18-N17-C1	118.148	H18-C14-C12	109.660
H20-C13-C11	111.424	O19-N17-C1	117.846	H19-C14-C12	111.359
H21-C13-C11	111.739	H20-O8-C4	109.712	H20-C14-C12	111.760
H22-C14-C10	110.763	H21-O16-N12	106.313	H21-C15-C11	110.551
H23-C14-C10	110.565	H22-C14-C10	110.497	H22-C15-C11	110.604
H24-C14-C10	110.585	H23-C14-C10	110.746	H23-C15-C11	110.735
H25-C6-C1	119.627	H24-C14-C10	110.614	H24-O17-N13	106.168
H26-C1-C6	120.005	H25-C13-C11	111.227	H25-O9-C5	109.068
H27-C2-C1	120.026	H26-C13-C11	109.675	H26-C7-C2	119.659
H28-C3-C2	121.452	H27-C13-C11	111.789	H27-C4-C3	120.812
		H28-C3-C2	121.118	H28-C3-C2	120.126
		H29-C2-C1	119.618		
		H30-C6-C1	118.778		

IMO-4		IMO-5		IMO-6	
C3-C2-Br1	119.601	C3-C2-N1	107.213	C3-C2-C1	120.882
C4-C3-C2	119.352	N4-C3-C2	105.316	C4-C3-C2	120.487
C5-C4-C3	121.568	C5-N1-C2	111.122	C5-C4-C3	118.334
C6-C5-C4	118.500	C6-C2-N1	120.313	C6-C1-C2	119.712
C7-C2-Br1	119.501	C7-C3-C2	132.231	C7-C5-C4	120.320
C8-C6-C5	120.905	C8-C5-N1	128.168	O8-C4-C3	118.814
O9-C5-C4	118.281	C9-C8-C5	120.392	N9-C7-C5	128.310
N10-C8-C6	127.965	C10-C9-C8	122.059	C10-N9-C7	111.086
C11-N10-C8	111.010	C11-C10-C9	118.884	C11-C10-N9	107.176
C12-C11-N10	107.201	C12-C11-C10	120.592	N12-C7-C5	127.293
N13-C8-C6	127.556	C13-C12-C11	120.983	C13-C11-C10	132.183
C14-C12-C11	132.130	O14-C11-C10	117.094	C14-C10-N9	120.334
C15-C11-N10	120.356	O15-N1-C5	125.406	O15-N9-C7	125.466
O16-N10-C8	125.482	O16-N4-C3	122.928	O16-N12-C7	125.099
O17-N13-C8	125.073	O17-C13-C12	117.863	H17-O8-C4	109.111
H18-C7-C2	119.958	H18-C6-C2	110.548	H18-O16-N12	106.062
H19-C3-C2	120.341	H19-C6-C2	110.597	H19-C13-C11	109.651
H20-C4-C3	120.850	H20-C6-C2	110.782	H20-C13-C11	111.424
H21-O17-N13	106.189	H21-C7-C3	111.780	H21-C13-C11	111.739
H22-C15-C11	110.540	H22-C7-C3	109.649	H22-C14-C10	110.763
H23-C15-C11	110.610	H23-C7-C3	111.437	H23-C14-C10	110.565
H24-C15-C11	110.740	H24-C9-C8	119.060	H24-C14-C10	110.585
H25-C14-	109.658	H25-C10-C9	121.473	H25-C6-C1	119.627

C12					
H26-C14-C12	111.352	H26-C12-C11	121.380	H26-C1-C6	120.005
H27-C14-C12	111.761	H27-O14-C11	109.656	H27-C2-C1	120.026
H28-O9-C5	109.096	H28-O16-C4	106.050	H28-C3-C2	121.452
		H29-O17-C13	109.054		

Selected dihedral angle (º)					
IMO-1		**IMO-2**		**IMO-3**	
O16-N12-C7-N9	-177.570	O16-N12-C7-N9	-177.700	O17-N13-C8-N10	-179.470
O16-N12-C7-C5	0.833	O16-N12-C7-C5	3.880	O17-N13-C8-C6	-1.010
C6-C5-C7-N9	-147.380	C6-C5-C7-N9	149.340	C7-C6-C8-N10	-147.580
C6-C5-C7-N12	34.579	C6-C5-C7-N12	-32.600	C7-C6-C8-N13	34.304
C4-C5-C7-N12	-143.860	C4-C5-C7-N12	145.390	C5-C6-C8-N10	33.960
C4-C5-C7-N9	34.178	C4-C5-C7-N9	-32.640	C5-C6-C8-N13	-144.140
C4-C3-C2-C1	0.913	C4-C3-C2-C1	-0.662	C5-C4-C3-C2	1.009
C5-C4-C3-C2	0.344	C5-C4-C3-C2	-0.517	C6-C5-C4-C3	0.070

Again, from the optimized geometry, it is evident that the C-C bond distance of all the aryl groups in the compounds IMO-1 to IMO-6 are in the range 1.382 to 1.433Å which suggests that the carbon atoms are highly conjugated and electrons are delocalized through resonance[23]

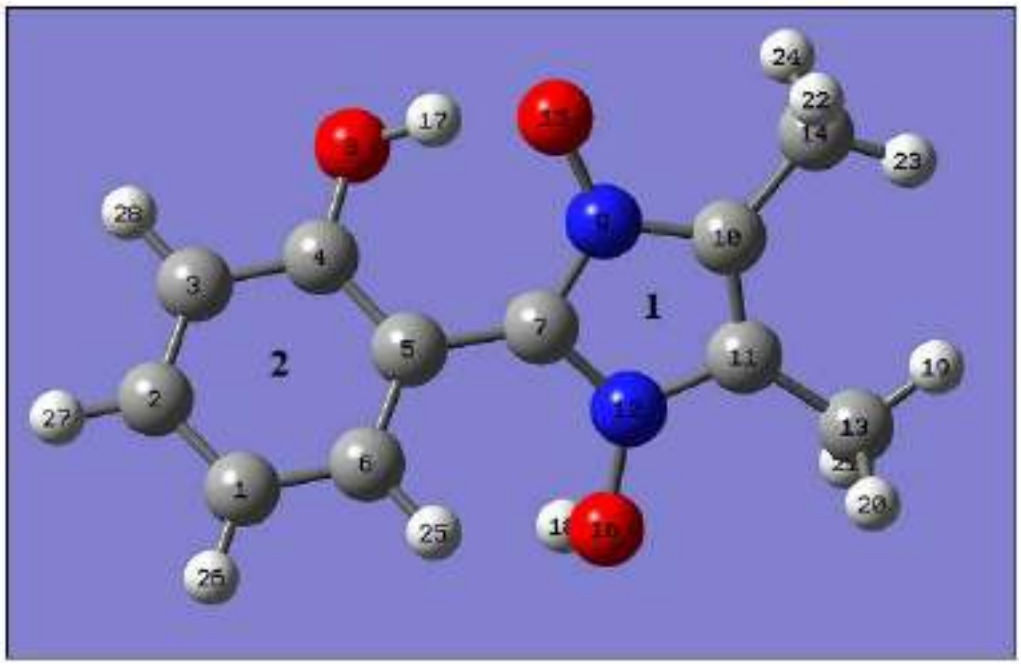

Fig. 5.B.1. Labeling of the phenyl ring and the imidazole ring in the studied compounds

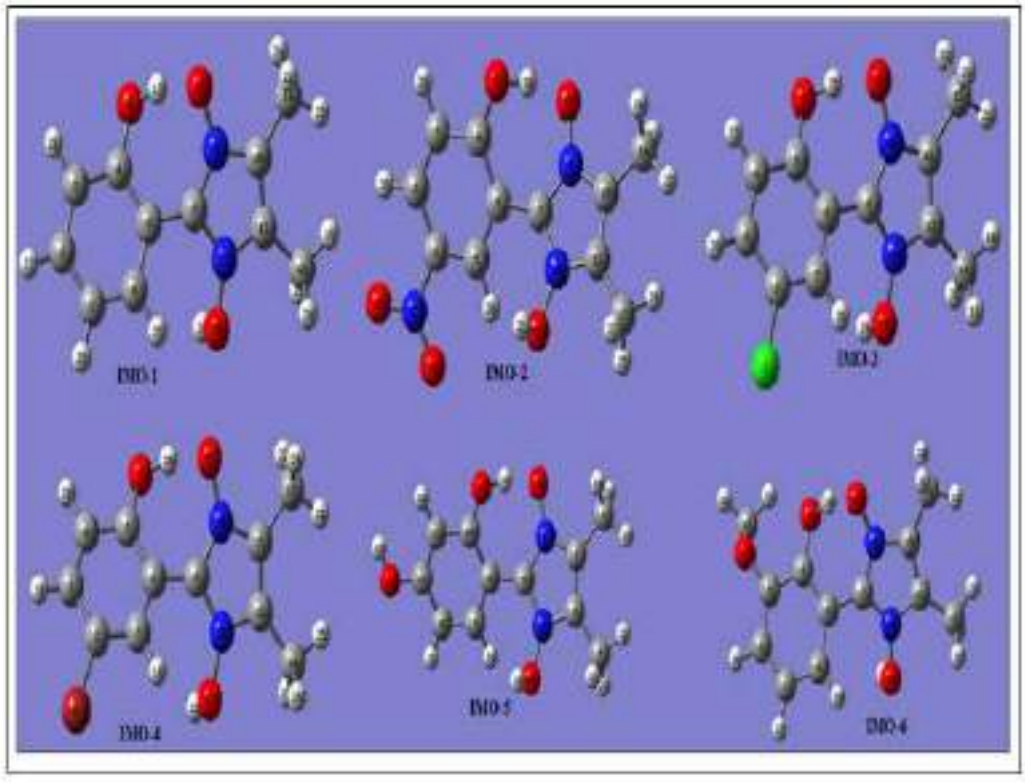

Fig. 5.B.2. DFT optimized geometry of the compounds IMO-1 to IMO-6 with atom labeling scheme

The N-O bond distance in the imidazole ring 1 of the studied compounds IMO-1 to IMO-6 are in the range 1.324-1.327 Å and the O-H bond distances in the imidazole ring1 of all the studied compounds are equal with a value of 0.973Å. The aromatic C-H, aliphatic C-H, C-O, O-H and C-Halogen bond distances for the studied compounds IMO-1 to IMO-6 are in the range 1.081-1.086 Å, 1.325-1.341Å, 1.023-1.047Å and 1.762-1.909 Å respectively.

5.B.2.1.2 Frontier Molecular Orbitals

The Frontier Molecular Orbitals namely the Highest Occupied Molecular Orbital (HOMO) and the Lowest Unoccupied Molecular Orbital (LUMO) are essential for calculating the most reactive positions in π -electron conjugated systems, in which the HOMO acts as an electron donor and the LUMO acts as an electron acceptor, which determine whether a system is stable or instable[24]. The energy difference between the HOMO and the LUMO called the energy gap is an important parameter for analyzing the charge transfer within a molecule. For organic molecules having a low energy gap, there is a significant intramolecular charge transfer within the molecule[25].

. The energies of HOMO and LUMO orbitals of the studied compounds (IMO-1 to IMO-6) are calculated using DFT/B3LYP method using 6-31G+ (d, 2p) level of basis set and shown in Fig.5.B.3. The energy of HOMO and LUMO orbitals of the studied compounds (IM-1 to IM-6) are listed in Table 5.B.2

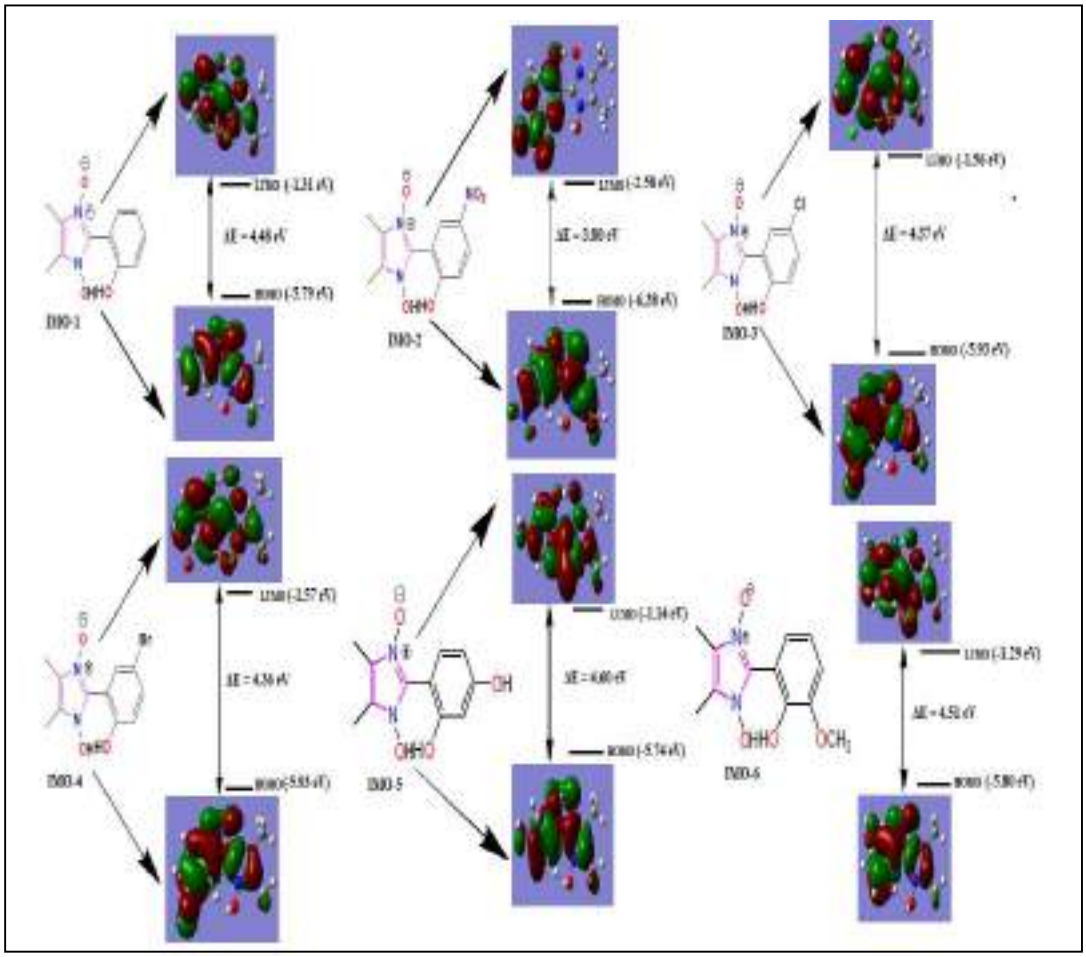

Fig. 5.B.3. Pictorial representation of the HOMO-LUMO of selected compounds (IMO-1 to IMO-6)

From the Table 5.B.2, it is evident that the energy of HOMO and LUMO orbitals are negative and this shows that the compounds under study (IMO-1 to IMO-6) are relatively stable[46]and the energy of HOMO and LUMO orbitals of the compounds are -5.79 eV(IMO-1), -6.38 eV(IMO-2), -5.93 eV(IMO-3), -5,93(IMO-4), -5.74(IMO-5), -5.80 eV(IMO-6) and -1.31 eV(IMO-1), -2.58 eV(IMO-2), -1.56 (IMO-3), -1.57(IMO-4), -1.14 eV (IMO-5), -1.29 eV(IMO-6). From the energies of the HOMO and LUMO, global chemical descriptors like chemical potential, global hardness and global electrophilicity can be determined which is helpful for understanding the reactivity and the structure of the molecule which in turn is essential for determination of the various pharmacological properties of the molecule for the process of drug design[26]. The ionization energy (I) and electron affinity (A) can be expressed in terms of HOMO and LUMO orbital energies as follows:

$$I = -E_{HOMO} \text{ and } A = -E_{LUMO}$$

The chemical reactivity descriptors such as chemical potential (μ), Electronegativity (χ), Global hardness (η) and global electrophilicity power (ω) can be calculated with the help of following relation;

$$\text{Chemical potential } (\mu) = (E_{HOMO} + E_{LUMO})/2 = -(I-A)/2$$

$$\text{Electronegativity } (\chi) = (I+A)/2$$

$$\text{Global Hardness } (\eta) = (-E_{HOMO} + E_{LUMO})/2 = (I-A)/2$$

$$\text{electrophilicity power } (\omega) = \mu^2/2\,\eta$$

Where I and A are the first ionization potential and electron affinity of the chemical species[27-29]. The ionization energy (I), electron affinity (A), Chemical potential (μ), Electronegativity (χ), Global hardness (η) and Global electrophilicity power (ω) of the studied compounds (IMO-1 to IMO-6) are listed in Table 5.B.2

Table. 5.B.2. Energies of HOMO and LUMO orbitals, ionization energy (I), electron affinity (A), Chemical potential (μ), Electronegativity (χ), Global hardness (η) and Global electrophilicity power (ω) of the studied compounds (IMO-1 to IMO-6)

Parameters (eV)	IMO-1	IMO-2	IMO-3	IMO-4	IMO-5	IMO-6
E_{HOMO}	-5.79	-6.38	-5.93	-5.93	-5.74	-5.80
E_{LUMO}	-1.31	-2.58	-1.56	-1.57	-1.14	-1.29
Δ E	4.48	3.80	4.37	4.36	4.60	4.51
Ionization Energy (I)	5.79	6.38	5.93	5.93	5.74	5.80
Electron Affinity (A)	1.31	2.58	1.56	1.57	1.14	1.29
Chemical potential (μ)	-3.55	-4.48	-3.74	-3.75	-3.44	-3.54
Electronegativity (χ)	3.55	4.48	3.74	3.75	3.44	3.54
Global hardness(η)	2.24	1.90	2.185	2.180	2.30	2.25
Electrophilicity power(ω)	2.81	5.28	3.20	3.22	2.57	2.78

It was observed that the chemical potential of all the studied molecules are negative and it suggest that they do not decompose spontaneously into its elements they are made up of.

Apparently, it is seen that the hard molecule has large HOMO-LUMO gap and soft molecule has small HOMO-LUMO gap[30]. Thus, from the table 5.B.2 it is evident that the hardness of the studied molecule follows the order IMO-5> IMO-

6>IMO-1>IMO-3>IMO-4>IMO-2. Moreover, the hardness signifies the resistance towards the deformation of electron cloud of chemical systems under small perturbation that occur during the chemical reaction. Thus, hard system is less polarizable than soft system[31]. Again, a large value of electrophilicity is assigned for good electrophile whereas nucleophile is described by low value of nucleophilicity[32].

5.B.2.1.3 FT-IR analysis

Study of the molecular vibrations of organic compounds is an important area of research as it is possible to correlate the theoretical and experimental FT-IR spectra of the studied compounds to figure out the different structural features in the molecules.

The theoretical vibrational spectra of the studied compounds (IMO-1 to IMO-6) was calculated using B3LYP/631G+(d,2p) basis set on the optimized geometry of the molecules in the gas phase. The experimental and theoretical vibrational frequencies of the studied compounds (IMO-1 to IMO-6) are given in Table 5.B.3 with proper assignment of the observed peaks.

Table 5.B.3 Theoretical vibrational spectra of the studied compounds (IMO-1 to IMO-6)

Unscaled frequency (cm^{-1}) (theoretical)	IR_i	R(A)	IR Frequency (cm^{-1}) Experimental	Assignments
		IMO-1		
3705.02	45.6127	107.6216	3431	ν OH stretch
3214.65	8.1747	196.2786	3338	νAr-H stretch
3207.92	10.5946	126.254		ν(as)Ar-H stretch
3196.54	11.179	137.9638		ν(as)Ar-H stretch
3180.19	2.9544	71.0119		ν(as)Ar-H stretch
3141.24	9.5178	79.2307		ν(as)CH_3 stretch
3134.3	9.791	53.93		ν (as)CH_3 stretch
3104.86	6.0324	81.7627		ν (as)CH_3 stretch
3093.32	9.7373	103.3131	3098	ν (as)CH_3 stretch
3048.73	22.8065	273.4913	3037	νCH_3 stretch
3041.98	30.0307	298.3652	3006	ν CH_3 stretch
2645.32	957.6912	44.5108		νOH stretch
1671.45	25.2853	33.3528	1650	ν C=C stretch
1653.62	51.9197	290.3311	1640	ν Ar C=C stretch
1614.47	51.3607	22.1022	1615	ν (as)Ar C=C stretch
1457.09	34.6840	78.6450	1457	υC-N stretch
1493.02	23.2802	13.2052	1542	υC-N stretch
1337.64	21.2356	61.8351	1343	ν N-O stretch
		IMO-2		
3708.7	54.7241	96.4733		ν OH stretch
3251.26	6.0628	20.7603	3318	νAr-H stretch
3236.79	3.0491	119.7162		ν (as)Ar-H stretch
3213.44	1.7457	109.6095		ν (as)Ar-H stretch
3144.57	8.1638	80.5279	3150	ν (as)CH_3 stretch
3137.92	8.1158	54.2632		ν (as)CH_3 stretch
3107.87	4.8485	83.504	3102	ν (as)CH_3 stretch
3098.01	7.3051	94.5127		ν (as)CH_3 stretch

3050.94	18.9379	280.0527	3049	ν CH_3 stretch
3043.61	23.5196	287.2019		ν CH_3 stretch
2301.78	1350.918	112.0266		ν OH stretch
1670.03	32.1487	30.5226		ν C=C stretch
1655.81	172.1217	199.7095	1635	ν Ar C=C stretch
1623.32	139.5832	67.2111	1621	ν (as)Ar C=C stretch
1397.38	47.9595	11.9295		C-N stretch
1471.94	17.3935	5.0781	1484	C-N stretch
1336.15	113.0832	90.2131	1327	ν N-O stretch
		IMO-3		
3706.21	48.4285	103.2254	3417	ν OH stretch
3230.73	0.4683	38.2996	3238	νAr-H stretch
3217.85	2.7715	204.6611	3213	ν (as)Ar-H stretch
3203.41	1.2489	69.7343		ν (as)Ar-H stretch
3142.52	8.9493	79.5551	3143	ν (as)CH_3 stretch
3135.4	9.2279	54.9416	3136	ν (as)CH_3 stretch
3105.99	5.5806	82.8585		ν (as)CH_3 stretch
3095.05	8.7991	100.241		ν (as)CH_3 stretch
3049.44	21.6612	281.2927	3054	ν CH_3 stretch
3042.59	27.531	295.8094		ν CH_3 stretch
2607.67	998.2402	38.2402		ν OH stretch
1670.39	27.7088	29.6206		ν C=C stretch
1648.04	11.8571	312.3336	1692	ν Ar C=C stretch
1608.44	32.1363	25.1459	1631	ν (as)Ar C=C stretch
1479.80	29.9446	13.3081	1482	C-N stretch
1394.27	50.1501	6.0786	1381	C-N stretch
1336.38	31.8164	54.6673	1365	ν N-O stretch
		IMO-4		
3705.55	47.6898	101.883	3418	ν OH stretch
3232.46	0.5041	31.1475	3366	νAr-H stretch
3217.69	2.5979	192.8309		ν (as)Ar-H stretch
3203.16	1.0309	67.4351		ν (as)Ar-H stretch
3142.52	9.0416	80.4962		ν (as)CH_3 stretch

3135.67	9.1412	55.1417		ν (as)CH_3 stretch
3105.89	5.5709	83.5943		ν (as)CH_3 stretch
3095.15	8.7228	98.7825	3084	ν (as)CH_3 stretch
3049.5	21.8497	285.2729	3060	ν CH_3 stretch
3042.7	27.2933	293.7105	3027	ν CH_3 stretch
2596.32	1025.3657	38.3236		ν OH stretch
1670.38	27.986	29.6608	1658	ν C=C stretch
1645.96	15.6418	323.3396		ν Ar C=C stretch
1606.74	34.2417	21.1009	1602	ν (as)Ar C=C stretch
1479.49	30.7870	13.4282	1488	C-N stretch
1394.38	52.5472	6.2468	1384	C-N stretch
1336.88	34.8166	55.404	1306	ν N-O stretch
		IMO-5		
3819.82	87.7808	177.7733		ν OH stretch
3703.1	44.3077	11.05166	3452	ν OH stretch
3221.67	3.8053	139.191	3288	νAr-H stretch
3206.4	1.7675	58.2336	3205	ν (as)Ar-H stretch
3183.19	9.1867	131.2378		ν (as)Ar-H stretch
3140.49	9.8455	82.7708		ν (as)CH_3 stretch
3133.95	9.9568	54.993	3126	ν (as)CH_3 stretch
3104.61	6.1979	82.7744	3113	ν (as)CH_3 stretch
3092	10.135	105.793		ν (as)CH_3 stretch
3048.57	23.8552	279.8837		ν CH_3 stretch
3040.99	32.4452	317.8999	2973	ν CH_3 stretch
2528.27	1060.9586	53.2578		ν OH stretch
1673.46	13.6042	43.8922	1678	ν C=C stretch
1661.69	393.0675	318.5151		ν Ar C=C stretch
1626.04	91.5295	2.8895	1619	ν (as)Ar C=C stretch
1498.43	24.8828	52.003	1445	C-N stretch
1394.80	34.3140	11.8589	1394	C-N stretch
1342.65	7.7212	20.3365	1364	ν N-O stretch
		IMO-6		
3707.9	45.7938	101.1333	3335	ν OH stretch

3218.18	6.1246	126.6136		νAr-H stretch
3204.66	7.5837	173.6928		ν (as)Ar-H stretch
3189.44	5.0698	65.7592		ν (as)Ar-H stretch
3146.69	13.9772	98.4095		ν (as)CH_3 stretch
3141.23	9.6342	81.3277		ν (as)CH_3 stretch
3134.51	9.681	53.8307		ν (as)CH_3 stretch
3108.43	35.3624	96.6261		ν (as)CH_3 stretch
3105.09	5.9275	80.2792		ν (as)CH_3 stretch
3093.85	9.511	104.4622	3098	ν (as)CH_3 stretch
3048.89	22.762	275.497	3065	ν CH_3 stretch
3042.3	29.8785	305.75		ν CH_3 stretch
3015.55	83.0457	145.7974	2998	ν CH_3 stretch
2514.14	1180.046	59.5506		ν OH stretch
1671.46	28.082	31.2389		ν C=C stretch
1641.2	17.9565	285.0536	1626	ν Ar C=C stretch
1622.17	11.2284	17.424		ν (as)Ar C=C stretch
1479.33	41.6254	14.9933	1479	νC-N stretch
1393.52	35.2125	9.8195	1366	νC-N stretch
1343.14	1.95	27.1136	1336	ν N-O stretch

5.B.2.1.3.1 C-H stretching vibrations

For the studied compounds (IMO-1 to IMO-6), C-H functional group is present at a number of positions. The characteristics region of C-H stretching vibration of aromatic ring falls in the range 3100-3000 cm^{-1}[133]. In the present investigation, theoretically calculated bands in the range 3214-3180 cm^{-1}, 3251-3213 cm^{-1}, 3230-3203 cm^{-1}, 3232-3203 cm^{-1}, 3221-3183- cm^{-1} and 3218-3189- cm^{-1} were assigned to aromatic C-H stretching vibrations for compounds IMO-1, IMO-2, IMO-3, IMO-4, IMO-5 and IMO-6 respectively. Pure symmetric bands were calculated at 3214 cm^{-1} in IMO-1, 3251 cm^{-1} in IMO-2, 3230 cm^{-1} in IMO-3, 3232 cm^{-1} in IMO-4, 3221 cm^{-1} in IMO-5 and 3218 cm^{-1} in IMO-6 respectively. Experimentally, symmetric bands were observed at 3338 cm^{-1}in IMO-1, 3318 cm^{-1} in IMO-3, 3366 cm^{-1} in IMO-4, 3288 cm^{-1} and 3205 cm^{-1} in IMO-5 respectively. Asymmetric vibrational bands were calculated with stretching frequencies3180 cm^{-1}, 3196 cm^{-1}, 3207 cm^{-1} in IMO-1, 3213, cm^{-1}, 3236 cm^{-1} in IMO-2, 3217 cm^{-1},3230 cm^{-1} in IMO-3, 3203 cm^{-1}, 3217 cm^{-1}in IMO-4, 3183 cm^{-1}, 3206 cm^{-1} in IMO-5 and 3189 cm^{-1} and 3204 cm^{-1} in IMO-6 respectively. Experimentally,

Asymmetric vibrational bands were observed at 3213 cm^{-1} in IMO-3and 3205 cm^{-1} in IMO-6 respectively (Table 5.B.3).

5.B.2.1.3.2 Aromatic C-C stretching vibrations

Generally, the bands observed in the range 1650-1400 cm^{-1} are assigned to C-C stretching mode of aromatic derivatives[34]. In our present study, the range for theoretically calculated C-C stretching vibrational mode showing sharp bands are in the range 1614-1671 cm^{-1}, 1632-1670 cm^{-1}, 1608-1670 cm^{-1}, 1606-1670 cm^{-1}, 1626-1673 cm^{-1} and 1622-1671 cm^{-1} for IMO-1, IMO-2, IMO-3, IMO-4, IMO-5 and IMO-6 respectively (Table 5.B.3). Experimentally, the aromatic C-C stretching frequencies for the studied compounds observed in the range 1615-1650 cm^{-1} in IMO-1, 1621-1632 cm^{-1} in IMO-2, 1631-1692 cm^{-1} in IMO-3, 1602-1658 cm^{-1} in IMO-4, 1619-1678 cm^{-1} in IMO-5 and 1626 cm^{-1} in IMO-6 respectively.

5.B.2.1.3.3 C-N bond stretching vibrations

For imidazole scaffolds, several bands of variable intensity are observed in the range of 1660-1450 cm^{-1} owing to C=N and C=C stretching vibrations[35]. Theoretically, for the studied compounds (IMO-1 to IMO-6), the C=N stretching vibrations are observed in the range of 1457-1493 cm-1 for IMO-1, 1471-1397 cm^{-1} for IMO-2, 1479-1394 cm^{-1} for IMO-3 and IMO-4, 1498-1394 cm^{-1} for IMO-5 and 1479-1393 cm^{-1} for IMO-6. The experimentally observed values for C=N stretching vibrations are found in the range of 1542-1457 cm^{-1} for IMO-1, 1484 cm^{-1} for IMO-2, 1482-1381 for IMO-3, 1488-1384 cm^{-1} for IMO-4, 1145-1394 cm^{-1} for IMO-5 and 1479-1366 cm^{-1} for IMO-6.

5.B.2.1.3.4 N-O bond stretching vibrations

N-O stretching vibration is an important stretching vibration for 1-hydroxy-2-(2-hydroxyphenyl)-4,5-dimethylimidazole-3-oxide derivatives to ascertain their structure. Theoretically, the N-O stretching frequency observed were at 1337.64 cm^{-1}, 1336.15 cm^{-1}, 1336.38 cm^{-1}, 1336.88 cm^{-1}, 1342.65 $cm^{-1}$and 1343.14 $cm^{-1}$for the compounds IMO-1, IMO-2, IMO-3, IMO-4, IMO-5 and IMO-6 respectively.

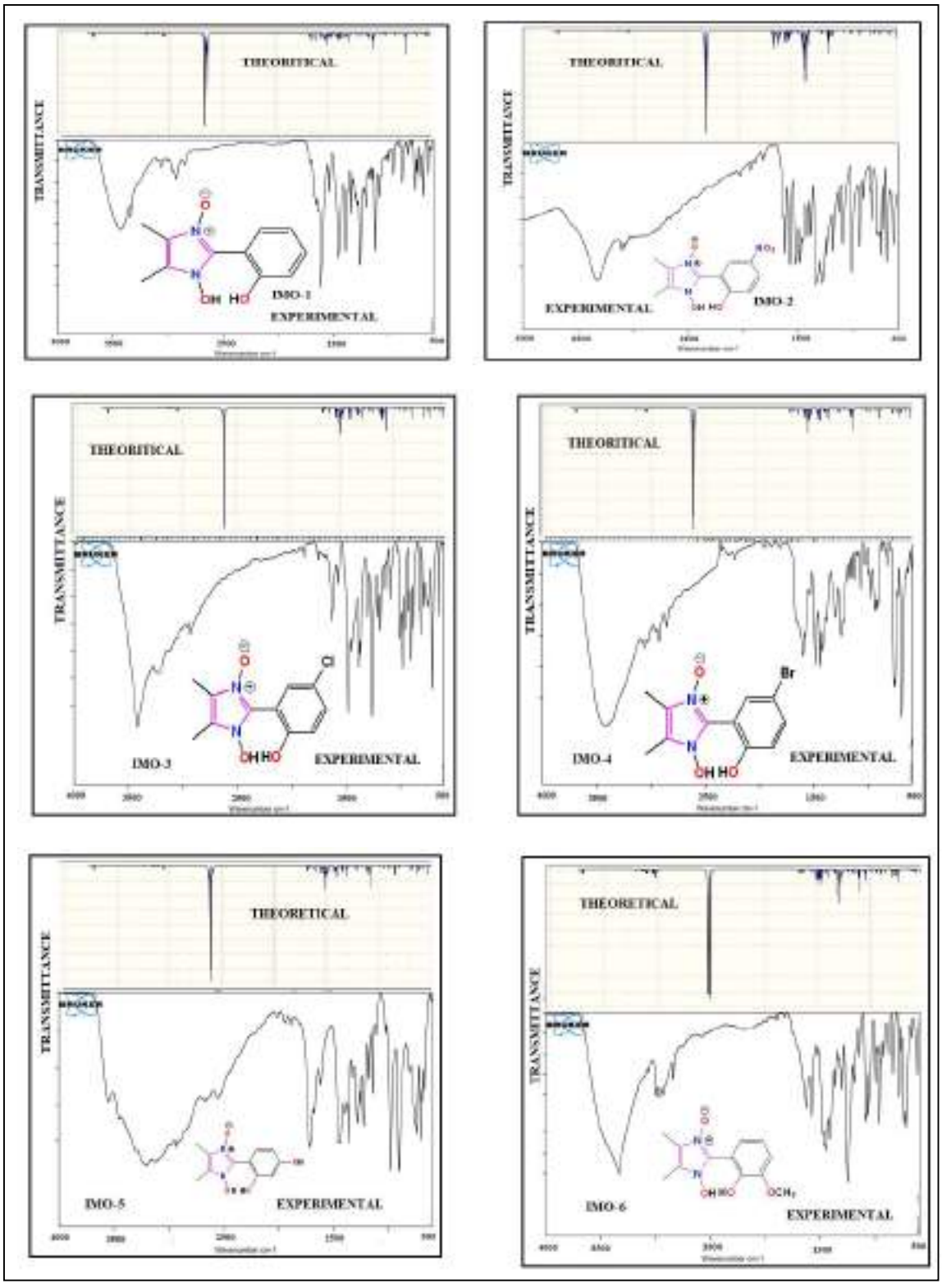

Fig. 5.B.4. Theoretical and experimental FTIR spectra of IMO-1 to IMO-6

The experimentally observed values for N-O stretching frequency were at 1343, 1327, 1365, 1306, 1364 and 1336 cm^{-1} for the compounds IMO-1, IMO-2, IMO-3, IMO-4, IMO-5 and IMO-6 respectively.

Thus, from the above discussions it is evident that the theoretically calculated vibrational frequency matched well with the experimental results for the studied compounds (Fig. 5.B.4)

5.B.2.1.4 Molecular Electrostatic Potential

Molecular Electrostatic Potential (MEP) is a useful parameter which gives information about the relative polarity of molecules along with other parameters like hydrogen bonding, reactivity, polarizability, sites for electrophilic and nucleophilic attack, etc[36]. To predict the reactive sites of electrophilic and nucleophilic attack for the investigated molecules (IMO-1 to IMO-6), MEP at B3LYP/6-31G+ (d, 2p) optimized geometry was calculated. The significance of MEP provides a visual method to understand the relative polarity of the given molecule and the different values of the electrostatic potential at the MEP surface are given by different colors such as red, blue and green. Red, blue and green color represents the region of most negative, most positive and zero electrostatic potential respectively. Thus, the electrostatic potential increases in the order blue > green > yellow > orange > red. The most negative electrostatic potential (red, orange and yellow region) in the MEP surface is assigned for the electrophilic reaction sites and the positive (blue region) corresponds to nucleophilic reaction site[37-38]. The MEP surface of the studied compounds (IMO-1 to IMO-6) is depicted in Fig. 5.B.5.

A detailed description of the MEP surface indicating the region of negative/ electrophilic reaction sites and positive/nucleophilic reaction site for the studied compounds (IM-1 to IM-6) are listed in Table 5.B.4.

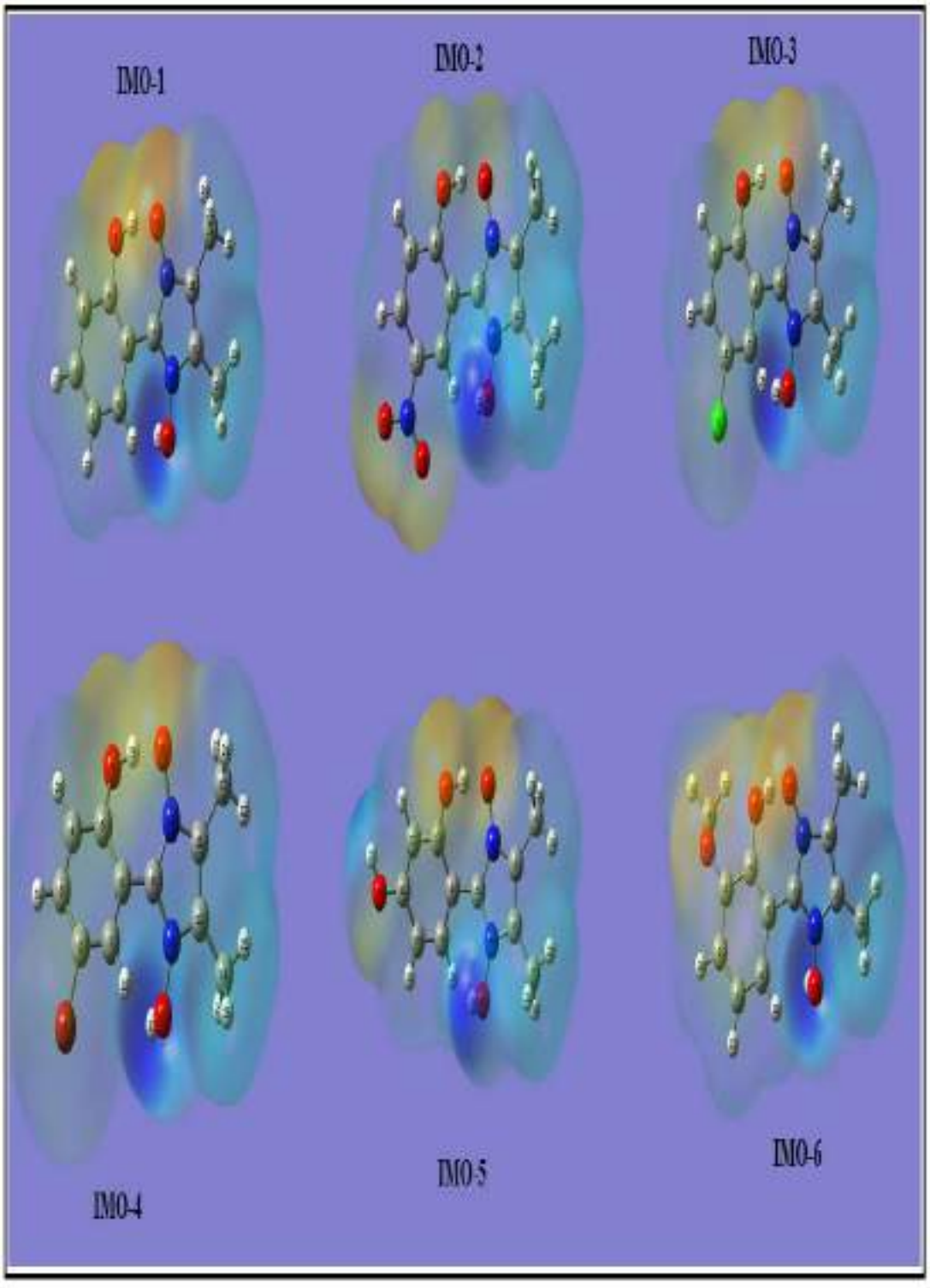

Fig. 5.B.5. MEP plot of studied compounds (IMO-1 to IMO-6)

Table 5.B.4. Detailed description of MEP surface for compounds IMO-1 to IMO-6

Entry	Negative region (red, orange, yellow)/Electrophilic reaction site	Positive region (blue)/ Nucleophilic reaction site
IMO-1	-OH group of 2-phenyl ring and N(3)-O^- group of imidazole core1	-OH group attached to N(4) and two CH_3 groups of imidazole core 1
IMO-2	NO_2 group and -OH group of phenyl ring 2 and N(3)-O^- group of imidazole core 1	-OH group attached to N(4) and two CH_3 groups of imidazole core 1
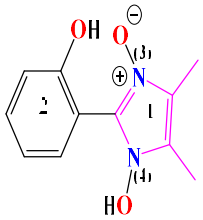 **IMO-3**	-OH group, Cl group of phenyl ring 2 and N(3)-O^- group of imidazole core 1	-OH group attached to N(4) and two CH_3 groups of imidazole core 1
IMO-4	-OH group, Br group of phenyl ring 2 and N(3)-O^- group of imidazole core 1	-OH group attached to N(4) and two CH_3 groups of imidazole core 1
IMO-5	-OH group at ortho position of phenyl ring 2 and N(3)-O^- group of imidazole core 1	-OH group attached to N(4) and two CH_3 groups of imidazole core 1 and -OH group at para position of the phenyl ring 2
IMO-6	-OH group at ortho position and -OCH_3 at meta position of phenyl ring 2 and N(3)-O^- group of imidazole core 1	-OH group attached to N(4) and two CH_3 groups of imidazole core 1

5.B.2.1.5 NLO Properties

With the rapid development in the field of non-linear optics, Organic molecules with strong non-linear properties has been a center of attention of many researchers working in the field of chemistry and material chemistry in the last few decades. Organic Molecules with π- conjugation has tremendous applications in the field of photonics, biomedicine, signal processing, etc[39-40]. Theoretically, the NLO properties of the given compound is calculated by determining the parameters such as magnitude of dipole moment (μ), polarizability (α), anisotropy of polarizability (Δα), first hyperpolarizability (β) and second order hyperpolarizability (γ). The polarizability tensors are calculated using the following relations:[41]

$$\text{Dipole moment } \mu = (\mu x^2 + \mu y^2 + \mu z^2)^{1/2} \quad \ldots\ldots (1)$$

$$\alpha(\text{total}) \text{or} < \alpha > = \frac{1}{3}(\alpha xx + \alpha yy + \alpha zz) \quad \ldots\ldots (2)$$

$$\Delta\alpha = 1/\sqrt{2}[(\alpha xx - \alpha yy)^2 + (\alpha yy - \alpha zz)^2 + (\alpha zz - \alpha xx)^2 + 6(\alpha xy^2 + \alpha xz^2 + \alpha yz^2)]^{1/2} \quad \ldots\ldots (3)$$

$$\beta x = \beta xxx + \beta xyy + \beta xzz \quad \ldots\ldots (4)$$

$$\beta y = \beta yyy + \beta yzz + \beta yxx \quad \ldots\ldots (5)$$

$$\beta z = \beta zzz + \beta zxx + \beta yyz \quad \ldots\ldots (6)$$

$$\beta\text{total} = (\beta x^2 + \beta y^2 + \beta z^2)^{1/2} \quad \ldots\ldots (7)$$

$$< \gamma > \textit{or } \gamma \text{ total} = 1/5\,(\gamma xxxx + \gamma yyyy + \gamma zzzz + 2(\gamma xxyy + \gamma yyzz + \gamma xxzz)) \quad \ldots\ldots (8)$$

Interstingly,1-hydroxy-2-arylimidazole-3-oxide derivatives also consists of extended π-conjugated system carrying a phenyl ring in conjugation with imidazole core and therefore, it was thought worthwhile to study the NLO properties of these type of molecules. The nonlinear optical properties such as dipole moments, dipole polarizabilities, first- and second order hyperpolarizabilities of the studied compounds (IMO-1 to IMO-6) were calculated by B3LYP/ 6-31G + (d, 2p) basis set and the computed results are listed in Table 5.B.5

Table 5.B.5. Dipole moments, dipole polarizabilities, anisotropic polarizabilities and First order hyperpolarizabilities of IMO-1 to IMO-6

Dipole moments, dipole polarizabilities and anisotropic polarizabilities							
Entry	**IMO-1**	**IMO-2**	**IMO-3**	**IMO-4**	**IMO-5**	**IMO-6**	**Ref.**
μ_x	-6.49	7.70	4.51	-4.83	-3.06	-3.82	0
μ_y	-6.87	-4.20	-7.82	-5.92	3.93	-5.04	-4.06
μ_z	0.02	0.01	-0.01	-0.02	1.80	3.35	0.0018
μ	**9.45**	**8.77**	**9.03**	**7.64**	**5.31**	**7.16**	**4.06**
α_{xx}	-70.30	-117.13	-87.40	-101.61	-80.72	-90.87	-16.62
α_{yy}	-96.27	-111.77	-108.92	-107.58	-104.85	-111.97	-24.64
α_{zz}	-98.43	-109.97	-109.87	-115.03	-100.28	-103.51	-27.03
α_{xy}	-0.08	-28.44	-14.39	23.37	-8.48	-1.1319	-0.0003
α_{xz}	-0.04	-0.08	-0.03	0.06	0.46	1.00	-0.07
α_{yz}	-0.10	0.01	-0.02	0.23	2.23	1.77	0.01
α_{tot} x 10^{-24}(esu)	**-13.09**	**-16.59**	**-15.12**	**-16.00**	**-14.12**	**-15.11**	**-3.37**
Δα x 10^{-24} (esu)	**4.01**	**7.36**	**4.92**	**6.24**	**4.43**	**2.79**	**1.39**
First order hyperpolarizabilities							
βxxx	-58.13	179.99	82.57	4.60	-25.97	-66.73	-0.0026
βxyy	-39.93	27.40	20.73	25.20	-0.24	9.33	-0.0004
βxzz	-16.06	-2.99	7.50	22.88	-5.96	0.15	0.001
Byyy	-62.87	-65.39	-106.74	-99.59	28.17	-17.20	-16.94
βxxy	-38.03	12.15	-32.43	-51.72	-40.49	-1.66	-0.63
βyzz	2.59	-6.63	-5.05	-13.39	13.10	-9.27	2.05
βzzz	1.31	1.31	-0.04	-0.02	8.51	24.28	-0.01
βxxz	-0.49	-1.28	0.19	-0.46	18.98	27.00	-0.09
βyyz	-0.84	-1.11	-0.44	-0.26	8.06	10.61	-0.03
βxyz	0.27	0.11	0.07	-0.80	-5.41	14.32	0.05
βtotal x 10^{-30} (esu)	**1.30**	**1.84**	**1.57**	**1.48**	**0.47**	**0.76**	**0.13**

A comparative study of the dipole moment in the studied system indicates that they have different charge distributions for different directions. The theoretically calculated dipole moments of the studied compounds are 9.45 D (IMO-1), 8.77 D (IMO-2), 9.03 D (IMO-3), 7.64 D (IMO-4), 5.31 D (IMO-5) and 7.16 D (IMO-6) respectively and the dipole moment increases in the order IMO-1 > IMO-3 > IMO-2 > IMO-4 > IMO-6 > IMO-5. It is clearly seen that the studied compounds IMO-1 to IMO-6 have dipole moments greater than the reference material urea (4.06 D). Also, the total dipole polarizabilities value of the studied compounds along all three directions is listed in Table 3.C.5. From the Table 5.B.5,

it is evident that the dipole polarizability of the studied compounds follows the order IMO-2 (-16.59 $\times 10^{-24}$esu) > IMO-4 (-16.00 $\times 10^{-24}$) > IMO-3 (-15.12 $\times 10^{-25}$) > IMO-6 (-15.11 $\times 10^{-24}$) > IMO-5 (-14.11 $\times 10^{-24}$) > IMO-1 (-13.09 $\times 10^{-24}$). The theoretically computed first-order hyperpolarizabilities and their individual components for the studied compounds (IMO-1 to IMO-6) are listed in Table 5.B.5. From the table, it is evident that the first-order hyperpolarizability of the studied compounds are IMO-1 (1.30$\times 10^{-30}$), IMO-2 (1.84 $\times 10^{-30}$), IMO-3 (1.57$\times 10^{-30}$), IMO-4 (1.48$\times 10^{-30}$), IMO-5 (0.47$\times 10^{-30}$), IMO-6 (0.76 $\times 10^{-30}$). A comparison of the first-order hyperpolarizability value of the studied compounds with the standard reference urea (0.134 $\times 10^{-30}$ esu) have shown that the studied compounds have far greater value of first-order hyperpolarizability value than urea.Thus, the order for the first-order hyperpolarizability of the studied compounds are IMO-2 > IMO-3 > IMO-1 > IMO-4 > IMO-6 > IMO-5.

The second order hyperpolarizabilities of the compounds IMO-1 to IMO-6 are given in Table 5.B.6. The second order hyperpolarizability of the studied compounds are -0.85 $\times 10^{-36}$esu, -1.22 x10^{-36}esu, -1.17x 10^{-36}esu, -1.20x 10^{-36}esu, -0.94x 10^{-36}esu and-1.08x 10^{-36}esu for IMO-1, IMO-2, IMO-3, IMO-4, IMO-5 and IMO-6 respectively and the order of second-hyperpolarizability of the studied compounds is given by IMO-2 > IMO-4 > IMO-3 > IMO-6 >IMO-5 > IMO-1.Thus it is evident that the second-hyperpolarizability of the studied compounds are much greater than the reference NLO material urea (Table 5.B.6).

Table. 5.B.6. Second order hyperpolarizabilities of compound IMO-1 to IMO-6

Second order hyperpolarizabilities							
Entry	γ_{xxxx}	γ_{yyyy}	γ_{zzzz}	γ_{xxyy}	γ_{yyzz}	γ_{xxzz}	γ_{total} **(x 10^{-36}) esu**
IMO-1	-3440.45	-1352.70	-121.08	-821.73	-264.63	-264.63	-0.85
IMO-2	-5333.19	-1970.72	-124.59	-1183.8	-352.36	-839.56	-1.22
IMO-3	-4767.79	-1950.03	-132.67	-1114.1	-360.95	-908.65	-1.17
IMO-4	-5037.13	-1907.64	-141.40	-1136.5	-361.76	-936.22	-1.20
IMO-5	-3958.78	-1308.62	-221.47	-900.79	-234.94	-791.54	-0.94
IMO-6	-4408.92	-1570.02	-463.25	-995.02	-321.04	-835.07	-1.08
Urea	-120.66	-117.90	-29.39	-44.02	-28.019	-39.86	-0.04

From the above discussion, it is evident that the studied molecules IMO-1 to IMO-6 have shown greater value of nonlinear optical parameters than the reference urea molecule and we may infer that this set of molecules could act as a better nonlinear optical material.

5. B.2.2 Molecular Docking study

According to Global Cancer Statistics 2020, Female breast cancer is the most commonly diagnosed cancer followed by lung cancer, colorectal cancer prostate cancer and stomach cancer[42]. In India alone, breast cancer contributes more than 27% of the total cancer patients[43]. Estrogens are a group of hormones which plays an important role in the sexual and reproductive development in women. They are also responsible for the regulation of growth and development of bone, breast and uterine pathology. Estrogen receptor is categorized into two subtypes, Er-alpha (Estrogen Receptor-α) and Er-beta (Estrogen Receptor-β). Er-alpha is found in endometrial, mammary epithelial cells which are the origin for growth in most breast cancers, ovarian stromal cell and hypothalamus[44]. The excessive secretion of estrogen hormone leads to the multiplication of the ER-α which is responsible for responsible for breast cancer. In early stages of breast cancer, some of the prescribed drugs like cyclophosphamide, methotrexate, fluorouracil, and doxorubicin, etc. are usually used in combination as

Chemotherapeutic agents for first- and second-line treatment of patients with metastatic breast cancer[45]. These chemotherapeutic drugs have their own side effects. Now a days, modern anti-cancer drugs are in use which target specific receptors and tumors, thus reducing the side effects of the traditional chemo-drugs and hence increasing the efficiency of the treatment. Molecular Docking process is generally used to find out various interactions between the ligand and the protein in a faster and cheaper way and this has made molecular docking an important tool in drug designing[46-47]. In this chapter, we have reported the molecular docking study of the selected 1-hydroxy-2-arylimidazole-3-oxide derivatives against the estrogen receptor protein (PDB ID: 3ERT)

5.B.2.2.1 Visualization of the Docking Result

Molecular docking study of the compounds (IMO-1 to IMO-6) against has been carried out using GUI interface programme of Autodock Tools (MGL tool or Molecular Graphics Laboratory tool developed by Scripps research Institute[48]. The docking results have been visualized with the help of Biovia Discovery Studio 2020 (DS), version 21.1.0.20298 and Edu Pymol version 2.5.2.

After successful docking of the compounds (IMO-1 to IMO-6) with the protein 3ERT, the docking result showed different types of protein-ligand interactions with particular binding energies. For better understanding of fitting of the ligand into the binding pocket of the protein, ligands are shown as blue green stick. The hydrogen bonding interactions between ligands and protein are shown by green dash line, the π-sulfur interaction as yellow dash line, π-anion/π-cation interactions as orange dash line, π-sigma interactions as purple dash line, π-π stacking/ π-π T-shaped interactions as dark pink dash line and π-alkyl interactions as light pink dash line respectively. The binding energy (ΔG) and the predicted inhibitory constant (pK_i) of the studied compounds (IMO-1 to IMO-6) are found to be -5.7Kcal/mole (IMO-1), -6.1Kcal/mole (IMO-2), -6.7Kcal/mole (IMO-3), -6.6Kcal/mole (IMO-4), -6.2Kcal/mole (IMO-5) and -5.7Kcal/mole (IMO-6) respectively and 54.14μM27.17μM, 9.66μM, 11.47μM, 22.87μM and 54.14μM respectively (Table 5.B.7)

Table. 5.B.7. Summary of docking of the compound (IM-1 to IM-6) against insulin receptor protein 1IR3 with corresponding binding energy (ΔG), predicted inhibitory constant (**pK_i**), interacting amino acid residues and type of interactions.

Ligands	Binding Energy (kcal/mol)	Predicted inhibitory constant (**pK_i**) μM	Amino Acid residues	Types of interactions
IMO-1	-5.7	54.14	His513 Ala430, Arg434, Ile510	π- Cation Alkyl, π- Alkyl
IMO-2	-6.1	27.17	Ala493	π-Sigma
IMO-3	-6.7	9.66	Met522 Trp383, Tyr526 Leu525	H-bonding, Alkyl, π-Alkyl, Unfavorable Acceptor-Acceptor Alkyl, π- Alkyl π-Sigma, Alkyl, π-Alkyl
IMO-4	-6.6	11.47	Lys481 Met315, Ile487 Ala312	H-bonding, Alkyl Alkyl π-Sigma
IMO-5	-6.2	22.87	Ala312 Lys481 Met315	H-bonding, π-Sigma H-bonding, Alkyl Alkyl
IMO-6	-5.7	54.14	Trp383, Met522 Leu525	H-bonding, Alkyl, π-Alkyl Alkyl, π- Alkyl

The visualization of the docking result of compound IMO-1 against the protein 3ERT showed an interaction with a binding constant value of -5.7 Kcal/mol and predicted inhibitory constant value of 54.14μM. For IMO-1, there were various types of interactions between the ligand and the protein. It was seen that a π -cation interaction was present between a phenyl ring of the ligand and amino acid His 513 at a distance of 4.88Å (Fig. 5.B.6). Another significant interaction that was observed was the alkyl interactions between the two CH_3 groups of the ligand and the CH_3group of Ala 430 at a distance of 4.18 and 4.27Å respectively followed by the pi-alkyl type of interactions between the phenyl ring of the ligand and the sigma bond between two CH_2 groups of the amino acid Arg 434 at a distance of

3.75 Å. Finally, a pi-alkyl interaction was also seen between the phenyl ring of the ligand and the sigma bond between the two CH_2 groups of Ile 510 amino acid at a distance of 4.85 Å.

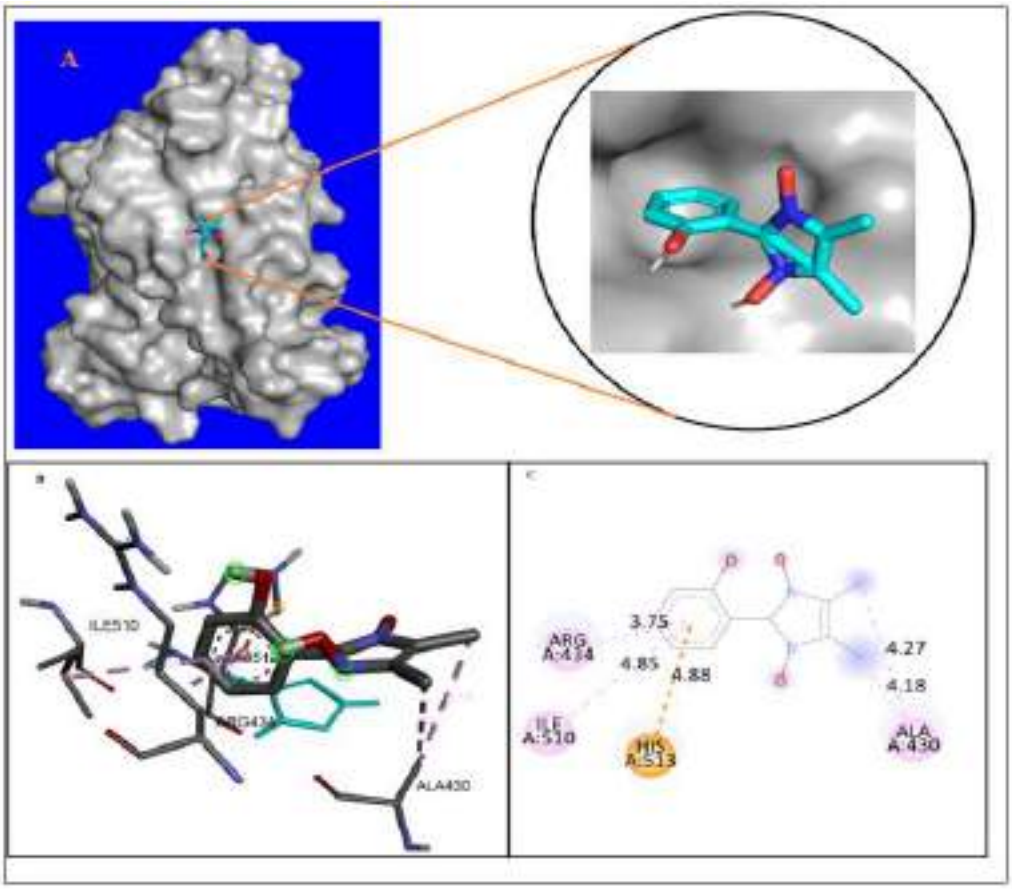

Fig. 5.B.6. Visualisation of docking results pf ligand IMO-1 with the protein 3ERT : (A) Optimal binding mode of the protein with IMO-1 ligand (ligand shown as blue and green stick model), (B) Amino acid residues involved in different interactions (light pink dashed lines shows alkyl and pi- alkyl interactions and brown dashed lines show pi-cation interactions), (C) 2D representation of bonding interaction of ligand IMO-1 with different amino acid residues of protein 3ERT.

A close visualization of the docking result of ligand IMO-2 with the receptor protein 3ERT revealed that the ligand binds with the protein with a binding energy (ΔG) -6.1Kcal/mole and predicted inhibitory constant (**pK_i**) 27.17μM. For IMO-2, it was found that there was only one kind of pi-sigma interaction between the phenyl ring of the ligand and the CH_3 group of the amino acid Ala 493 at a distance of 3.42Å (Fig. 5.B.7)

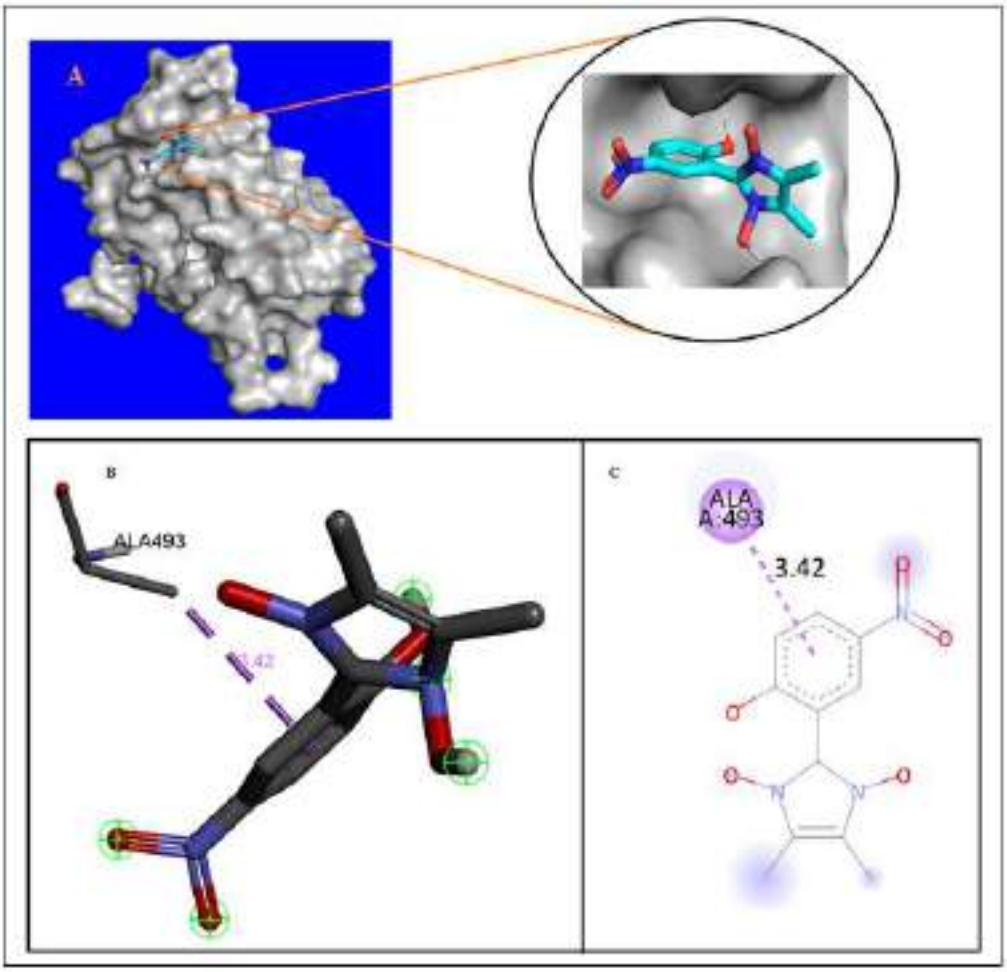

Fig. 5.B.7. Visualization of docking results of ligand IMO-2 with the protein 3ERT : (A) Optimal binding mode of the protein with IMO-2 ligand (ligand shown as blue and green stick model), (B) Amino acid residues involved in different interactions (purple dashed lines shows pi- sigma interactions (C) 2D representation of bonding interaction of ligand IMO-2 with different amino acid residues of protein 3ERT.

Docking results of the ligand IMO-3 shows the highest affinity interaction among the ligands IMO-1 to IMO-6 binding energy value of -6.7 Kcal/mol and the predicted inhibitory constant was found to be 9.66μM. A Conventional Hydrogen bonding was seen between the hydrogen atom of the -OH group attached to a nitrogen atom of the imidazole ring present in the ligand and the oxygen atom of the amino acid Lys 481 at a distance of 2.87Å (Fig. 5.B.8). A pi-sigma interaction was also seen between the phenyl ring of the ligand and the CH_3 group of Ala 312 at a distance of 3.79 Å followed by an alkyl interaction between the chlorine atom of the ligand with the sigma bond between the (CH_3) CH group and CH_2 group of the Ile 487 amino acid at a distance of 5.49 Å. Two more kinds of alkyl interactions were seen between the CH_3 groups of the ligand and the sigma bond

between Sulfur atom and CH_2 group in Met315 at a distance of 4.31 Å and between the CH_3 groups of the ligand with the CH_3 group of the amino acid Lys 481 at a distance of 3.55Å and 3.74 Å respectively.

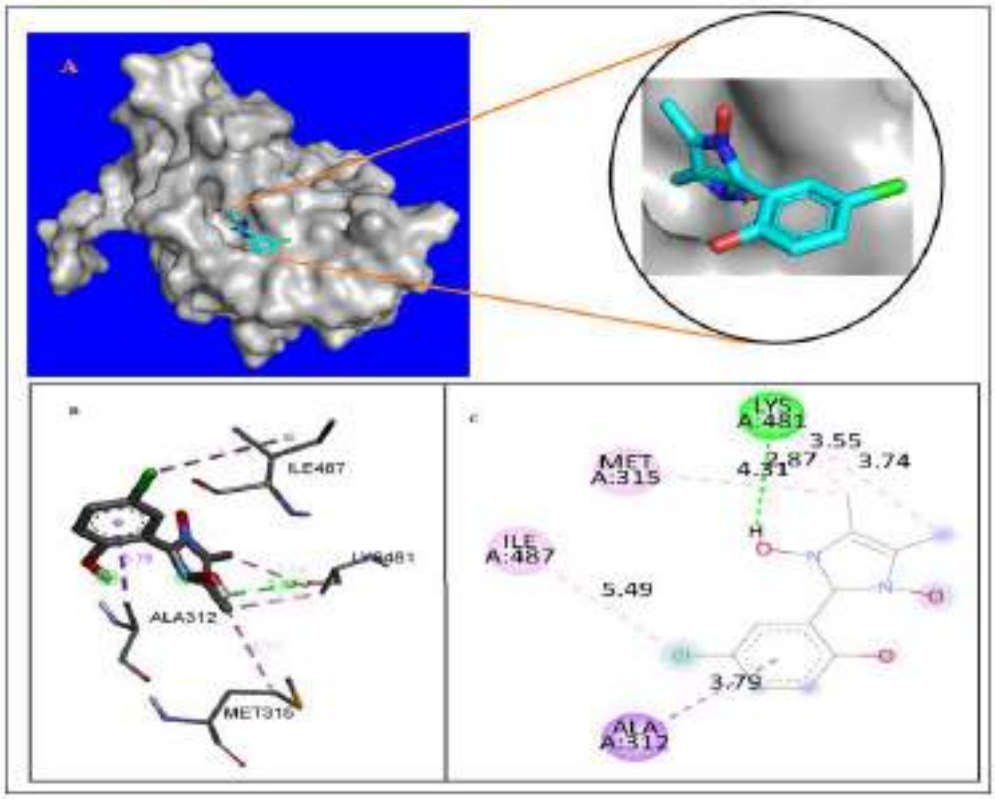

Fig. 5.B.8. Visualization of docking results of ligand IMO-3 with the protein 3ERT : (A) Optimal binding mode of the protein with IMO-3 ligand (ligand shown as blue and green stick model), (B) Amino acid residues involved in different interactions (purple dashed lines shows pi- sigma interactions, light pink dashed lines show alkyl interactions and green dashed lines show conventional hydrogen bonding interactions), (C) 2D representation of bonding interaction of ligand IMO-3 with different amino acid residues of protein 3ERT.

Docking results of the ligand IMO-4 shows the second highest affinity interaction after NO-3with a binding energy value of -6.6 kcal/mol and the predicted inhibitory constant was found to be 11.47µM. A Conventional Hydrogen bonding was seen between the hydrogen atom of the -OH group attached to a nitrogen atom of the imidazole ring present in the ligand and the sulfur atom of the amino acid Met 522 at a distance of 2.52Å (Fig 5.B.9). A pi-sigma interaction was also seen between the phenyl ring of the ligand and the CH_2 group of Leu 525 at a distance of 3.61Å followed by a pi-alkyl interaction between the CH_3 of the ligand with the phenyl ring of the amino acid Tyr 526 at a distance of 4.76Å. Another pi-alkyl interaction was seen between the bromine atom of the ligand with the benzimidazole ring present in amino acid Trp 383 at a distance of 4.96 Å. Two

more alkyl interactions were also seen between the bromine atom of the ligand and the $C(CH_3)_3$group of the amino acid Leu 525 at a distance of 4.29 Å and between the CH_3 group of the ligand with the sigma bond present between the CH_2 group and Sulfur atom in the amino acid Met 522 at a distance of 4.57 Å. Finally, an unfavorable interaction was seen between the oxygen atom attached to the OH group in the ligand with the Oxygen atom present in amino acid Met 522 at a distance of 2.99Å.

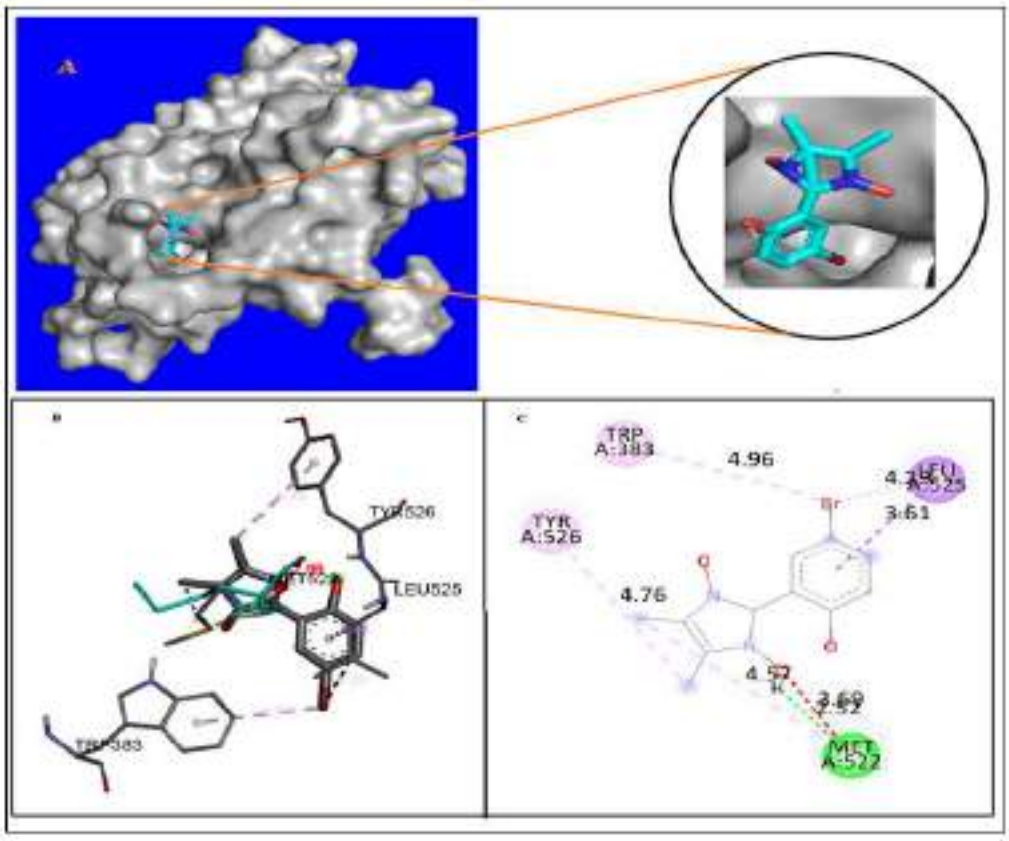

Fig. 5.B.9. Visualization of docking results of ligand IMO-4 with the protein 3ERT : (A) Optimal binding mode of the protein with IMO-3 ligand (ligand shown as blue and green stick model), (B) Amino acid residues involved in different interactions (purple dashed lines shows pi- sigma interactions, light pink dashed lines show alkyl and pi-alkyl interactions and green dashed lines show conventional hydrogen bonding interactions), (C) 2D representation of bonding interaction of ligand IMO-4 with different amino acid residues of protein 3ERT.

The interaction of ligand IMO-5 with 3ERT showed an interaction with a binding constant value of -6.2 Kcal/mol and predicted inhibitory constant value of 22.87 µM.For IMO-5, there were various types of interactions between the ligand and the protein. It was seen that a conventional Hydrogen bonding interaction was present between the oxygen atom of the ligand and the hydrogen atom of the NH_2

group found in amino acid Ala 312 at a distance of 2.00Å. Another significant conventional hydrogen bonding interaction was also observed between the oxygen atom of the OH group of the ligand with the oxygen atom of the C=O group of the amino acid Lys 481 at a distance of 3.10Å.A pi-sigma interaction was also seen between the phenyl ring of the ligand with the CH_3 group of the amino acid Ala 312 at a distance of 2.00 Å followed by two alkyl interactions between the CH_3 group of the ligand with CH_2 group present in Lys 481 at a distance of 3.58Å and 3.65Å respectively . Finally, an alkyl interaction was also seen between the CH_3 group of the ligand with the sigma bond present between Sulfur and carbon atoms present in the amino acid Met 315 at a distance of 4.25Å (Fig. 5.B.10).

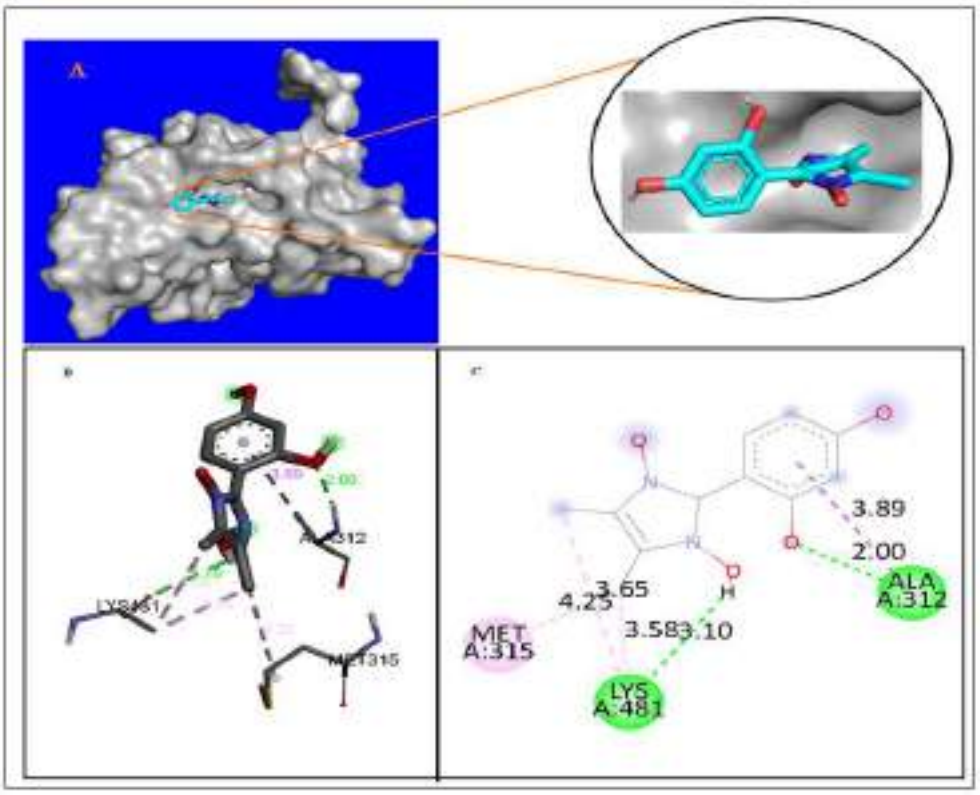

Fig. 5.B.10. Visualization of docking results of ligand IMO-5 with the protein 3ERT : (A) Optimal binding mode of the protein with IMO-5 ligand (ligand shown as blue and green stick model), (B) Amino acid residues involved in different interactions (purple dashed lines shows pi- sigma interactions, light pink dashed lines show alkyl and pi-alkyl interactions and green dashed lines show conventional hydrogen bonding interactions), (C) 2D representation of bonding interaction of ligand IMO-5 with different amino acid residues of protein 3ERT.

The interaction of IMO-6 with 3ERT showed an interaction with a binding constant value of -5.7 kcal/mol and predicted inhibitory constant value of 54.14 µM. For IMO-6, there were various types of interactions between the ligand and the protein. It was seen that a conventional Hydrogen bonding interaction was present between the oxygen atom of the ligand and the hydrogen attached to nitrogen of the indole ring found in amino acid Trp 383 at a distance of 3.08Å.

Another significant conventional hydrogen bonding interaction was also observed between the hydrogen atom of the OH group of the ligand with the oxygen atom of the C=O group of the amino acid Met 522 at a distance of 2.24Å .A pi-alkyl interaction was also seen between the phenyl ring of the ligand with the sigma bond between carbon and sulfur atoms in amino acid Met 522 at a distance of 4.98 Å followed by an alkyl interaction between the O-CH_3 group of the ligand with the sigma bond between carbon and sulfur atoms in amino acid Met 522 at a distance of 4.74 Å . Yet another pi-alkyl interaction was seen between the CH_3 group of the ligand with the indole ring in Trp 383 at a distance of 4.79 Å. Finally, an alkyl interaction was observed between the CH_3 group of the ligand with the -$CH(CH_3)_2$ group of the amino acid Leu525 at a distance of 4.55 Å (Fig 5.B.11).

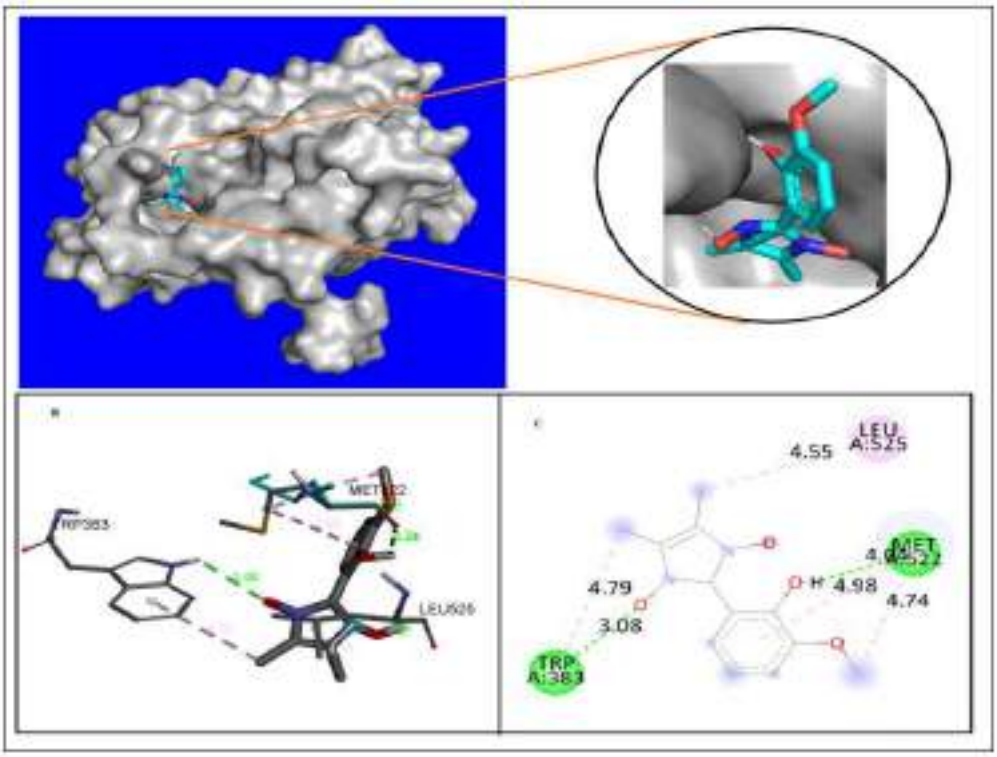

Fig. 5.B.11: Visualization of docking results of ligand IMO-6 with the protein 3ERT : (A) Optimal binding mode of the protein with IMO-6 ligand (ligand shown as blue and green stick model), (B) Amino acid residues involved in different interactions (purple dashed lines shows pi- sigma interactions, light pink dashed lines show alkyl and pi-alkyl interactions and green dashed lines show conventional hydrogen bonding interactions), (C) 2D representation of bonding interaction of ligand IMO-6 with different amino acid residues of protein 3ERT.

5.B.2.3 In silico Pharmacokinetics analysis of IMO-1 to IMO-6

In silico predictions of the pharmacokinetic ADMET properties like adsorption, distribution, metabolism, excretion and toxicity are very important for a molecule to be selected as a drug candidate in a much lesser time as compared to the conventional procedures[49]. Properties such as gastrointestinal adsorption (GI), water soluble capability (Log S), lipophilicity (Log P_o/W), CYP1A2 inhibitor and Blood-Brain Barrier (BBB) are also very important for any compound to be considered as a drug candidate[50]. These pharmacokinetic properties of the studied ligands (IMO-1 to IMO-6) have been determined with the help of computer aided online SAR studies using SwissADME database (http://www.swissadme.ch) and the results of the pharmacokinetic properties as well as Lipinski's property have been summarized in the Table 5.B.8.

Table 5.B.8. Lipinski's properties and pharmacokinetic properties (ADME) of 1-hydroxy-2-arylimidazole-3-oxide derivatives (IMO-1 to IMO-6)

	Compounds					
Properties	**IMO-1**	**IMO-2**	**IMO-3**	**IMO-4**	**IMO-5**	**IMO-6**
Molecular weight (gm/mole)	220.22	406.35	254.67	299.12	236.22	250.25
Rotatable bonds	1	2	1	1	1	2
H-bond acceptor	3	5	3	3	4	4
H-bond donor	2	2	2	2	3	2
Violations	0	0	0	0	0	0
Log Po/W	1.40	0.68	1.68	2.03	1.00	1.47
Log S	-2.82(S)	-2.85(S)	-3.40(S)	-3.71(S)	-2.66(S)	-2.86(S)
GI	High	High	High	High	High	High
BBB	No	No	Yes	Yes	No	No
CYP1A2	Yes	No	No	Yes	No	Yes
Bioavailability Score	0.55	0.55	0.55	0.55	0.55	0.55
Topological Surface Area ($A^{\circ 2}$)	48.91	94.73	48.91	48.91	69.14	58.14

*S: Soluble, BBB: Blood-Brain Barrier, CYP: Cytochrome P450, GI: Gastrointestinal absorption.

Analysis of Table 5.B.8, reveals that all the studied ligands (IMO-1 to IM-6) with a bioavailability score in the range of 55 % have consensus lipophilicity (Log P_o/W) value in the range of 0.68 to 1.68 and a high gastrointestinal absorption (GI). The positive value of the consensus lipophilicity indicates that all the ligands can pass through the lipid bilayer of the cellular membrane[50]. The solubility parameter (Log S) value of the ligands reveals that the ligands are soluble in water. This suggests that the all the studied ligands could serve as a potential drug candidate with no violations of Lipinski's rule and hence qualifies the drug likeliness criteria.

5.B.2.4 Computational details

5.B.2.4.1 DFT study

All Quantum Mechanical calculations were carried out on a hp-Z640 desktop P.C. with an Intel Xeon processor (Specifications: E5-2630 V4 @ 220GHz) using Gaussian 16 W package. Density functional theory (DFT) with Becke's (B)three parameter hybrid model, Lee, Yang and Parr's (LYP) using 631G+(d,2p) basis set has been employed to optimize the geometry of the 1-hydroxy-2-arylimidazole-3-oxide derivatives (IMO-1 to IMO-6).

A set of theoretical calculations of selected compounds (IMO-1 to IMO-6) were performed with Gaussian 16W, Revision A.03 programme package using B3LYP/631G+(d,2p) basis sets to optimize geometry and minimize energy for faster and accurate calculations. With the optimized geometry, theoretical Raman and IR spectra were also calculated from the so chosen basis set. From the optimized geometry, the energy of HOMO and LUMO molecular orbitals along with the energy of HOMO-LUMO gap has also been measured. For analyzing the result of the theoretical calculations, a visual representation was obtained by Gauss View program 6.0 and it has been used to construct the molecular electrostatic potential surface (MESP) as well as the shape of HOMO and LUMO molecular orbitals. Also, nonlinear Optical property (NLO) of the selected 1-hydroxy-2-arylimidazole-3-oxide derivatives have also been calculated taking urea as a reference NLO material.

5.B.2.4.2 Preparation of Protein and ligand for docking Study

The X-ray crystallographic structures of the Estrogen receptor protein (PDB ID 3ERT) has been downloaded from the Protein Data Bank (PDB) (http: //www.pdb.org.) database. Graphical User Interface program "Auto Dock Tools (ADT) 1.5.6" from Molecular Graphics Laboratory (MGL) developed by Scripps Research Institute has been used for the preparation of protein for docking study[48]. Input file of receptor protein for the blind docking study were created by taking specific chain (Chain A) of the protein (3ERT). In a typical receptor protein preparation, water molecules and hetero atoms along with the co-crystallized ligands in PDB crystal structure was removed and subsequently, the receptor

.pdbqt file has been prepared by adding polar hydrogen atoms and Kollman united atom charges[46-47]. The three-dimensional (3D) structures of ligands (IM-1 to IM-6) were drawn using Chemsketch (ACD/Structure Elucidator, version 12.01, Advanced Chemistry Development, Inc., Toronto, Canada, 2014, http://www.acdlabs .com.) and geometry optimization of the ligands (IM-1 to IM-6) were carried out using MM2 program incorporated in Chem. Draw Ultra 8.0 and further optimization of geometry of each molecule were carried out with the MOPAC 6 package using the semi-empirical AM1 Hamiltonian[51]. The input .pdbqt file of the ligands was generated using Auto Dock Tools (ADT). As the ligand molecules (IMO-1 to IMO-6) were non peptides, therefore, Gasteiger charge was assigned and then non-polar hydrogen was merged.

5.B.2.4.3 Molecular docking study using Autodock vina

All molecular docking calculations of the studied ligands (IMO-1 to IMO-6) with protein 3ERT were carried out in the AutoDock Vina programe 1.1.2 developed by Scripps Research institute[52-53] and the results of the docking study and the intermolecular interactions between receptors protein and the ligand molecules were analyzed using BIOVIA Discovery Studio 2020 (DS), version 20.1.0.0 (Dassault Systèmes BIOVIA, Discovery Studio Modeling Environment, Release 2017, San Diego: Dassault Systèmes, 2016) and Edu pymol version 1.7.4.4[52-53]. The three-dimensional (3D) affinity (grid) maps and electrostatic a grid boxes of 100×100×100 Å grid points and grid centre (X, Y, Z) of 22.395 ,5.644, 21.987with a spacing of 1.00 Å generated by AutoGrid auxiliary program for each of the receptor protein for blind docking were generated to cover the entire active site of the receptor protein in order to eliminate biasness arising during the docking simulation[54]. Lamarckian genetic algorithm and a standard protocol with default setting of other run parameters were used for docking simulation. For each docking experiments, several runs were performed by the program with one predicted binding mode with each run. All the torsions were allowed to rotate. The predicted inhibitory constant (pK_i) has been calculated using the following standardized equation[55]

$$pK_i = 10^{\frac{Binding\ Energy\ Score}{1.336}}$$

5. B.4.4 Pharmacokinetic study

The pharmacokinetic properties like like absorption, distribution, metabolism, excretion and toxicity (ADMET) of the compounds (IMO-1 to IMO-6) have been studied using the computer aided online SwissADME database (http://www.swissadme.ch).

5.B.5 References

(1) M. Waheed, N. Ahmed, M. A Alsharif, M. I. Alahmdi, S. Mukhtar., *ChemistrySelect*, **2017**, *2* (26), 7946–7950.

(2) A. Verma, S. Joshi, D. Singh., *Journal of Chemistry*, **2013**, *2013* (Article ID 392412).

(3) L. H. Abdel-Rahman, A. A. Abdelhamid, A. M. Abu-Dief, M. R. Shehata, M. A. Bakheet., *Journal of Molecular Structure*, **2020**, *1200*, 127034.

(4) A. P. Taylor, R. P. Robinson, Y. M. Fobian, D. C. Blakemore, L. H. Jones, O. Fadeyi., *Organic & Biomolecular Chemistry*, **2016**, *14* (28), 6611–6637.

(5) T. Shan, Z. Gao, X. Tang, X. He, Y. Gao, J. Li, X. Sun, Y. Liu, H. Liu, B. Yang, P. Lu, Y. Ma., *Dyes and Pigments*, **2017**, *142*, 189–197.

(6) R. B. da Silva, V. B. Loback, K. Salomão, S. L. de Castro, J. L. Wardell, S. M. S. V. Wardell, T. E. M. M. Costa, C. Penido, M. D. G. M. de Oliveira Henriques, S. A. Carvalho, E. F. da Silva, C. A. M. Fraga., *Molecules*, **2013**, *18* (3), 3445–3457.

(7) M. Witschel., *Bioorganic & Medicinal Chemistry*, **2009**, *17* (12), 4221–4229.

(8) T. B. Stensbøl, P. Uhlmann, S. Morel, B. L. Eriksen, J. Felding, H. Kromann, M. B. Hermit, J. R. Greenwood, H. Braüner-Osborne, U. Madsen, F. Junager, P. Krogsgaard-Larsen, M. Begtrup, P. Vedsø., *Journal of Medicinal Chemistry*, **2002**, *45* (1), 19–31.

(9) M. L. Richardson, K. A. Croughton, C. S. Matthews, M. F. G. Stevens., *Journal of Medicinal Chemistry*, **2004**, *47* (16), 4105–4108.

(10) O. K. Kim, L. K. Garrity-Ryan, V. J. Bartlett, M. C. Grier, A. K. Verma, G. Medjanis, J. E. Donatelli, A. B. Macone, S. K. Tanaka, S. B. Levy, M. N. Alekshun., *Journal of Medicinal Chemistry*, **2009**, *52* (18), 5626–5634.

(11) G. Mloston, M. Celeda, M. Jasinski, K. Urbaniak, P. J. Boratynski, P. R. Schreiner, H. Heimgartner., *Molecules*, **2019**, *24* (23), 4398.

(12) A. D. Bochevarov, M. A. Watson, J. R. Greenwood, D. M. Philipp., *Journal of Chemical Theory and Computation*, **2016**, *12* (12), 6001–6019.

(13) M. Mutailipu, Z. Xie, X. Su, M. Zhang, Y. Wang, Z. Yang, M. R. S. A. Janjua, S. Pan., *J Am Chem Soc*, **2017**, *139* (50), 18397–18405.

(14) M. Xiang, Y. Cao, W. Fan, L. Chen, Y. Mo., *Combinatorial Chemistry & High Throughput Screening*, **2012**, *15* (4), 328–337.

(15) M. Evecen, H. Tanak., *Materials Science - Poland*, **2016**, *34* (4), 886–904.

(16) X. Ma, D. Chang, C. Zhao, R. Li, X. Huang, Z. Zeng, X. Huang, Y. Jia., *Journal of Materials Chemistry C*, **2018**, *6* (48), 13241–13249.

(17) S. Naseem, M. Khalid, M. N. Tahir, M. A. Halim, A. A. C. Braga, M. M. Naseer, Z. Shafiq., *Journal of Molecular Structure*, **2017**, *1143*, 235–244.

(18) A. D. Becke., *The Journal of Chemical Physics*, **1993**, *98* (7), 5648–5652.

(19) C. Lee, W. Yang, R. G. Parr., *Physical Review B*, **1988**, *37* (2), 785–789.

(20) M. J. Frisch, G. W. Trucks, H. B. Schlegel, G. E. Scuseria, M. A. Robb, J. R. Cheeseman, G. Scalmani, V. Barone, G. A. Petersson, H. Nakatsuji, X. Li, M. Caricato, A. v Marenich, J. Bloino, B. G. Janesko, R. Gomperts, B. Mennucci, H. P. Hratchian, J. v Ortiz, A. F. Izmaylov, J. L. Sonnenberg, D. Williams-Young, F. Ding, F. Lipparini, F. Egidi, J. Goings, B. Peng, A. Petrone, T. Henderson, D. Ranasinghe, V. G. Zakrzewski, J. Gao, N. Rega, G. Zheng, W. Liang, M. Hada, M. Ehara, K. Toyota, R. Fukuda, J. Hasegawa, M. Ishida, T. Nakajima, Y. Honda, O. Kitao, H. Nakai, T. Vreven, K. Throssell, J. A. Montgomery Jr., J. E. Peralta, F. Ogliaro, M. J. Bearpark, J. J. Heyd, E. N. Brothers, K. N. Kudin, V. N. Staroverov, T. A. Keith, R. Kobayashi, J. Normand, K. Raghavachari, A. P. Rendell, J. C. Burant, S. S. Iyengar, J. Tomasi, M. Cossi, J. M. Millam, M. Klene, C. Adamo, R. Cammi, J. W. Ochterski, R. L. Martin, K. Morokuma, O. Farkas, J. B. Foresman, D. J. Fox., *Gaussian, Inc., Wallingford CT, Gaussian 16 Revision C.01*, **2016**.

(21) R. Dennington, T. A. Keith, J. M. Millam., *GaussView Version 6, Semichem Inc., Shawnee Mission, KS*, **2016**.

(22) G. Varvounis, V. Gkalpinos, P. Theodorakopoulou, E. Tsemperlidou., In *Comprehensive Heterocyclic Chemistry IV (Chap 4.02 - Imidazoles)*; Black, D. S., Cossy, J., Stevens, C. V., Eds.; Elsevier: Oxford, **2022**; Vol. 4, pp 113–307.

(23) P. Sykes., *A Guidebook to Mechanism in Organic Chemistry*, 6th ed.; Pearson Education: New Delhi, India, **2004**.

(24) K. B. Benzon, H. T. Varghese, C. Y. Panicker, K. Pradhan, B. K. Tiwary, A. K. Nanda, C. van Alsenoy., *Spectrochimica Acta Part A: Molecular and Biomolecular Spectroscopy*, **2015**, *151*, 965–979.

(25) K. Fukui, T. Yonezawa, H. Shingu., *The Journal of Chemical Physics*, **2004**, *20* (4), 722–725.

(26) L. G. Ferreira, R. N. dos Santos, G. Oliva, A. D. Andricopulo., *Molecules*, **2015**, *20* (7), 13384–13421.

(27) M. Snehalatha, C. Ravikumar, I. Hubert Joe, N. Sekar, V. S. Jayakumar., *Spectrochimica Acta Part A: Molecular and Biomolecular Spectroscopy*, **2009**, *72* (3), 654–662.

(28) T. A. Koopmans., *Physica*, **1934**, *1* (1–6), 104–113.

(29) R. G. Parr, R. G. Pearson., *J Am Chem Soc*, **1983**, *105* (26), 7512–7516.

(30) R. G. Parr, L. V. Szentpály, S. Liu., *J Am Chem Soc*, **1999**, *121* (9), 1922–1924.

(31) R. G. Pearson., *Journal of Chemical Sciences*, **2005**, *117* (5), 369–377.

(32) S. Mandal, D. K. Poria, D. K. Seth, P. S. Ray, P. Gupta., *Polyhedron*, **2014**, *73*, 12–21.

(33) P. Jaramillo, P. Pérez, R. Contreras, W. Tiznado, P. Fuentealba., *Journal of Physical Chemistry A*, **2006**, *110* (26), 8181–8187.

(34) N. P. G. Roeges., *A Guide to the Complete Interpretation of Infrared Spectra of Organic Structures*; John Wiley and Sons Inc.: New York, **1994**.

(35) B. C. Smith., *Infrared Spectral Interpretation, A Systematic Approach*, 1st ed.; CRC Press: Washington, DC, **1999**; Vol. 2.

(36) A. Madanagopal, S. Periandy, P. Gayathri, S. Ramalingam, S. Xavier, V. K. Ivanov., *Journal of Taibah University for Science*, **2017**, *11* (6), 975–996.

(37) E. Scrocco, J. Tomasi., *Advances in Quantum Chemistry*, **1978**, *11* (C), 115–193.

(38) P. Politzer, J. S. Murray., In *Theoretical Biochemistry and Molecular Biophysics: A Comprehensive Survey, Protein*; Beveridge, D. L., Lavery, R., Eds.; Adenine Press: Schenectady, New York, **1991**; Vol. 2.

(39) E. Scrocco, J. Tomasi., *Topics in Current Chemistry*, **1973**, *42*, 95–170.

(40) E. M. Maya, A. W. Snow, J. S. Shirk, R. G. S. Pong, S. R. Flom, G. L. Roberts., *Journal of Materials Chemistry*, **2003**, *13* (7), 1603–1613.

(41) Z. Sofiani, S. Khannyra, A. Boucetta, M. ElJouad, K. Bouchouit, H. Serrar, S. Boukhris, A. Souizi, A. Migalska-Zalas., *Optical and Quantum Electronics*, **2016**, *48* (282).

(42) S. Muthu, T. Rajamani, M. Karabacak, A. M. Asiri., *Spectrochimica Acta Part A: Molecular and Biomolecular Spectroscopy*, **2014**, *122*, 1–14.

(43) H. Sung, J. Ferlay, R. L. Siegel, M. Laversanne, I. Soerjomataram, A. Jemal, F. Bray., *CA : A Cancer Journal for Clinicians*, **2021**, *71* (3), 209–249.

(44) L. A. Torre, F. Bray, R. L. Siegel, J. Ferlay, J. Lortet-Tieulent, A. Jemal., *CA: A Cancer Journal for Clinicians*, **2015**, *65* (2), 87–108.

(45) Z. Bai, R. Gust., *Arch Pharm (Weinheim)*, **2009**, *342* (3), 133–149.

(46) N. Kerru, L. Gummidi, S. Maddila, K. K. Gangu, S. B. Jonnalagadda., *Molecules*, **2020**, *25* (8), 1909.

(47) X.-Y. Meng, H.-X. Zhang, M. Mezei, M. Cui., *Current Computer-Aided Drug Design*, **2011**, *7* (2), 146–157.

(48) R. Huey, G. M. Morris., *Using AutoDock 4 with AutoDocktools: A Tutorial.*; The Scripps Research Institute, Molecular Graphics Laboratory, pp. 54-56: La Jolla, CA, USA, **2008**.

(49) S. Hari., *Journal of Applied Pharmaceutical Science*, **2019**, *9* (7), 18–26.

(50) F. Ntie-Kang, L. L. Lifongo, J. A. Mbah, L. C. Owono Owono, E. Megnassan, L. M. Mbaze, P. N. Judson, W. Sippl, S. M. N. Efange., *In Silico Pharmacology*, **2013**, *1(1)* (Article 12), 1–11.

(51) K. Ohtawara, H. Teramae., *Chemical Physics Letters*, **2004**, *390* (1–3), 84–88.

(52) J. Eberhardt, D. Santos-Martins, A. F. Tillack, S. Forli., *Journal of Chemical Information and Modeling*, **2021**, *61* (8), 3891–3898.

(53) O. Trott, A. J. Olson., *Journal of Computational Chemistry*, **2010**, *31* (2), 455–461.

(54) G. M. Morris, D. S. Goodsell, R. S. Halliday, R. Huey, W. E. Hart, R. K. Belew, A. J. Olson., *Journal of Computational Chemistry*, **1998**, *19* (14), 1639–1662.

(55) M. A. Alamri, M. Tahir ul Qamar, M. U. Mirza, R. Bhadane, S. M. Alqahtani, I. Muneer, M. Froeyen, O. M. H. Salo-Ahen., *Journal of Biomolecular Structure and Dynamics*, **2021**, *39* (13), 4936–4948.